JOURNAL OF APPLIED PHYSICS

JOURNAL OF APPLIED PHYSICS

Vol. 18, No. 5 MAY, 1947

In This Issue

Page

Special Issue on High Polymers

Measurements of the Refractive Index of Films FRED W. BILLMEYER, JR. 431

Sound Velocity Method for Determination of Molecular Weight of Liquid Polymers ALFRED WEISSLER, JAMES W. FITZGERALD, AND IRVING RESNICK 434

Instrument for Measuring Particle Diameters and Constructing Histograms from Electron Micrographs E. E. HANSON AND J. H. DANIEL 439

Torsion of a Rubber Cylinder R. S. RIVLIN 444

Elastic Losses in Some High Polymers as a Function of Frequency and Temperature H. S. SACK, J. MOTZ, H. L. RAUB, AND R. N. WORK 450

Electrical Conductivity of GR-S and Natural Rubber Stocks Loaded with Shawinigan and R-40 Blacks P. E. WACK, R. L. ANTHONY, AND E. GUTH 456

Elastic Properties of Cork. II. Stress-Temperature Relationship of Compressed Cork S. L. DART AND EUGENE GUTH 470

Elastic Properties of Cork. III. Hydrostatic and Ordinary Load-Compression Curves for Cork S. L. DART, HOWARD A. ROBINSON, AND EUGENE GUTH 474

Contributed Original Research

Cold Cathode Rectifier WILLARD H. BENNETT 479

Hydrodynamic Lubrication of Finite Sliders CHARLES P. BOEGLI 482

Letters to the Editor:

Measurements of Base Pressure on a Missile in Free Flight F. K. HILL AND R. A. ALPHER 489

Direction of Maximum Crystal Elongation during Metal Cutting G. H. TOWNEND 489

In Every Issue

Here and There 490
Calendar of Meetings 492
New Booklets 492
Index to Advertisers xxxiv

BOARD OF EDITORS

ELMER HUTCHISSON, *Editor*

Associate Editors

R. BOWLING BARNES
OTTO BEECK
W. F. BUSSE
SELIG HECHT
W. JAMES LYONS
PHILIP MORRISON
PAUL E. SABINE
FREDERICK SEITZ
J. R. TOWNSEND
JOHN VON NEUMANN

Publication of the American Institute of Physics

ADMINISTRATIVE STAFF

HENRY A. BARTON, *Director*

MARGARET S. GRIFFIN, *Publications Manager*

THEODORE VORBURGER, *Business Manager*

JOHN T. TATE, *Adviser on Publications*

GOVERNING BOARD

GEORGE R. HARRISON, *Chairman*

WALLACE WATERFALL, *Secretary*

GEORGE B. PEGRAM, *Treasurer*

E. U. CONDON
A. J. DEMPSTER
W. F. FAIR, JR.
FLOYD A. FIRESTONE
HARVEY FLETCHER
R. C. GIBBS
K. S. GIBSON
PAUL E. KLOPSTEG
A. H. PFUND
JOHN T. TATE
M. W. WHITE
A. G. WORTHING

The JOURNAL OF APPLIED PHYSICS, published monthly at Prince and Lemon Sts., Lancaster, Pa., is devoted to physics in its role as the science basic to other natural sciences and to the arts and industries. Previous to 1937 this publication was known as PHYSICS. The JOURNAL OF APPLIED PHYSICS publishes editorials, news of physicists, and reviews, as well as technical papers of applied physics.

Manuscripts should be submitted to Elmer Hutchisson, Editor, Case School of Applied Science, Cleveland 6, Ohio.

Subscriptions and orders for back numbers should be addressed to Prince and Lemon Streets, Lancaster, Pa. or to the American Institute of Physics, 57 East 55 Street, New York 22, N. Y.

Subscription Price

	U.S. AND CANADA	ELSEWHERE
To members and associate members of the American Institute of Physics	$5.00	$5.70
To all others	7.00	7.70

Back Number Prices

Complete set: Vol. 1, July, 1931–Vol. 17, 1946—$124.00
Yearly back number rate: $10.00
Single copies: $1.00 each.

Changes of address and proofs should be addressed to the Publications Manager.

Advertising rates supplied on request. Orders, advertising copy, and cuts should be sent to the American Institute of Physics.

Entered as second class matter January 22, 1937, at the Post Office at Lancaster, Pennsylvania, under the Act of March 3, 1879. Accepted for mailing at the special rate of postage provided for in the Act of February 28, 1925, authorized May 2, 1932.

Copyright 1947, by the American Institute of Physics.

Journal of
Applied Physics

Volume 18, Number 5 May, 1947

Special Issue on High Polymers

The following six papers were presented at the meeting of the Division of High Polymer Physics of the American Physical Society at Columbia University, January 30–February 1, 1947.

Measurements of the Refractive Index of Films*

FRED W. BILLMEYER, JR.
E. I. du Pont de Nemours and Company, Plastics Department, Arlington, New Jersey

The refractive index of a film of transparent or translucent material may be determined by immersing the film in a suitable liquid mixture and observing the intensity of light reflected from the surface of the specimen. The composition of the immersion liquid is varied, and a record is made of its refractive index (measured on a refractometer) and of the reflected light intensity. The refractive index of the film is the same as that of the immersion liquid giving the lowest reflected intensity. This has been confirmed by experiments with a glass plate, whose refractive index was known. According to Fresnel's laws of reflection, the experimental data should fit a parabola with its minimum at the refractive index of the film. On fitting the data by the method of least squares, the minimum is obtained with a standard deviation of the order of 0.002 refractive index units. The method has been applied to several plastic materials.

INTRODUCTION

A METHOD has been developed for measuring the refractive index of a solid material. Originally used with thin films of translucent plastics, it may be applied as well to thicker specimens, of more highly absorbing or colored material. Mentioned by R. W. Wood[1] and used to some extent in the investigation of anomalous dispersion phenomena, the procedure consists in immersing the specimen in a suitable mixture of liquids and observing the intensity of light reflected from its surface. The composition of the immersion liquid is varied, and a record is made of its refractive indices (measured by a refractometer) and of the corresponding intensities of the reflected light. The refractive index of the sample is the same as that of the immersion liquid which gives the lowest intensity of reflected light.

THEORY

When a material of refractive index n_0, immersed in a liquid of refractive index n not too far different from n_0, is illuminated with unpolarized light striking its surface at an angle i (see Fig. 1), the fraction of the light reflected is given by Fresnel's Law as[2]

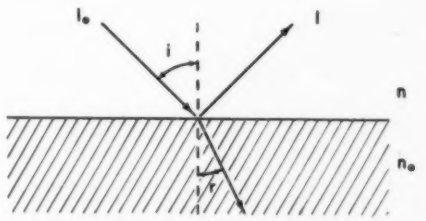

FIG. 1.

* Presented at the meeting of the Division of High Polymer Physics, American Physical Society, January 30–February 1, 1947.

[1] R. W. Wood, *Physical Optics* (The Macmillan Company, New York, 1934), third edition, pp. 411–12, 509.

[2] The coefficient $\frac{1}{2}$ in these equations becomes nearly 1 when reflections from the back face of a transparent sample are included. For these experiments its actual value is immaterial.

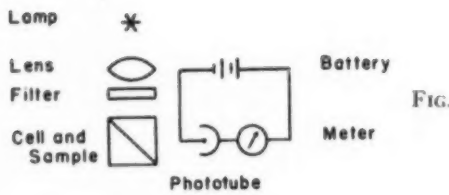

FIG. 2.

$$\frac{I}{I_0}=\frac{1}{2}\left[\frac{\sin^2(i-r)}{\sin^2(i+r)}+\frac{\tan^2(i-r)}{\tan^2(i+r)}\right], \quad (1)$$

where I_0 and I are the initial and reflected light intensities, respectively, and i and r are the angles of incidence and refraction. The angle r is given by Snell's Law:

$$n \sin i = n_0 \sin r. \quad (2)$$

If i is chosen as 45°, a convenient angle experimentally, and n is nearly equal to n_0, r becomes nearly 45°, and Eq. (1) reduces to

$$I/I_0=\tfrac{1}{2}(\tan^2(i-r)-\tan^4(i-r)). \quad (3)$$

Use of Eq. (2) then gives, for $i-r$ small,

$$I/I_0=\tfrac{1}{2}\left(\frac{n-n_0}{n_0}\right)^2+\cdots \quad (4)$$

which is a parabola with its minimum at $n=n_0$.

EXPERIMENTAL

Apparatus

A diagram of the essentials of the apparatus is shown in Fig. 2.

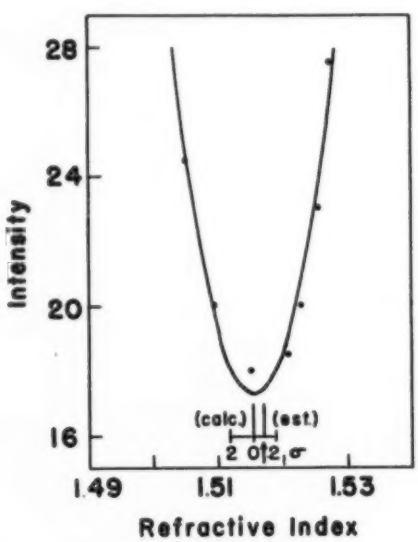

FIG. 3. Glass plate.

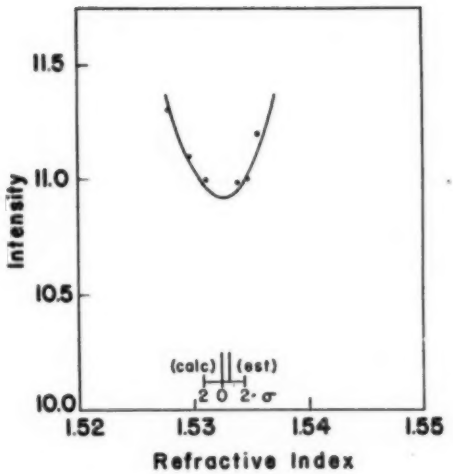

FIG. 4. Type FM-3 Nylon.

In the actual experiments two sets of apparatus were used. One consisted of a Bausch and Lomb projection microscope illuminator as light source and a Photovolt photometer, model 500, as detector. The tungsten lamp was run from a voltage-stabilizer, and a Wratten 62 filter was used to approximate mercury green light.

Later experiments were made with the light-scattering apparatus built by the author (to be described elsewhere). A stabilized incandescent lamp was used in conjunction with Wratten filters 11 and 22 to approximate sodium yellow light. Occasionally the filters were omitted.

In each case the sample was a thin film held between two pieces of polythene approximately 0.080 inch thick, arranged so as to fit tightly along the diagonal of a 4-centimeter square glass cell. The polythene was cut away so as to allow the light to hit the film and to allow free circulation of the immersion liquid. Polythene is especially suitable because of its general insolubility.

The immersion liquids must be miscible with one another and must not dissolve, swell, or otherwise affect the sample. Some liquid pairs which have been used are benzyl alcohol and carbon tetrachloride for the range in refractive index around 1.5, and carbon tetrachloride and benzene, or carbon tetrachloride and ethanol, for lower indices.

Measurements were carried out by starting with a liquid mixture about 0.01 refractive index

unit away from the index of the film (chosen by experience or in a preliminary experiment) and adding small increments of a liquid with index beyond that of the sample. For each liquid mixture used, the refractive index and the intensity of reflected light were measured.

The measurements of refractive index were carried out either on a Bausch and Lomb "Precision" refractometer using mercury green light, or on a Bausch and Lomb Abbé refractometer, which gives a reading for sodium light. All experiments were carried out at room temperature (approximately 25°C) and the refractometers were checked against standard glass plates occasionally.

Glass Plate Experiment

To test the accuracy of the procedure, the refractive index of a microscope slide was measured both by the method described here and directly by the Abbé refractometer, with the following result:

by refractometer,

$$n=1.5171$$

by light reflection,

$n=1.5156\pm0.0036$ (95 percent reliability).

The two values agree within one standard deviation. The data are presented in Fig. 3, with the refractometer value indicated by an arrow.

TABLE I. Refractive indices of films.

Material	Index	Color of light	Notes
polythene	1.515	mercury green	PM-1, lot 720
	1.519	mercury green	PM-1, lot 859
tetrafluoroethylene	1.378	white	"Teflon," density 2.18
	1.376	sodium yellow	"Teflon," density 2.12
hexamethylene sebacamide	1.532	sodium yellow	Type FM-3 Nylon

COMPUTATIONS

The refractive index of the test specimen may be obtained from the experimental data either by inspection or from the equation of the parabola fitted to the observed points by the method of least squares.

In the latter case, the reflected intensity is represented by the equation

$$I=a+bn+cn^2 \tag{5}$$

and the position of the minimum is

$$n_0=-\frac{b}{2c} \tag{6}$$

In the experiments carried out on films of plastics, the standard deviation in the value of n_0 was computed directly from the experimental data for the case of the glass plate. For each of the other cases the standard deviation was estimated from this value and the relative magni-

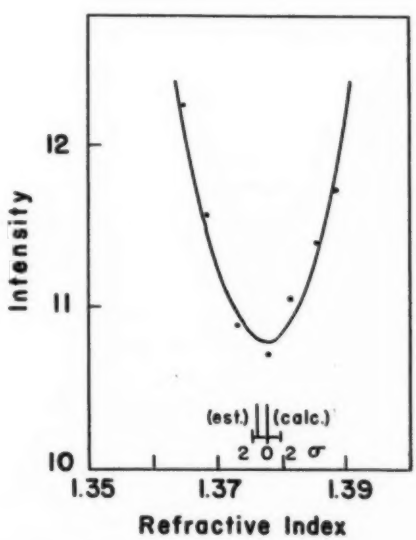

FIG. 5. "Teflon," density 2.18.

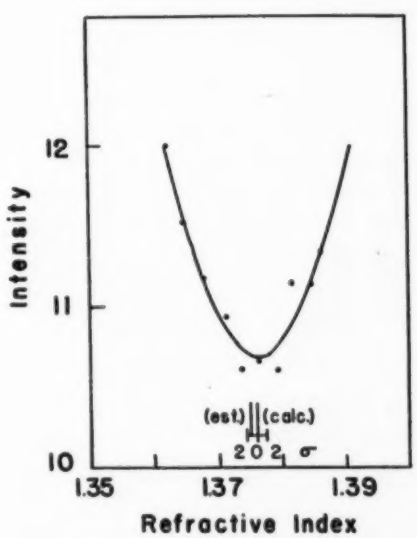

FIG. 6. "Teflon," density 2.12.

tudes of the "chi-square" index of precision[3] for glass and for the case in question.

Whenever the refractive index as determined by a visual inspection of the data was compared with that computed by least squares, the difference between the two was less than twice the standard deviation of the computed value.

Some experimental results are presented in the following table, and a few of the computed curves are shown in Figs. 4, 5, and 6. Included on the graphs are the estimated and computed indices of refraction of the respective films, and a scale of standard deviation, σ. The intensity is represented in arbitrary units, with the zero of intensity considerably below the axis.

The intensity at the minimum will depend upon the transparency of the film. For a very transparent material such as glass, it will be limited chiefly by the scattered and stray light in the apparatus. The value of n_0 is not influenced by the magnitude of this residual intensity.

[3] See, for example, R. A. Fisher, Statistical Methods for Research Workers (Oliver and Boyd, 1941), eighth edition.

CONCLUSION

A method similar to the mineralogical immersion technique for measuring the refractive index of a solid has been presented. The test specimen may be a thick or thin piece with a reasonably plane face, or a film. The material may be clear or translucent, and may also be colored. The optical quality of its surface need only be fair. For these reasons this technique has proved successful in several cases where other methods, such as the determination of Brewster's angle, have failed.

Some experimental results are given in the accompanying table and figures.

A Sound Velocity Method for Determination of Molecular Weight of Liquid Polymers†

ALFRED WEISSLER, JAMES W. FITZGERALD,* AND IRVING RESNICK**
Naval Research Laboratory, Washington, D. C.

A new method is presented for determining number average molecular weights of liquid polymers, by means of easily performed measurements. The molecular weight is an explicit function

$$M=\frac{Bd}{v^4-A\left(\frac{n^2-1}{n^2+2}\right)}$$

of the sound velocity v, density d, refractive index n, and the two empirical constants A and B. Accuracy of about 2 parts per hundred was attained for the lower polyethylene glycols. The method seems suitable for molecular weights up to several thousand. Sound velocities were measured by an acoustic interferometer, at one megacycle frequency.

THE molecular weight of a polymer is so fundamental a property, and the methods available for its determination are so few in number, that any new technique warrants a certain interest. This paper presents such a new method, suitable for liquids, which is based on the relatively simple measurements of sound velocity, density, and refractive index.

I. BASIS OF THE METHOD

Sound velocity in liquids became useful for the investigation of molecular structure after the discovery by M. R. Rao[1] of the empirical constant

$$R=Mv^{\frac{1}{3}}/d \qquad (1)$$

where M is the molecular weight, v and d are the sound velocity and density measured at the same temperature, and R may be called the molar sound velocity. For each pure liquid (except water) the molar sound velocity is a constant independent of temperature; therefore, density and the cube root of velocity vary in such a way that their ratio is fixed.

† Presented at the meeting of the Division of High Polymer Physics, American Physical Society, January 30–February 1, 1947.

* Now at Engineering Research Associates, Washington, D. C.

** Now at Johns Hopkins University, Baltimore, Maryland.

[1] M. R. Rao, Ind. J. Phys. 14, 109 (1940); J. Chem. Phys. 9, 682 (1941).

TABLE I. Physical properties of polyethylene glycols at 30°C.

Glycol	Mol. wt.	Density	Sound velocity	n_D	Viscosity	Boiling point
Ethylene	62.1	1.1068 g/cc	1642.9 m/s	1.4295	13.95 c.p.	69°/1.2 mm
Diethylene	106.1	1.1094	1567.7	1.4438	22.55	105°/2.0
Triethylene	150.1	1.1158	1593.3	1.4531	29.96	123°/1.2
Tetraethylene	194.2	1.1159	1580.1	1.4567	35.16	138°/0.5
Pentaethylene	238.2	1.1165	1580.0	1.4593	42.37	176°/0.5
Poly 200	200±10	1.1168	1592.2	1.4572	39.71	
Poly 300	300±15	1.1176	1578.0	1.4618	59.02	
Poly 400	400±20	1.1182	1576.0	1.4636	74.70	
Poly 600	600±30	1.1183	1570.2	1.4653	104.62	

Although the velocity of sound varies irregularly within a given homologous series, such as the alcohols or ketones, the molar sound velocity was found to be an additive property of the atoms (or bonds) in the molecule. From the published tables of R increments for atoms of carbon, hydrogen, oxygen, etc., the molar sound velocity may be calculated with good accuracy, just as in the familiar case of molar refraction.

Further, Lagemann and Dunbar[2] showed that, within a homologous series, linear relationships exist between any two of the following molar constants: (a) molar sound velocity, (b) molar refraction

$$N=\frac{M}{d}\left(\frac{n^2-1}{n^2+2}\right) \tag{2}$$

where n is index of refraction, (c) molar viscosity as defined by Souders[3]

$$I=(2.9+\log\log\eta)\frac{M}{d} \tag{3}$$

where η is viscosity in millipoises, (d) molar magnetic rotation, (e) parachor, (f) critical volume, and (g) van der Waals' b.

An example of such a relationship is the one involving refraction and sound velocity

$$R=AN+B \tag{4}$$

where A and B are, respectively, the slope and intercept. Upon substitution of Eqs. (1) and (2), this immediately yields an expression for the molecular weight

$$M=\frac{Bd}{v^{\frac{1}{4}}-A\left(\frac{n^2-1}{n^2+2}\right)} \tag{5}$$

in terms of the two empirical constants and the observed sound velocity, density, and refractive index. Similar expressions may be obtained from other pairs of molar constants; for example:

$$M=\frac{B'd}{v^{\frac{1}{4}}-A'(2.9+\log\log\eta)} \tag{6}$$

and

$$M=\frac{B''d}{\left(\frac{n^2-1}{n^2+2}\right)-A''(2.9+\log\log\eta)} \tag{7}$$

where A', A'', B', and B'' are the analogous slopes and intercepts of the other linear relations.

These results should be applicable not only to a homologous series, in which the difference between two successive members is $-CH_2-$, but also to a polymer homologous series, where the difference is any monomer structural unit.

II. EXPERIMENTAL

It was therefore decided to test the validity of Eq. (5), and incidentally of (6) and (7), by using it to determine the molecular weights of several pure members and commercial mixtures of the polyethylene glycol series. These polymers, of type formula $HO-(-CH_2-CH_2-O-)_n-H$, have been studied intensively in the past.[4,5] The

[2] R. T. Lagemann and W. S. Dunbar, J. Phys. Chem. **49**, 428 (1945).
[3] M. Souders, J. Am. Chem. Soc. **60**, 154 (1938).
[4] H. Staudinger, *Der Aufbau der hochmolekülaren organischen Verbindungen*, (Julius Springer, Berlin, 1932).
[5] R. Fordyce and H. Hibbert, J. Am. Chem. Soc. **61**, 1910, 1912 (1939).

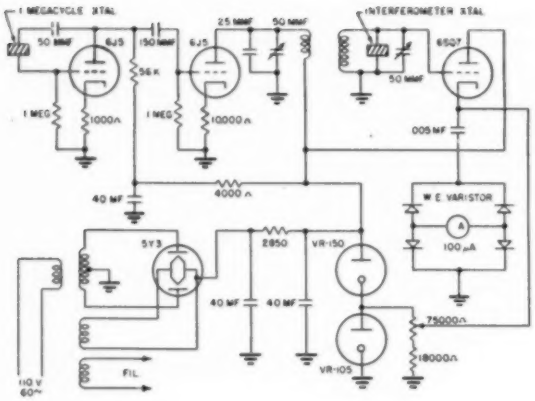

FIG. 1. Circuit design for interferometer.

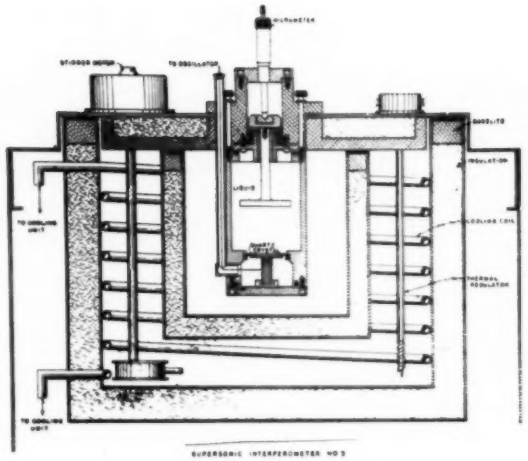

FIG. 2. Interferometer in thermoregulated oil bath. The inner tank shown has since been removed.

chemical individuals (the monomer, dimer, trimer, tetramer, and pentamer) were purified by fractional distillation through a 40 cm Widmer column, at about 1 mm pressure. The mixtures were those of average molecular weight 200, 300, 400, and 600, as manufactured by Carbide and Carbon Chemicals Corporation.

Several physical properties of these nine liquids were measured at $30°\pm0.1°$: refractive index for sodium light by the Abbé refractometer, density by a 25 ml pycnometer, sound velocity by the acoustic interferometer described below, and viscosity by the Ostwald-Fenske viscometer. These properties are listed in Table I.

The acoustic interferometer[6] was of conventional type,[7–9] energized by a one megacycle crystal-controlled oscillator. Figure 1 shows the circuit used. Figure 2 is a sectional view of the brass interferometer cell, containing the quartz crystal source and the movable reflecting plate, immersed in the thermoregulated oil bath. About 300 ml of liquid are required for a measurement. As the reflector is moved vertically through the liquid by the micrometer head, cyclical variations in the standing wave pattern recur at distances of integral half-wave-lengths. These cause corresponding cycles in the current through the interferometer crystal, which are observed on a suitable microammeter. The micrometer-head travel required for an interval of two current maxima, then, is equal to the wave-length; and the velocity of sound is, of course, the product of this wave-length and the frequency. In practice, one measures the travel for twenty maxima, which makes possible a precision of a few hundredths of a percent.

[6] Designed by one of us (J. W. F.) and Mr. Burton G. Hurdle.

[7] G. W. Pierce, Proc. Am. Acad. **60**, 269 (1925).

[8] J. C. Hubbard and A. L. Loomis, Phil. Mag. **5**, 1177 (1928).

[9] E. Klein and W. D. Hershberger, Phys. Rev. **37**, 760 (1931).

III. DISCUSSION

From the physical properties of the nine liquids, there were computed the molar refractions, viscosities, and sound velocities. These observed molar constants agree reasonably well (Table II) with the values calculated[10] from the molecular structures, using the published tables[2,3,10] of the bond increments for each type of constant. In the case of molar sound velocity, the agreement is better than 1 percent, which is less than the dispersion in values among the original com-

TABLE II. Molar constants of polyethylene glycols.

	Molar sound velocity		Molar refraction		Molar viscosity	
Glycol	Observed	Calculated	Observed	Calculated	Observed	Calculated
Ethylene	661.7	652.0	14.47	14.49	181.2	176.0
Diethylene	1111.2	1106.1	25.40	25.39	312.9	316.9
Triethylene	1571.6	1560.1	36.37	36.31	443.2	457.8
Tetraethylene	2027.1	2014.2	47.36	47.28	575.3	598.7
Pentaethylene	2485.1	2468.2	58.36	58.27	708.3	739.6
Poly 200	2091	2075	48.79	48.87	593.6	617.5
Poly 300	3125	3105	73.71	73.56	897.3	937.5
Poly 400	4163	4135	98.63	98.48	1201.3	1257.5
Poly 600	6236	6195	148.40	148.17	1813.4	1897.5

[10] Molar refraction was calculated by the method of K. Fajans, *Physical Methods of Organic Chemistry*, edited by A. Weissberger (Interscience Publishers, New York, 1946), Vol. I, pp. 672, 679.

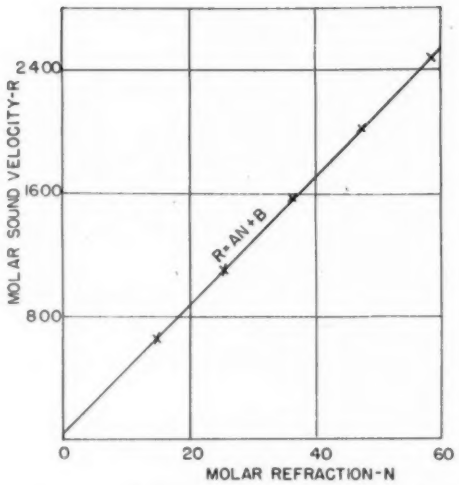

FIG. 3. Linear relation between molar sound velocity and molar refraction.

pounds used for constructing the table of increments. Compared to values previously reported[11] for 20°, the molar refractions show the customary increase of 0.01–0.02 percent per degree, attributed by Fajans[10] to loosening of the electron shell. The agreement is poorest for the molar viscosities.

Next, the existence of a linear relation between molar sound velocity and molar refraction was verified for the five pure compounds. The points lie on the straight line of Fig. 3, of which the slope A is 41.59 and the intercept B is 57.7. The slope may also be calculated from the tables of bond increments: for each $-CH_2-CH_2-O-$ structural unit, the R increment is 454 and the N increment is 10.88. The quotient of these two, which should be the slope, is 41.73, so that the agreement is a few parts per thousand.

TABLE III. Determination of molecular weight by sound velocity.

$$M=\frac{57.7d}{v^4-41.59\left(\frac{n^2-1}{n^2+2}\right)}$$

Glycol	Theoretical Mole. wt.	Mole. wt. by sound velocity	Deviation	Mole. wt. number avg.	Mole. wt. wt. avg.
Ethylene	62.1	59.9	−3.5%	60.8	62
Diethylene	106.1	111.5	5.1	101.6	109
Triethylene	150.1	147.3	−1.9	148.5	155
Tetraethylene	194.2	195.7	−0.8	195.4	190
Pentaethylene	238.2	237.7	0.2	234.5	238
Poly 200	200±10	186.2	−2.0+	183	219
Poly 300	300±15	302.7	0.0+	315	359
Poly 400	400±20	381.8	0.0+	384	480
Poly 600	600±30	546.9	−4.0+	561	720

[11] A. F. Gallaugher and H. Hibbert, J. Am. Chem. Soc. 58, 813 (1936).

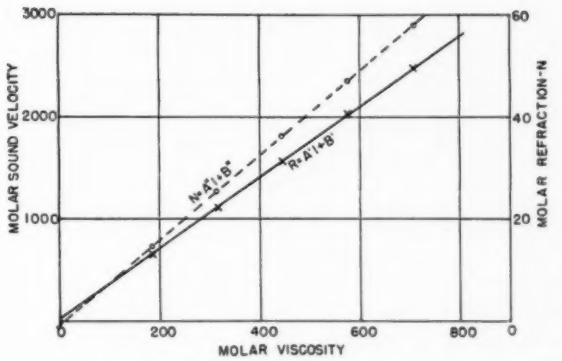

FIG. 4. Verification of other linear relations.

As expected, linear relations were found (Fig. 4) for the two other pairs of molar constants, sound velocity and viscosity, and refraction and viscosity. For the former pair, slope $A'=3.466$ and intercept $B'=31.9$; for the latter, $A''=0.08337$ and $B''=-0.640$. The agreement between observed and calculated slopes is not as good in these cases.

Next came the crux of the entire work. For each of the nine liquids, the molecular weight was calculated as indicated by Eq. (5), from the density, sound velocity, index of refraction, A, and B. The results show an average accuracy of about 2 percent (Table III) on the basis of the theoretical molecular weights, which compares well with that of other methods.

For purposes of comparison, the number average molecular weight was determined by freezing-point depression in water as solvent.[12] Measurements were made at concentrations of approximately 2 percent and 4 percent, and the values extrapolated to infinite dilution. The precision is estimated at about 3 parts per hundred. It is apparent from Table III that, within experimental error, the sound velocity molecular weight is the same as the number average

[12] Using water as solvent avoided the anomalous results encountered in ethylene dibromide solution by Gallaugher and Hibbert, reference 11, presumably because the glycols tend to be solvated, rather than associated, in aqueous solution. The apparent molecular weights obtained in the present work decreased slightly with increasing concentration, which indicates that association of glycol molecules is negligible compared to solvation.

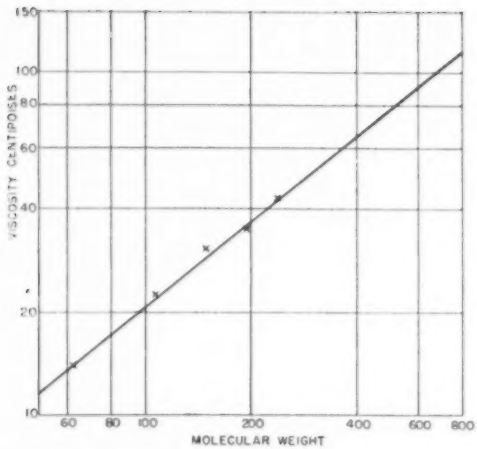

FIG. 5. Bulk viscosities of polyethylene glycols at 30°.

molecular weight. In addition, a weight average molecular weight was determined from the log-log plot of bulk viscosity against molecular weight[13] (Fig. 5). As would be expected, for the heterogeneous mixtures the weight average results shown in Table III are considerably higher than the number average or sound velocity molecular weights.

Attempts were also made to calculate the molecular weights from Eqs. (6) and (7), the analogous relations involving the other two pairs of properties. However, the errors are large, as demonstrated in Table IV. This may be due partly to the fact that the precision of measurement of viscosity is only about one-tenth as good as that of sound velocity or refractive index. Unfortunately, the errors increase for higher molecular weights because the calculations involve a decreasing difference between the two terms in the denominator of the expression for M.

[13] These lower polyethylene glycols appear not to conform to the relation $\log\eta = A + BM^{\frac{1}{2}}$ suggested for bulk viscosities by P. J. Flory, J. Am. Chem. Soc. **62**, 1057 (1940).

IV. SUMMARY

A new method for determining molecular weights of polymeric liquids has been shown to yield results of about 2 percent accuracy in the case of the lower members of the polyethylene glycol series. This method, which gives the number average molecular weight, consists of calculating M from two empirical constants and the observed sound velocity, density, and refractive index. We intend to investigate extension of its applicability to solid polymers or solutions of solids.

V. ACKNOWLEDGMENTS

Grateful acknowledgments are made to the many physicists and chemists at the Naval Research Laboratory who were generous with their facilities, materials, and advice during the prosecution of this work; and also to the Dow Chemical Company and to the Carbide and Carbon Chemicals Corporation, for generously supplying samples of these polyethylene glycols.

TABLE IV. Molecular weight determinations using other pairs of molar constants.

Glycol	Theoretical Mol. wt.	Refraction and velocity	Velocity and viscosity	Refraction and viscosity
Ethylene	62.1	59.9	63.6	62.5
Diethylene	106.1	111.5	131.4	98.2
Triethylene	150.1	147.3	138.0	167.2
Tetraethylene	194.2	195.7	186.0	205.2
Pentaethylene	238.2	237.7	237.9	221.9
Poly 200	200±10	186.2	187	183
Poly 300	300±15	302.7	479	185
Poly 400	400±20	381.8	1677	168
Poly 600	600±30	546.9	Infinite	137

An Instrument for Measuring Particle Diameters and Constructing Histograms from Electron Micrographs*

E. E. Hanson and J. H. Daniel
Chemical and Physical Research Laboratories, The Firestone Tire and Rubber Company, Akron, Ohio

An instrument for shortening the time and labor required in constructing particle size histograms from electron micrographs is described. Representative histograms obtained with the instrument for GR-S latices are shown. Linear, surface, and volume-equivalent diameters of non-spherical particles are defined, and variations in the instrument for plotting such diameters are proposed.

INTRODUCTION

In certain studies of the polymerization of synthetic rubbers, it is desirable to obtain particle-diameter distribution curves or histograms for the rubber latices. Such diameter histograms may be obtained from electron microscope photographs of the latex particles.

The technique used in this laboratory for preparing latex specimens for the electron microscope[1] consists essentially of forming a film from a dilute water solution of polyvinyl alcohol containing a small amount of the latex.

The construction of particle diameter histograms is tedious and time consuming. In the usual procedure, the "longest" and "shortest" diameters of the projected image (or of a photographic enlargement) of a particle are measured with a rule, their arithmetic mean is computed, and finally the number of particles with mean diameters lying in chosen diameter intervals is plotted against the diameters. Multiplication by a scale factor, containing the reciprocal of the magnification, converts the diameter axis of the histogram to read directly in Angstrom units. To obtain a representative distribution, at least 200 particles should be measured.

The instrument to be described here was developed to reduce the time and labor required in constructing such histograms. It will be called a "histogram computer."

In the development of the histogram computer, consideration was given to the question of whether the arithmetic or the geometric mean, or some other function of the "longest" and "shortest" diameters of a particle, should be plotted. With an unbroken film in the electron microscope, the latex particles usually appear approximately spherical in shape. However, when holes are present in the film, as frequently is the case, the particle contours are elliptical. The problem, then, is to compute the diameter of the equivalent spherical particle having either the same volume, or the same surface area, as the actual ellipsoidal particle. The two cases require, of course, calculation of different functions of the major and minor axes. In addition, the

Table I. Comparison of arithmetic and geometric mean diameters with volume and surface equivalent diameters.

				Prolate Spheroid						Oblate Spheroid					
					% Error			% Error			% Error			% Error	
Ratio a/b	Arith. Mean $\frac{a+b}{2}$	Geom. Mean $(ab)^{\frac{1}{2}}$	Difference %	D_v	Arith. Mean	Geom. Mean	D_s	Arith. Mean	Geom. Mean	D_v	Arith. Mean	Geom. Mean	D_s	Arith. Mean	Geom. Mean
1.0	b	b	0.0	b	0.0	0.0	b	0.0	0.0	b	0.0	0.0	b	0.0	0.0
1.5	$1.25b$	$1.225b$	1.0	$1.145b$	9.2	7.0	$1.16b$	7.8	5.6	$1.31b$	−4.6	−6.5	$1.33b$	−6.0	−7.9
2.0	$1.50b$	$1.414b$	2.9	$1.260b$	19	12.2	$1.31b$	14	7.9	$1.587b$	−5.5	−11	$1.66b$	−9.6	−15
2.5	$1.75b$	$1.58b$	5.1	$1.357b$	29	16	$1.44b$	22	9.7	$1.842b$	−5.0	−14	$1.99b$	−12	−21

a = Major Axis
b = Minor Axis

D_v = Diameter of sphere of equal volume.
D_s = Diameter of sphere of equal surface.

* Presented at the meeting of the Division of High Polymer Physics, American Physical Society, New York, January 30–February 1, 1947.

[1] R. H. Kelsey and E. E. Hanson, J. App. Phys. **17**, 675 (1946).

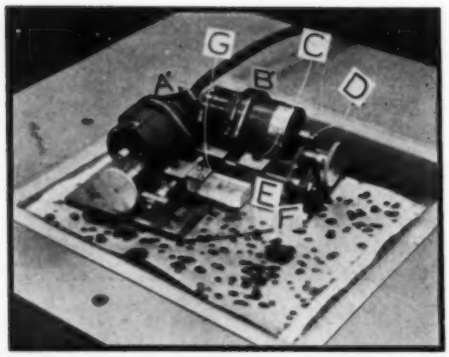

FIG. 1. The scanning mechanism.

particles may be either prolate or oblate, or some shape in between. Without going through some time-consuming process, such as taking stereo-photographs, there is no way of determining what volumetric shape a particle has.

A comparison between the diameters of the volume-equivalent and the surface-equivalent spheres, and the arithmetic and geometric mean diameters for both prolate and oblate spheroids is given in Table I. In some cases the geometric mean is the closer approximation, and in others the arithmetic mean is the closer. It was therefore decided to design the simplest of possible mechanisms, which gives the arithmetic mean. In general, the measurements should be restricted to particles having a major to minor axis ratio of less than two.

APPARATUS

The histogram computer consists essentially of a scanning mechanism for setting manually two pairs of mutually perpendicular lines on the outline of the particle, and a coupled recording mechanism for dropping a steel ball into a compartment corresponding to a range of diameters containing the arithmetic average of the two measured diameters of the particles.

Figures 1 and 2 are photographs of the scanning and the recording mechanisms, respectively. The scanning mechanism consists of a steel baseplate with a right angle section cut out for viewing the electron micrograph field, two mutually perpendicular screws (one labelled *E*) for translating non-rotating nuts to which clear Lucite blocks are attached, two equal gear trains coupling the rotations of the screws to their

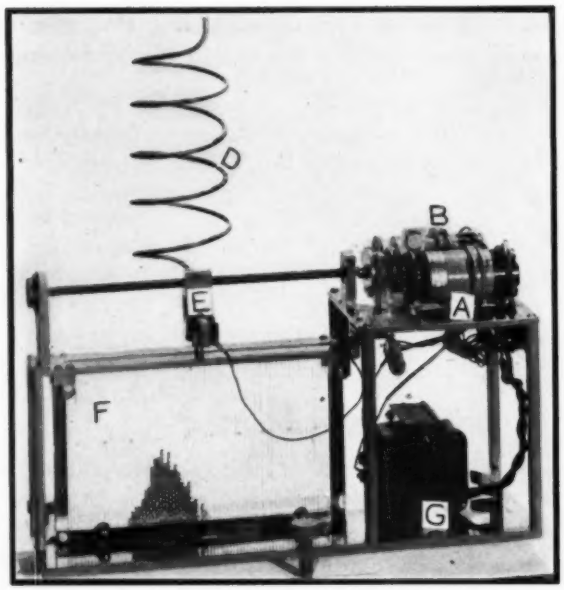

FIG. 2. The recording mechanism.

respective Selsyn motors, and a sub-base plate of clear Lucite on the under side of which are two scribed, inked-in lines drawn parallel with, and perpendicular to the two screws. Each of the movable Lucite blocks has a scribed, inked-in line drawn on its top and bottom surface, in a vertical plane parallel to a line in the sub-base plate. This enables the operator to set the lines without parallax on the edge of the particle. Each of the two Selsyn motors is coupled to a corresponding motor on the recorder so as to transmit its rotation.

In the recorder unit, the Selsyn motors, *A* and *B*, transmit their rotations additively through a differential gear, *C*, to a screw 10 inches long. The screw serves to position the ball-dispensing mechanism *E*. Directly below the ball-delivery

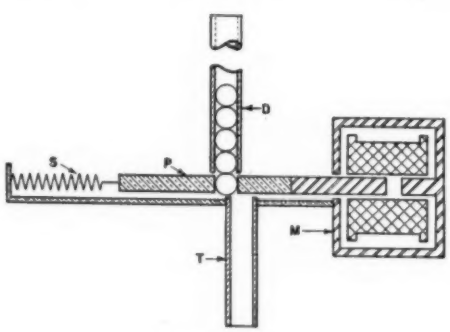

FIG. 3. The ball release mechanism.

tube, and parallel to the screw, is a thin rectangular Lucite box, F, divided into 80 compartments for receiving the steel balls as they are dropped.

The ball-dispensing unit consists of a $\frac{1}{8}''$ I.D. copper-tubing magazine, D, for holding a supply of $\frac{3}{32}''$ diameter steel balls, and an electromagnetically controlled "valve" by which the operator can cause the balls to be dropped one at a time. A cross-sectional diagram of the valve is shown in Fig. 3. The axis of the delivery-tube is sufficiently offset from the magazine, D, to prevent the balls from falling through. The flat plunger, P, normally held by the spring, S, in the position shown, is pierced by a hole slightly larger in diameter than the steel balls. When the circuit to the magnet, M, is closed, the plunger carries one ball over and discharges it into the delivery tube. The delivery tube projects between two parallel guides to a position $\frac{3}{16}''$ above the opening in the recorder compartments. The parallel guides also serve the purpose of preventing any rotation of the dispensing unit nut.

The recorder compartment box, F, was made by bolting together the two ends of two pieces of $6''\times11''\times\frac{1}{4}''$ Lucite blocks against .096" thick spacers. Strips of .010" thick shim stock were inserted into grooves which had been accurately milled into the inner surfaces of the plates on $\frac{1}{8}''$ centers. The bottom of the box is a metal blade which can be removed at the end of a run to release the accumulated balls into a flat box below.

End-play was taken out on the three screws by special thrust bearings. Back-lash was eliminated through the use of split-nuts engaging the screws.

The Selsyn motors were designed to be operated normally at 115 volts and 400 cycles. However, since no 400 cycle source was available, they were operated from the transformer, G, at 60 cycles and 24 volts.

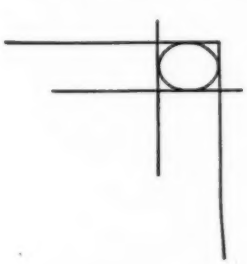

FIG. 4. Appearance of the scanning lines set on a particle.

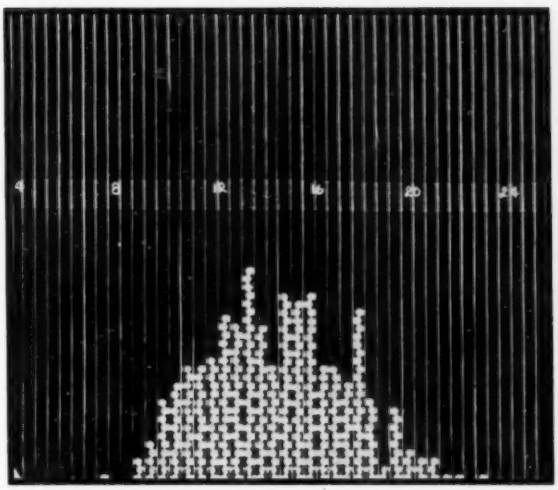

FIG. 5. Contact print of the recorder compartmented box showing distribution from which histogram of run 3, Fig. 6, was obtained.

The gear train normally used gave an amplification factor of 18 from the scanning to the recorder units. Therefore, a total magnification of 35,300 diameters was required in the electron micrograph to give a value of 50 Angstroms to each $\frac{1}{8}''$-long compartment interval. Other values could be given to the compartment interval by a suitable choice of gears and total magnification of the electron micrograph.

In practice, a particle count can be made either from a photographic enlargement, or directly from an image of the electron micrograph plate projected at the desired magnification on a ground-glass screen. The procedure is first to set the scanner unit on the zero position (scribed lines directly over each other), and the ball dispensing unit approximately at the zero position of the recorder box, and finally to shift the compartmented box slightly by hand until the balls fall equally often on both sides of the chosen zero wall. The scanning unit is then set successively on the particles to be measured, so that each particle is bracketed by the scribed lines as shown in Fig. 4. As each particle in turn is thus bracketed, the ball release switch is closed to record that particle. A counter, coupled to the switch, automatically totals the number of particles as the measurements proceed.

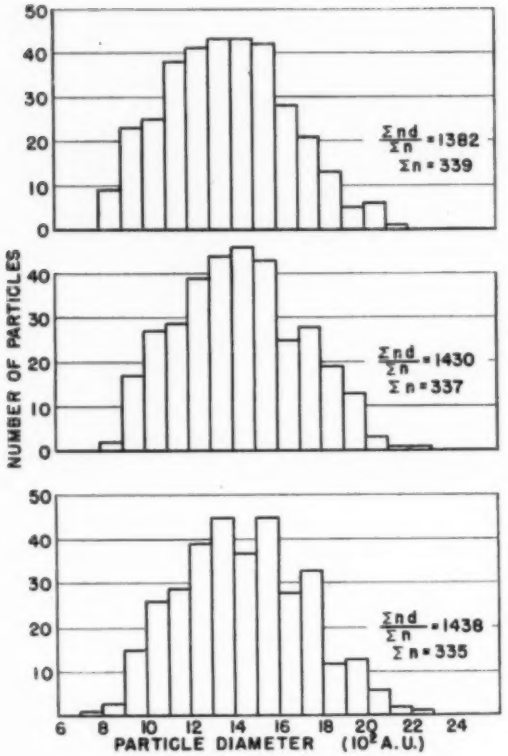

FIG. 6. Histograms of experimental latex. Each run made from same electron micrograph field.

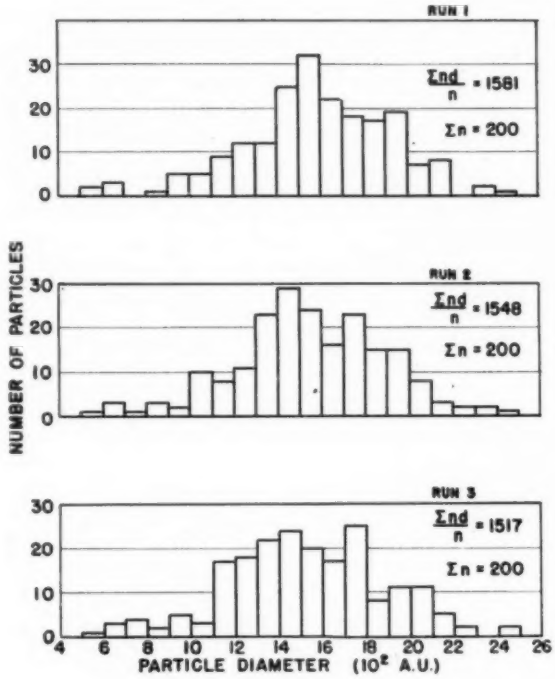

FIG. 7. Histograms of another experimental latex. Each run made from same electron micrograph field.

TYPICAL RESULTS

Figure 5 is a direct contact print of the record given by the histogram computer of 335 particles of an experimental GR-S latex. The print was made by placing F-2 contact paper against the back of the recorder compartments, and illuminating the front of the box for 15 seconds with a 60 watt Mazda bulb placed 7 feet away. In this case the electron microscope magnification was 5600, and the photographic enlargement was 6.3× to give a total magnification of 35,300×.

In Fig. 6 are three histograms of an experimental GR-S latex. All were constructed from the same electron micrograph field, and are, therefore, indicative of the reproducibility of the instrument. In these measurements an interval of 100 Angstrom units was chosen. Since the limit of resolution of the electron microscope was about 50 Angstroms for the specimens used, it was concluded that the sharp variations between 50 Angstrom intervals, shown in Fig. 5, were not significant.

Figure 7 is similarly a record of three successive histograms constructed from the same field of an electron micrograph of another GR-S type latex.

In general, the reproducibility of the curves is considered satisfactory.

It has been our experience that it is much less tedious to operate the computer than to measure particles with a rule, that the accuracy is increased, and that the time required to construct a histogram is reduced by about one-half.

OTHER POSSIBLE MECHANISMS

Construction of an electronic servo-system, to replace the Selsyns and differential in the histogram computer, was not justified in this laboratory because of extra complications, but would give added features which might be desirable in some applications. Among such features may be listed the following:

1. Distribution of the geometric as well as arithmetic means of major and minor axes.
2. Distribution of surface area (approximate) or of volume (exact), assuming particle shape to be an ellipsoid of revolution.
3. Flexibility of size of histogram increments.

One such scheme is shown in Fig. 8. Circular

potentiometers, P_1 and P_2, have resistances linear with their respective angles of rotation, θ_1 and θ_2, to the desired degree of accuracy. In use, θ_1 and θ_2 are set proportional to the major and minor axes, D_1 and D_2, respectively. Similar potentiometers, P_3 and P_4, are mechanically inter-connected so that their angles of rotation remain always equal to the single angle θ. This angle θ is determined by the position of the servo-motor, which also runs the ball dispenser of the recorder (minus differential gear). In Fig. 8, the two voltages, V_2 and V_3, applied to the sum amplifier will always differ 180° in phase, so when their magnitudes are equal, the sum amplifier output to the servo-motor will be zero. The direction of rotation of the servo-motor when V_2 and V_3 are not equal will depend on which voltage is the greater. The blocks labeled CF are cathode followers with amplification, A_{CF}, extremely constant and slightly less than unity. Setting $R_1=R_2=0$ for the moment, the following relations will exist:

$$V_2=V_1A_{CF_1}\theta_2=V_1A_{CF_1}k_2D_2$$
$$=k_1D_1C_1V_0A_{CF_1}k_2D_2, \quad (1)$$

$$V_3=V_4A_{CF_2}\theta=-A_{CF_2}\theta^2C_4V_0, \quad (2)$$

where $\theta_1=k_1D_1$; $\theta_2=k_2D_2$; voltage across $P_1=C_1V_0$; voltage across $P_4=-C_4V_0$.

When the servo-motor has equalized V_3 and $-V_2$, and the recorder ball dispenser comes to rest, the following relation will exist:

$$A_{CF_2}\theta^2C_4V_0=k_1D_1C_1V_0A_{CF_1}k_2D_2,$$

$$\theta=\left(k_1k_2\frac{C_1}{C_4}\frac{A_{CF_1}}{A_{CF_2}}\right)^{\frac{1}{2}}(D_1D_2)^{\frac{1}{2}}. \quad (3)$$

Hence the position of the recorder ball dispenser is proportional to the geometric mean of the particle major and minor axes.

Since V_0 does not appear in Eq. (3), line voltage regulation is unnecessary. Rheostat R_1 allows the increment of diameter for the histogram to be varied. The combination of R_1 and R_2 allows a shift of recorder zero for cases where no small particles are present.

To obtain a histogram of approximate surface areas, a switching arrangement feeds V_4 instead of V_3 to the sum amplifier, thus giving θ proportional to the product D_1D_2.

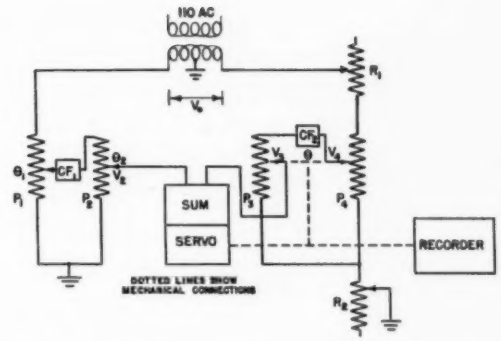

FIG. 8. Schematic diagram of proposed servo-mechanism for histogram computer.

To obtain a histogram of the arithmetic mean of particle diameters, a switching arrangement removes CF_1 and CF_2 from the circuit, connects the ungrounded ends of P_1 and P_2, and feeds V_1 and V_2 separately, and V_4 instead of V_3, to the sum amplifier (for this arrangement k_1 must equal k_2, as would normally be the case).

To obtain a histogram of volumes, V_4 instead of V_3 is fed to the sum amplifier, P_3 is connected mechanically and electrically to P_2 in the same manner it was formerly connected to P_4, and the series outputs of P_1, P_2, and P_3, are fed to the sum amplifier. In the case of a prolate spheroid, θ_1 must be set proportional to the major axis; for an oblate spheroid, θ_1 must be set proportional to the minor axis. Obviously, only a small range of particle sizes can be covered in volume histograms as compared to diameter histograms.

ACKNOWLEDGMENTS

It is a pleasure to acknowledge the assistance given by Mr. George Cervana in laying out the design of the instrument and in operating it. Mr. F. S. Grover and Mr. Howard Hentzell did the constructional work and contributed valuable ideas to the design. We are indebted to Mr. G. E. White of the Sperry Gyroscope Company, Inc., for the gift of the small differential gear used in the recorder. Thanks are due the Firestone Tire & Rubber Company for permission to publish this paper, and to Dr. J. H. Dillon and Dr. F. W. Stavely for their interest in the problem.

Torsion of a Rubber Cylinder*

R. S. Rivlin
British Rubber Producers' Research Association, Welwyn Garden City, Herts., England, and National Bureau of Standards, Washington, D. C., U. S. A.

It has been predicted theoretically that, in general, a right-circular cylinder of incompressible, highly elastic material, which is isotropic in its undeformed state, cannot be held in a state of pure torsional deformation by means of a torsional couple alone. In addition, normal surface tractions must be exerted over the plane ends of the cylinder. These normal surface tractions depend on the amount of torsion and on position on the plane ends of the cylinder. Experiments are reported here in which this phenomenon is observed in a right-circular cylinder of pure gum compound. The dependence of the surface traction on amount of torsion and its distribution over the surface of the cylinder is studied by measuring the bulging of the rubber into small holes in a metal plate on one end of the cylinder.

I. INTRODUCTION

In a series of papers which is pending publication elsewhere,[1] the mechanical properties of highly elastic materials, such as rubber, which can be assumed incompressible and isotropic in their undeformed state, are discussed in terms of a stored-energy function W. This stored-energy function is specified in terms of the invariants of strain. It is shown that, once W is specified in this manner, the forces, which must be applied in order to support any given state of deformation, can be calculated. This calculation has been carried out for the pure torsional deformation of a right circular cylinder, for an assumed stored-energy function of simplest possible type and subsequently for any general form of stored-energy function.

The theory predicts that in order to produce a pure torsion in the cylinder, a torsional couple must be exerted on the plane ends of the cylinder, as in the classical theory of elasticity for small deformations. In addition, normal tractions must be exerted over these surfaces. The distribution of these normal tractions over the ends of the cylinder and their dependence on the amount of torsion have been calculated for any specified form of the stored-energy function.

In this paper experiments are reported in which this distribution and dependence on amount of torsion is measured for a cylinder of pure gum compound, on the assumption that the surface traction is measurable by the bulging of the rubber into small holes in a metal plate on one end of the cylinder. The results obtained are compared with those derived theoretically for two simple forms of the assumed stored-energy function. Agreement, within the accuracy of the experiments, is obtained if the stored-energy function has a form equivalent to that put forward for rubber by Mooney.[2] This form involves two physical constants for the material.

II. SPECIFICATION OF THE STORED-ENERGY FUNCTION

The stored-energy function for an ideal perfectly elastic material may be completely defined in the following manner. If a cube of the material, of unit edge, is subjected to a pure, homogeneous deformation in which it is deformed into a cuboid of dimensions λ_1 by λ_2 by λ_3, then the strain invariants I_1, I_2, and I_3 are defined as

$$I_1=\lambda_1^2+\lambda_2^2+\lambda_3^2,$$
$$I_2=\lambda_2^2\lambda_3^2+\lambda_3^2\lambda_1^2+\lambda_1^2\lambda_2^2$$

and

$$I_3=\lambda_1^2\lambda_2^2\lambda_3^2. \qquad (1)$$

If the material is isotropic in its undeformed state, the energy stored in the deformed cube is defined as the stored-energy function for the material. It must be a function of I_1, I_2, and I_3, provided it depends only on the state of deformation of the cube and not on the manner in which the deformation is reached. Once the form of this

* Presented at the meeting of the Division of High Polymer Physics, American Physical Society, January 30–February 1, 1947.

[1] R. S. Rivlin, Phil. Trans. Roy. Soc. **A** (pending publication).

[2] M. Mooney, J. App. Phys. **11**, 582 (1940).

function is specified, the mechanical properties of any body of this material are, in principle, completely determinate and are purely a matter for calculation, provided such phenomena as internal friction and creep are negligible.

For an incompressible material, the volume of the cube considered is unaltered in the deformation, so that

$$I_3=\lambda_1^2\lambda_2^2\lambda_3^2=1. \tag{2}$$

Then W, the stored-energy function, is given by

$$W=W(I_1, I_2). \tag{3}$$

In general, the form of the function $W(I_1, I_2)$ will be such that when the body is undeformed $W=0$.

III. THE TORSION OF A RIGHT-CIRCULAR CYLINDER

Let us consider a right-circular cylinder of radius a and length l of incompressible material, for which the stored-energy function W is given by (3). It has been shown that, in such a body, a pure torsion, in which each circular cross section of the cylinder is turned in its own plane through an angle $\phi(=\psi z)$ proportional to its distance z from one end, can be maintained by the application of surface tractions alone. The necessary system of surface tractions is indeterminate to the extent of an arbitrary hydrostatic pressure, but if the surface tractions applied to the curved surface of the cylinder are zero, then the surface tractions which must be applied to the plane ends have been calculated as

(*i*) tangential surface tractions Θ acting azimuthally in the deformed state of the cylinder (these effectively act as a torsional couple on the cylinder), and
(*ii*) normal surface tractions Z.

Θ and Z are measured per unit area of the surfaces on which they act and their distribution over the plane ends of the cylinder and dependence on ψ are given by

$$\Theta=2\psi r\left(\frac{\partial W}{\partial I_1}+\frac{\partial W}{\partial I_2}\right)$$

and

$$Z=-2\psi^2a^2\frac{\partial W}{\partial I_2}+2\psi^2\int_a^r r\left\{\left(\frac{\partial W}{\partial I_1}-2\frac{\partial W}{\partial I_2}\right)-2\left[\frac{\partial^2 W}{\partial I_1^2}+(3+\psi^2r^2)\frac{\partial^2 W}{\partial I_1\partial I_2}+(2+\psi^2r^2)\frac{\partial^2 W}{\partial I_2^2}\right]\right\}\cdot dr. \tag{4}$$

r is the distance of the point considered from the axis of the cylinder. $\partial W/\partial I_1$, $\partial W/\partial I_2$, $\partial^2 W/\partial I_1^2$, etc., are, in general, functions of I_1 and I_2 which can be calculated if the form of $W(I_1, I_2)$ is known. For the deformation considered,

$$I_1=I_2=3+\psi^2r^2. \tag{5}$$

We shall consider here two particular choices of the form of the stored-energy function W for which Eq. (4) are considerably simplified.

In the series of papers[1] mentioned above, particular attention was paid to the stored-energy function given by

$$W=C_1(I_1-3), \tag{6}$$

when C_1 is a physical constant characterizing the material. Materials for which Eq. (6) are valid were described as incompressible, neo-Hookean materials.

The particular interest residing in this choice of the stored-energy function rests on the facts that

(*i*) it is the simplest choice that can be made, from the point of view of the formulation of a theory of large elastic deformations;
(*ii*) it is the form derived by Treloar,[3] for an ideal rubber, on the basis of the kinetic theory of large elastic deformations.

Equation (6) is a particular form, obtained by making $C_2=0$, of the relation

$$W=C_1(I_1-3)+C_2(I_2-3), \tag{7}$$

which was first suggested by Mooney[2] as suitable for describing the elastic properties of rubber. It is noted that Eq. (7) involves two physical constants for the material, C_1 and C_2.

If the relation (7) is introduced into (4), we

[3] L. R. G. Treloar, Trans. Faraday Soc. **39**, 241 (1943).

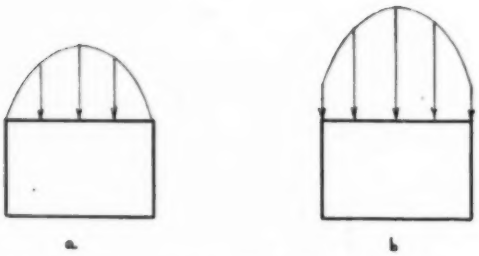

FIG. 1. Distribution of normal surface traction over plane ends of cylinder in pure torsion.
(a) When $W=C_1(I_1-3)$
and
(b) when $W=C_1(I_1-3)+C_2(I_2-3)$.

obtain

$$\theta=2\psi r(C_1+C_2)$$

and

$$Z=-2\psi^2a^2C_2-\psi^2(a^2-r^2)(C_1-2C_2). \qquad (8)$$

The equations for Θ and Z, when W takes the form (6) can, of course, be obtained by putting $C_2=0$ in (8).

We see that if the physical properties of the material are represented by either Eqs. (6) or (7), the force Z which must be exerted at each point is proportional to the square of the amount of torsion. If Eq. (6) applies, Z must everywhere have the nature of a thrust (since C_1 is essentially positive), which is distributed over the diameter of a plane end as shown in Fig. 1(a). If Eq. (7) applies, then Z does not vanish at the periphery (where $r=a$) and provided C_2 is positive and sufficiently small compared with C_1, its distribution will have the form shown in Fig. 1(b).

IV. EXPERIMENTAL PROCEDURE

The experiments which will be described in this paper have as their object the study of the distribution of the normal force Z defined in the previous section and its dependence on the amount of torsion.

In a preliminary qualitative experiment a rubber cylinder of pure gum compound, with brass plates bonded onto its plane ends, was subjected to a torsional couple by means of a lever attached to one of the ends while the other end was held in a vise. It was found that unless a longitudinal thrust was intentionally exerted parallel to the axis of the cylinder, the cylinder elongated, its axial cross section before and after torsion being shown roughly in Fig. 2. This simple experiment bears out the mathematical conclusion that a pure torsional couple does not give rise to a pure torsion. Clearly, if a pure torsion is to be obtained, normal compressive forces, whose resultant must have the nature of a thrust, must be exerted over the plane ends of the cylinder. This is in general agreement with the theoretical predictions outlined in the previous section.

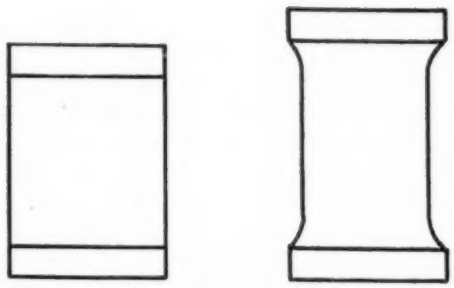

FIG. 2. Axial cross section of cylinder before and after twisting by a couple.

Consequently, an apparatus was designed in which the pure gum cylinder, to whose plane ends brass disks are bonded, is restrained from elongating. So, when one disk is rotated with respect to the other by the application of a torsional couple, the longitudinal thrusts required for the production of a pure torsion in the rubber cylinder are automatically called into play. The upper brass disk A contains five circular holes, each $\frac{1}{2}$-inch in diameter, varying in distance from the center and spaced as shown in Fig. 3, in order to have as little mutual interaction as possible. The lower disk B has rigidly attached to it a steel disk C.

The assembly of rubber cylinder and disks A, B, and C is held in a robust steel frame D, as shown in Fig. 4. The upper disk is rigidly attached to the frame and the lower disk is capable of being rotated in its own plane about its axis, by means of a crowbar which is introduced into one of a series of holes in the steel disk C. Provision is made for holding the cylinder in a state of torsion by means of steel pegs, which can be introduced into one of the holes E in the frame. A scale is also provided for measuring the angle through which the lower disk is rotated.

When this disk is rotated, the rubber bulges slightly in the holes in disk A and the amount of

this bulging is assumed to be proportional to the thrust which would have to be exerted to prevent the bulging.

The bulging represents a small deformation superposed on a relatively large torsional deformation. At each of the holes this torsional deformation approximates to a state of simple shear of an amount depending on the amount of the torsion and the position of the hole considered. The assumption that the amount of bulging is proportional to the normal force tending to produce it is equivalent to an assumption that the former does not depend greatly on the state of simple shear on which the bulging deformation is superposed. There are certain theoretical reasons for assuming that this is approximately valid in the experiments described here.

In order to produce a simple extension in a cylinder superposed on the simple torsion, an additional normal surface traction must be exerted over each of the plane ends. If the stored-energy function for the material of the cylinder has the form (6), it has been shown[1] that this additional normal surface traction is independent of the amount of torsion and of position on the surface of the cylinder. The stress distribution in the neighborhood of the hole is complex, but for small deformations, it is reasonable to assume that the amount of bulge in each hole is dependent only on the force tending to produce the bulging and not on the amount of torsion or position of the hole, except insofar as this force is determined by them. This conclusion should be approximately valid if the stored-energy function has the form (7), provided C_2 is small compared with C_1. However, there is no reason to believe that it should be true for every possible form of the stored-energy function.

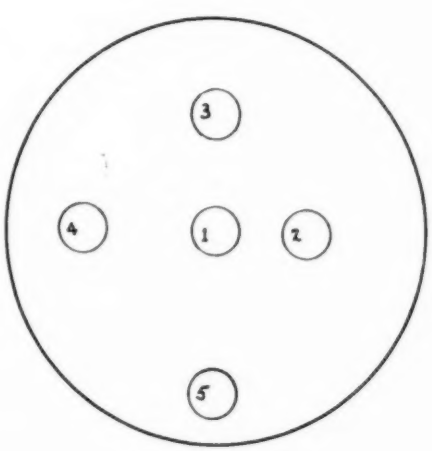

FIG. 3. Upper brass disk vulcanized to rubber cylinder.

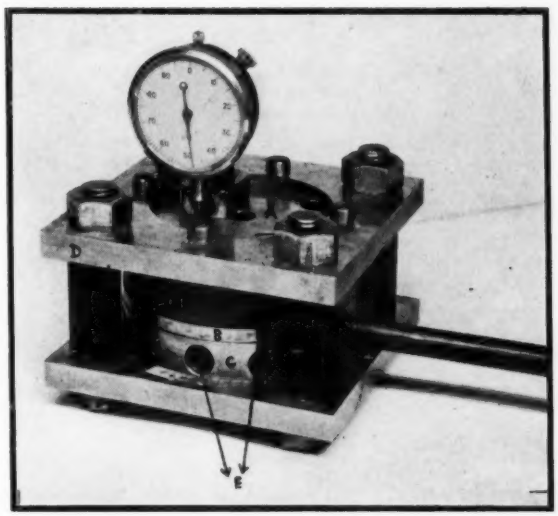

FIG. 4. The torsion apparatus.

The amount d of the bulging in each of the holes is measured at the center of the hole, for various angles of rotation θ of the disk B, by means of a dial gauge. The top of the disk B is ground flat and used as a reference plane in carrying out this measurement.

V. EXPERIMENTAL RESULTS

If Eq. (8) is valid for Z, then the relation between d and θ should be

$$d=K\theta^2[2a^2C_2+(a^2-r^2)(C_1-2C_2)], \qquad (9)$$

where K is some constant of proportionality. r is now taken as the distance of the center of the hole from the center of the disk. This assumption is justified if the radius of each hole is small compared with that of the cylinder, but it is impracticable to make it too small as the values of d are thereby reduced. The repeatability with which d could be measured in the experiment was estimated as ± 0.002 in. using the same dial gauge. The accuracy with which θ could be measured in the arrangement employed was $\pm\frac{1}{2}°$.

The gum compound used had the following

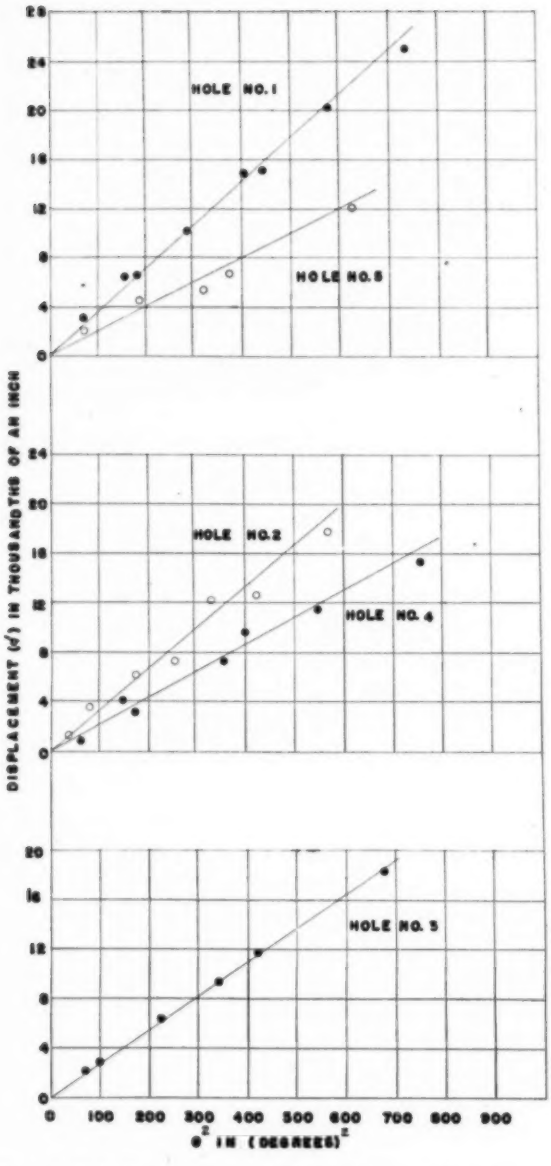

FIG. 5. Relation between displacement and the square of the angle of torsion.

composition in parts by weight:

Rubber	100
Sulphur	3.0
Captax	0.8
Stearic acid	1.0
Agerite	1.0
Zinc oxide	5.0
Tuads	0.08

The mix was vulcanized for 30 min. at 134°C.

In order to produce a strong bond between the brass plates, a "tie gum" layer, less than $\frac{1}{32}$" thick, was introduced between the main rubber cylinder and each of the brass plates, and a cement marketed as "Reanite, No. 3615" was employed. The composition of the "tie gum" layer was, in parts by weight,

Rubber	100
Stearic acid	1.0
Sulphur	3.5
Captax	1.0
Zinc oxide	5.0
Thermatomic black	40

The rubber cylinder employed had a radius of 2.12 in. and length of 1 in. The holes in disk B each had a diameter of $\frac{1}{2}$ in. and the distances of their centers from the center of the disk are given in the following table:

Hole number	1	2	3	4	5
r in inches	0	.85	1.18	1.47	1.69

Equation (9) suggests that the results of the experiments be plotted as a relation between d and θ^2 on linear graph paper. This should yield a straight line passing through the origin for each hole.

This is done in Figs. 5 for each of the five holes, and it is seen that the linear relation between d and θ^2 of Eq. (9) is borne out within the accuracy of the experiment.

The slope m of the straight line obtained for each hole is the value of $K[2a^2C_2+(a^2-r^2)\times(C_1-2C_2)]$ for that hole, and if this is plotted against (a^2-r^2) a straight line should be obtained, which passes through the origin if $C_2=0$ and otherwise gives an intercept of $2a^2C_2K$ on the m-axis. If m is plotted against (a^2-r^2) as in Fig. 6, it is seen that within the accuracy of the experiment the relation (9) between d/θ^2 and (a^2-r^2) is again borne out.

If m_0 is the intercept of the straight line in Fig. 6 on the m-axis and b is its slope, we have $m_0=2a^2C_2K$ and $b=K(C_1-2C_2)$. Whence

$$\frac{C_1}{C_2}=\frac{2b}{m_0}a^2+2. \tag{11}$$

From measurements on Fig. 6, we obtain

$$m_0=10\times10^{-6}\text{ in. deg.}^{-2},$$

and

$$b=5.65\times10^{-6}\text{ in.}^{-1}\text{ deg.}^{-2}$$

so that

$$\frac{C_1}{C_2}=7.1.$$

Mooney[2] uses the constants C_1 and C_2 to define three additional constants as follows:

$$G=2(C_1+C_2)$$
$$H=2(C_1-C_2)$$

and

$$\alpha=H/G.$$

He then shows that the constant G is the modulus of rigidity of the material. The constant α is named the coefficient of asymmetry. From the definitions it follows that

$$\alpha=\frac{C_1/C_2-1}{C_1/C_2+1}.$$

Consequently, the experimental results presented here lead to a value of 0.75 for the coefficient of asymmetry of the pure-gum compound studied. This is somewhat larger than the values found for two compounds studied by Mooney. Further work would be required to establish the variation of α with the nature of the compound.

VI. CONCLUSIONS

The experiments bear out the general conclusion of the theory that in order to produce pure torsion in a rubber cylinder, normal surface tractions must be exerted on the plane ends and that these surface tractions vary with the amount of torsion and the position on the plane end of the cylinder. If the assumption is made that the amount of bulging in each hole is proportional to the force producing it and does not depend on the state of local strain on which the bulging is superposed, then the results of the experiments are in accordance with the assumption of an expression of the form (7) for the stored-energy function of the rubber. It has already been pointed out by Mooney that a stored-energy function of this form describes the linear shearing stress *vs.* amount of shear relation for rubber in simple shear, with a fair measure of accuracy,

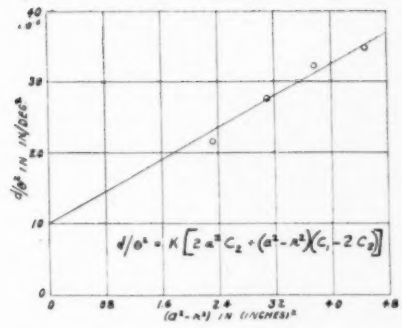

FIG. 6. Relation between slopes of lines in Fig. 5 and positions of holes.

up to reasonably large deformations. Also, Treloar[4] has recently obtained results in agreement with this for pure, homogeneous strain of a sheet of rubber.

The form (6) for the stored-energy function is that derived from the kinetic theory of rubber-like elasticity. Load *vs.* deformation relations derived from this have been compared with experimental results for simple types of deformation and have yielded fairly good agreement, depending on the type of deformation employed.

It appears then that the form (6) for the stored-energy function provides a first approximation to the stored-energy function for vulcanized rubber and that a second approximation is provided by the form (7). The differences between these forms are more or less accentuated depending on the type of deformation studied.

VII. ACKNOWLEDGMENTS

This work forms part of a program of fundamental research on rubber undertaken by the Board of the British Rubber Producers' Research Association. The work was carried out at the National Bureau of Standards, Washington, D. C., where the author is at present a guest worker. The author is indebted to W. L. Holt of the National Bureau of Standards for advice and assistance in connection with the mechanical design of the apparatus.

[4] L. R. G. Treloar, Trans. Faraday Soc. (pending publication).

Elastic Losses in Some High Polymers as a Function of Frequency and Temperature*

H. S. Sack, J. Motz,** H. L. Raub, and R. N. Work
Cornell University, Ithaca, New York

The frequency and temperature dependence of the elastic losses of polyvinyl chlorides (0° to 80°C, 60 to 1400 c.p.s.) and of natural rubber and butadiene-styrene copolymers (GRS) of different relative concentration (−50° to 35°C, 20 to 3500 c.p.s.) was studied by 3 methods, in which the motion of a reed in free or forced vibration is observed. Natural rubber at temperatures above 20°C, and polyvinyl chloride exhibit frequency independent losses, the mechanism of which is not yet clear. The results for rubber below 20° and for GRS can be explained by a relaxation theory. The behavior of the elastic losses also reflects the existence of a second-order transition, below which rotation of chain segments is hampered.

1. INTRODUCTION

AMONG the theories of elastic losses in solids, the so-called relaxation theory has lately received considerable attention.[1] According to this theory the reaction of a body to an applied strain is not instantaneous but requires a finite time which is determined by the molecular constitution of the material.[2] The time which is characteristic of the speed with which molecules will move towards their new equilibrium position when a stress is set up is called the relaxation time. This theory is the analogue to Debye's[3] theory of anomalous dispersion of dielectrics, and has been discussed for simple and more complicated models in many publications. It will suffice, here, to recall that according to this theory the elastic losses—defined as energy loss per cycle (often called Q^{-1})—should rise linearly with frequency ω for low frequencies, and decrease as $1/\omega$ for high frequencies. The shape of the maximum in the intermediate region depends on the number of relaxation processes and, therefore, on the relaxation times that are present. This analogy between dielectric and elastic properties has been emphasized particularly in a recent publication of Kirkwood,[4] in which he applied to elastic phenomena a treatment which he formerly had applied to dielectric behavior where he calculated the distribution of relaxation times on the basis of a diffusion process of the single groups of the long chain molecules in high polymer substances.[5]

So far, little experimental evidence for the existence of this relaxation phenomena has been found, at least in experiments in which the elastic losses under alternating stresses are measured.[6] The aim of the work here presented was to find cases in which the relaxation theory would apply. High polymer molecules seem particularly suited for such a study because these molecules show a high degree of mobility, and their motion seems to be sufficiently slow so that it can be hoped that a relaxation time may be found in a low frequency region. It is also known from dielectric measurements that such relaxation phenomena do exist in these substances.

As a starting-point the series of polyvinyl chlorides were chosen because Fuoss[7] observed dielectric relaxation in a region around 1000 c.p.s. However as will be discussed later, no elastic

---

* Presented at the meeting of the Division of High Polymer Physics, American Physical Society, January 30–February 1, 1947. Early results of this investigation were presented at the APS meeting in November, 1943. It was not possible to publish these results earlier except for a short summary (H. S. Sack, J. Motz, and R. N. Work, J. App. Phys. **15**, 396 (1944).) As they are in direct connection with the paper presented at the January 1947 meeting, and in order to avoid duplication in publication, the former work, in its essential lines, is included in the present contribution. Part of the later work was sponsored by the Office of Naval Research.

More details can be found in Cornell theses of J. Motz, R. N. Work and H. L. Raub.

** Now at the Armour Research Foundation, Chicago, Illinois.

[1] R. Simha, J. App. Phys. **13**, 147 (1942); T. Alfrey and P. Doty, J. App. Phys. **16**, 700 (1945); W. Kuhn, Zeits. f. physik. Chemie **B42**, 1 (1939).

[2] The relaxation theory can also be applied in cases where the relaxation is not due to a molecular rearrangement, but rather to heat flow. In this case the relaxation time is a function of the boundary conditions and therefore of the external shape of the body or of the grain structure of the substance. In this article we will refer only to relaxation phenomena which are governed by the motion of the molecules. C. Zener, Metals Tech. [5], **13** (1946). K. Bennewitz and H. Rötger, Physik. Zeits. **37**, 578 (1936); **40**, 416 (1939).

[3] See e.g. P. Debye and H. Sack; Handb. Rad. (1934); Vol.VI, part 1, p. 141.

[4] J. G. Kirkwood, J. Chem. Phys. **14**, 180 (1946).

[5] R. M. Fuoss and J. G. Kirkwood, J. Am. Chem. Soc. **63**, 385 (1941).

[6] The relaxation theory has been tested for nonperiodic motions, as for instance in the case of creep, etc.

[7] R. M. Fuoss, J. Am. Ch. Soc. **63**, 369 (1941).

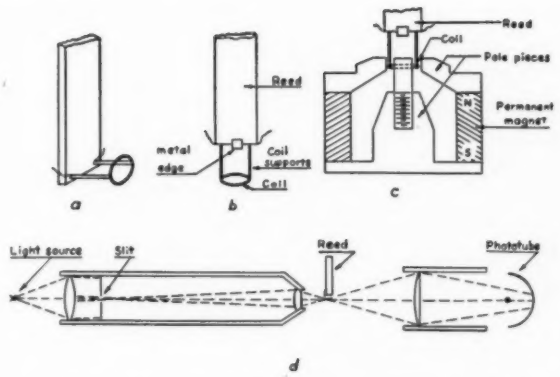

FIG. 1. Diagram of experimental arrangement. (a) and (b) coil attachment; (c) arrangement of magnet; (d) optical system.

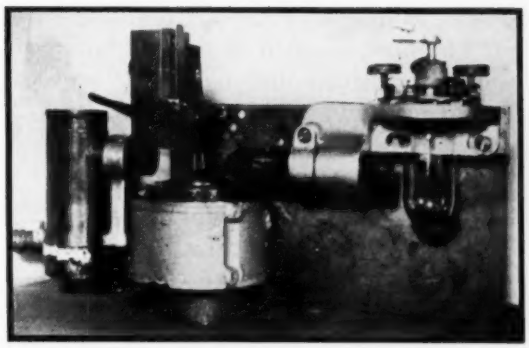

FIG. 2. Photograph of vibrator-unit.

relaxation was observed. More success was obtained with elastomers, in particular with synthetic rubber. The experimental procedure and results will be discussed in the following.

2. EXPERIMENTAL PROCEDURE

Three different methods for the determination of the elastic losses were used: (a) The observation of the half-widths of the resonance curve of a reed in forced vibration, (b) the measurement of the damping properties of a free vibrating body, and (c) the measurement of the (elastic) hysteresis loop.

The first and second methods are only applicable if the damping is relatively low. The last method is, in principal, free from this restriction, but the interpretation of the measurements is easier for high damping. The last method has the advantage, that it permits the measurement of the elastic losses over a wide range of frequencies, without need for changing the sample, while for methods (a) and (b) samples of different lengths have to be studied, in order to measure the elastic losses at different frequencies.

In all three cases, the sample, in the form of a reed approximately 2 mm thick and 4–15 mm wide, and of appropriate length, was clamped on one end, while an alternating force could be applied to the other end. In the first experiments this force was applied by an electrostatic method: One side of the reed was covered with a very thin metal foil and opposite the reed, separated by a few mm, was placed an electrode so that an alternating potential could be applied between the reed and this electrode. This gives rise to an alternating force of twice the frequency of the applied potential. (If a d.c. potential is superimposed, it is possible to create an alternating force of the same frequency.) In later measurements a small coil was attached to the end of the reed, and the reed was so mounted that this coil is in the air-gap of a strong speaker magnet. An alternating current set up in the coil then creates an alternating force on the reed.

The motion (vibration) of the end of the reed is observed by an optical method. The end of the reed protrudes into a light beam. If the reed vibrates, this light beam is thus modulated, and in falling on a photo-cell creates an a.c. signal proportional to the amplitude of vibration. This signal is then amplified. Figure 1 shows diagrammatically the optical arrangements and the attachment of the coil to the reed, in (a) for a lateral vibration, and in (b) for a longitudinal vibration. In the later experiments the whole device was made as small and compact as possible in order to avoid outside disturbances. Figure 2 reproduces a photo of the complete assembly mounted on a solid base plate. This picture represents the case of longitudinal vibration. For flexual vibrations a different clamping block is used. The screws on top of the light-bulb holder serve to adjust the light beam so that maximum modulation and, therefore, maximum sensitivity are obtained. For the study of variations with temperature the complete system was put in an automatically controlled constant-temperature box. (This arrangement is, of course, only workable for temperatures not higher than approximately 70°C.)

With the compact optical system as shown in Fig. 2, it was necessary to define the end of the

reed more sharply by attaching to it a thin metal edge. The photo-current is first amplified by a preamplifier driven by batteries, and then by a conventional audiofrequency amplifier. The driving potential or current was delivered by an audio oscillator, and kept constant over the whole frequency range. The frequency could be recorded within 1 percent.

In case (a) (resonance curve), the output of the photo-amplifier was read on an a.c. meter giving a direct measure of the amplitude of vibration, which, when plotted as a function of frequency, gives a resonance curve whose half-width is easily determined. This method is precise for low or moderately high damping. For higher damping, the resonance peak becomes very wide and may be distorted by higher harmonics or parasitic reasonances in the system.

In case (b) (free vibration), the reed is deflected from its rest position by a d.c. potential or current. By opening a switch, the current or potential is interrupted and the reed returns to its equilibrium position executing a damped vibration. The output of the photo-amplifier is applied to the deflecting plates of an oscilloscope. At the time, the switch is opened, starting the vibration of the reed, a linear sweep of adjustable speed is applied to the other set of the plates of the oscilloscope. Thus, on the screen appears the picture of the damped vibration, from which the logarithmic decrement can be calculated by measuring successive amplitudes. Figure 3 reproduces two sets of pictures obtained with two materials of different constitution. The four pictures in each set represent different frequencies of vibration as indicated by the time-scale. The set at the left represents a material in which the damping increases very strongly with increasing frequency, whereas in the set at the right the damping is nearly independent of frequency. Again, this method is only usable for low damping.

In case (c) (hysteresis loop), the procedure is somewhat more complicated. The output of the photo-amplifier is again applied to one set of plates of the oscilloscope. To the other pair of plates a potential is applied which is taken across a resistor in series with the driving coil. Since the driving force is proportional to the current in the coil, this signal is proportional to the force. Thus

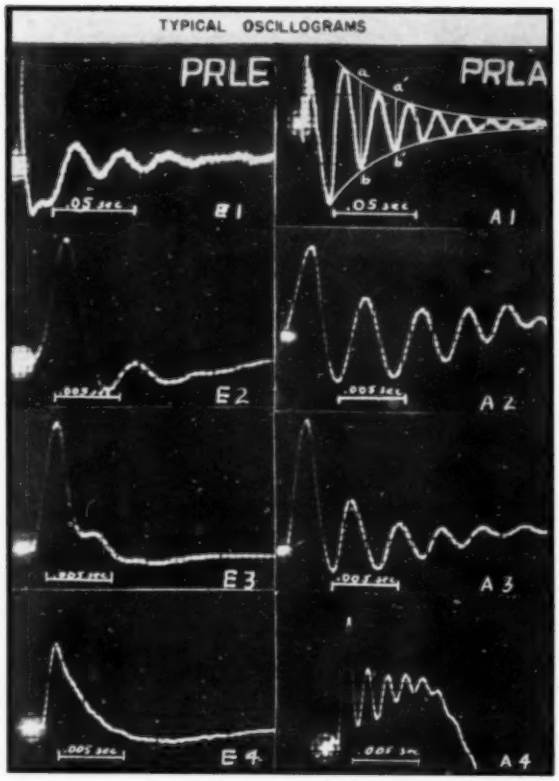

FIG. 3. Examples of damped free vibrations: butadiene-styrene, left 50/50, right 70/30.

there will appear on the screen the elastic hysteresis loop of the material (stress-strain diagram). The area of this hysteresis loop is a measure of the damping qualities of the material. In fact, if divided by the square of the amplitude, it is proportional to the energy dissipated per cycle divided by the total energy of vibration. In this method, the two signals must appear on the oscilloscope screen without phase differences caused by the electric system. As phase differences in amplifiers are unavoidable, a phase shifter is added to the system. This phase shifter is calibrated for each frequency by replacing the sample by a metal reed. It is known that for a metal like brass the phase shift between the vibration and the applied force is near 0 or 180°, except for a narrow region around resonance. If with this metal reed the stress-strain curve appearing on the oscilloscope screen is not a straight line, then there exists a phase shift in the electrical system, and it can be compensated for by an adjustment of the phase shifter. The accuracy

of this phase adjustment proved to be one of the main difficulties of this method, especially for measurements at frequencies far away from resonance.

In order to have a relative measure of the amplitude, another signal derived from a resistance in series with the coil is passed through the photo-amplifier system. As the current in the coil is kept constant, a variation of this signal as it appears on the oscilloscope screen is a measure of the change in amplification of the photo-amplifier.

The pattern on the oscilloscope screen is photographed, and the area of the hysteresis loop measured with a planimeter. This area is then divided by the square of the maximum amplitude as determined with the help of the calibration line mentioned above.

3. INTERPRETATION OF MEASURED QUANTITIES

The quantities determined by the three sets of experiments are: the half-width of the resonance curve $\Delta\omega/\omega_r$ (where $\Delta\omega$ is the difference in frequency for two points where the amplitude of vibration is $\frac{1}{2}$ the amplitude at resonance frequency ω_r); the logarithmic decrement δ; and the energy W dissipated during one cycle, divided by the square of the amplitude y, i.e., W/y^2. In order to discuss the elastic properties in terms of molecular properties, it is necessary, first, to relate the measured quantities to material constants. In the case of forced vibrations this can be done by introducing a complex modulus of elasticity, e.g., a complex Young's modulus for longitudinal vibrations, $E'+iE''$, which might be frequency dependent. For small damping ($E''/E' \ll 1$) the same complex modulus can be used in treating the case of free vibrations. In the case of $(E''/E') \ll 1$, the following relations exist $\Delta\omega/\omega_r = \sqrt{3}(E''/E')$; $\delta = \pi(E''/E')$, where E'' and E' have the values at the resonance, or free vibration frequency, respectively. W/y^2 is proportional to E'', with a proportionality constant which depends, in contrast to the two other formulas, on the dimensions of the reed, the boundary conditions etc. (For a free-clamped, thin reed of length l this constant is $\pi^2/8l$.) This proportionality is only valid for frequencies below a certain frequency, which is low for low damping and high, for high damping. For frequencies beyond this limit, deviations from proportionality occur that have to be calculated for each particular case. The same complication arises for the other two methods if the damping is no longer small. In all these cases of non-proportionality it is necessary, in order to calculate the higher approximations to know the exact mechanism which gives rise to the losses, and which determines the frequency dependence of the elastic modulus. These calculations were made under the assumptions of a thin reed, clamped at one end, and acted upon by the external force on the other end, whose motion was observed. The damping mechanism was assumed to be of the viscous type, and the frictional force was written as $K(\partial\epsilon/\partial t)$, where ϵ is the deformation. In this case $E''=K\omega$. Further calculations were made with putting $E''=$const., without specifying the mechanism that would yield this type of loss, since such a mechanism is not yet known. The experimental results were then corrected with the help of the formulas thus derived. Since the assumptions are only approximations to the real case, no data were used where the corrections exceeded 30 percent.

In the hysteresis loop method, the evaluation of W/y^2 in absolute units is rather cumbersome. Therefore the width of the resonance curve was measured simultaneously, at least at one temperature. This value was used to calculate the proportionality constants. The results were expressed directly in terms of $\Delta\omega/\omega_r$, and are plotted in these terms in the figures. ($E''(\omega)$ is then the value taken from the graph multiplied by E' at the resonance frequency and at the temperature where resonance is observed, and divided by $\sqrt{3}$.)

4. EXPERIMENTAL RESULTS AND DISCUSSION

(a) Generalities

In all the experiments the amplitude of vibration was so small that the maximum strain was not bigger than 0.1 percent. Under these conditions it proved that all the effects are linear. With the exciting force varying by a factor 5 to 10 in amplitude, no change in the losses was observed. Also the vibration remained sinusoidal (no appearance of harmonics). Furthermore the hysteresis loop has the form of an ellipse within a very good approximation (deviations from the ellipse

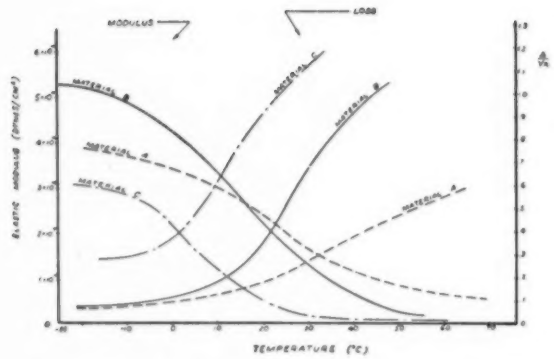

FIG. 4. Young's modulus and elastic losses of polyvinylchloride with 20 percent (*A*), 30 percent (*B*) and 40 percent (*C*) plasticizer.

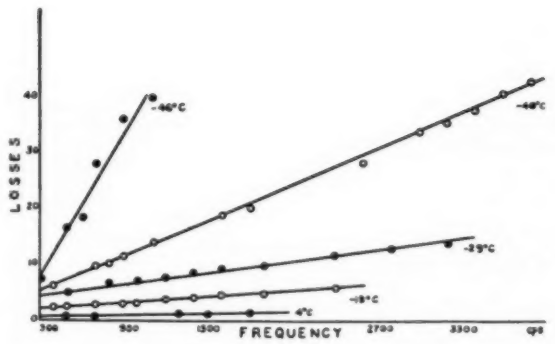

FIG. 5. Losses of natural rubber.

correspond to an harmonic content of not more than 1 or 2 percent).

The influence of the "tightness" of clamping appears to be negligible for the loss measurement.

The metal foil glued to the reed in the electrostatic method, and the coil and coil supports used in the electrodynamic method, were replaced by similar attachments of different weight or geometric form, and proved to have no influence upon the measured elastic losses.

In most cases measurements were repeated, if possible with reeds of different width or length. Good reproducibility was observed. The error for the losses is approximately ± 10 percent.

As will be seen later, very high losses, of an equivalent of approximately 100 for $\Delta\omega/\omega$, were observed under certain conditions. Such high values have to be interpreted with caution, as they mean that all the energy supplied by the outside force is dissipated in a very small region near the point where the force acts, and it is not excluded that the way in which the coil is connected to the reed has an effect; also the formula used for the calculation will probably receive additional correction terms, which cannot be evaluated exactly.

(b) Polyvinyl Chlorides

Three samples were measured.[8] Material *A* contained 80 percent polyvinyl chloride and 20 percent tricresyl phosphate, *B*, 70 and 30 percent, and *C*, 60 and 40 percent. All measurements were made by the first method (resonance curve). In Fig. 4 the results for Young's modulus and the half-widths of the resonance curve are indicated as a function of temperature. Young's modulus was calculated from the measured resonance frequency assuming a free-clamped, thin reed (or a clamp-clamped reed) in flexural vibration. By choosing different lengths of the reed, and by vibrating it as free-clamped or clamp-clamped, a series of resonance frequencies are obtained in the range of approximately 100 to 1400 c.p.s. The values obtained at these different frequencies agree within the experimental error with the curves drawn in Fig. 4. We can, therefore, conclude that in this frequency range, no dispersion occurs. This means that in our experiments we do not find a relaxation phenomena as it would have been suggested by the dielectric measurements made by Fuoss on the same substances in the same frequency and temperature range. This does of course not necessarily mean that such relaxation phenomena are absent, but if they are present, they are masked by other processes which are of greater importance and yield frequency independent losses.

From Fig. 4 it can be seen that Young's modulus decreases with increasing temperature, while the losses increase. This can be explained by the "loosening" of the structure, and the increased tendency to flow. It should also be mentioned that static measurements of Young's modulus, at room temperature and with small stresses, were made, which yielded from 4 to 10 times higher values than those obtained by the vibration method. This seems to indicate that a dispersion zone must be present below the frequency range here studied.

[8] We are obliged to Dr. Fuoss, at that time at General Electric, for providing us with these samples.

(c) Natural Rubber

The sample studied was natural gum stock with 3 percent sulphur. For temperatures between 5 and 55°C measurements were made with all 3 methods, yielding identical resuts; for lower temperature, down to −46°C, only the hysteresis-loop method proved workable. The frequency range was 20 to 900 c.p.s. for the first two methods, and 300 to between 1500 and 3500 (depending on the temperature) for the third method. Figure 5 reproduces the results for temperatures below 4°C, and shows that the losses rise linearly with frequency (but the line does not go through the zero). Measurements at temperatures above 10°C are not included in the diagrams. They yield for 20 to 1300 c.p.s., a constant value of 0.2 for 22°C, and slightly lower for higher temperature. (A slight rise of approximately 10 percent would also be compatible with the measurements.)

Where a comparison can be made, our results are in good agreement with those of Stambaugh,[9] and other earlier investigators. The frequency independent losses at higher temperatures can be represented, in a formal way, by a constant E''. However, as mentioned, no simple mechanism is known that would yield this result. Some speculations concerning this mechanism were given earlier,[10] but no new evidence in favor of or against it has been obtained. The losses at lower temperatures can be represented by the superposition of a frequency independent part and a viscous term, $E''=K\omega$, where K could be called a coefficient of viscosity. The same frequency dependence would result from a relaxation phenomenon with measurements made below the relaxation time (or zone of relaxation times). In fact, for low frequency, the relaxation theory gives a molecular picture of viscous flow. Figure 6 shows how this coefficient of viscosity increases with decreasing temperature.

Resonance frequencies could be observed above −18°C. These values indicate that Young's modulus is rising slightly with decreasing temperature (20 percent increase from 22°C to −18°C).

(d) Butadiene-Styrene Polymers

The samples[11] were unloaded and contained 1 percent sulphur, 0.5 percent BLE and 0.3 percent tetramethylthiuramonosulfide. The content of butadiene to styrene was 70/30; 65/35; 60/40; 55/45; 50/50. For the first 4 samples, at 22°C, all 3 methods were used, and gave identical results. The last sample at all temperatures, and the others below 22° were only investigated by the hysteresis-loop method. As an example Fig. 7 reproduces a set of curves observed for the 60/40 sample. For higher temperatures than those given in the figure, the losses are lower, and the bending is less pronounced. In Fig. 6 the slope of the linear part (low frequencies) is given as a function of temperature for this sample, and for 70/30 and 50/50. It appears that the temperature variation of this slope has the same shape, but is shifted to higher temperatures wih higher styrene content.

The characteristic feature in Fig. 7 as compared to the figure for natural rubber (Fig. 5) is the

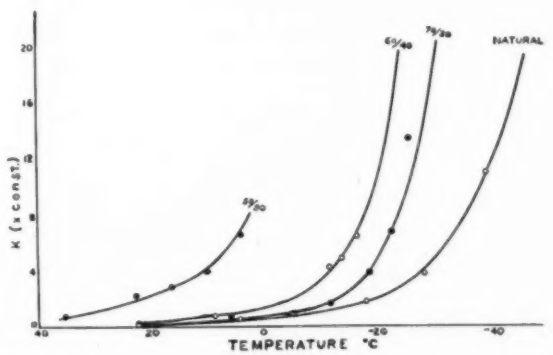

FIG. 6. Temperature dependence of "viscosity coefficient" (slope of loss-frequency curve).

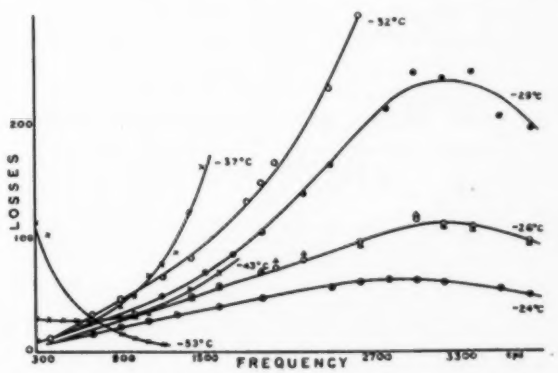

FIG. 7. Losses for 60/40 butadiene-styrene copolymer.

[9] R. B. Stambaugh, Ind. Eng. Chem. **34**, 1358 (1942).
[10] H. S. Sack, J. Motz, and R. N. Work, J. App. Phys. **15**, 396 (1944).
[11] These samples were kindly given to us by the U. S. Rubber Company.

appearance of a peak in the curve. Again, the other samples show a similar behavior, except that the temperature at which the bending of the curve occurs, in the frequency range here studied, is higher for higher styrene content. For the 70/30 sample it does not yet occur above −26°C, while for 50/50 the bending is already pronounced at 16°C. This appearance of a peak can be interpreted as the result of a relaxation phenomenon, though the curves do not correspond exactly to those calculated with a single relaxation time.

Finally it is of interest to note that while at a constant frequency the losses increase first slowly and then more and more rapidly with decreasing temperature, this trend is reversed at very low temperatures (approx. −40°C for 60/40), and the losses decrease again. This fact stands out particularly well in looking at the change of the resonance curve. In lowering the temperature the resonance becomes wider, then is no longer observable, reappears again and becomes narrow. This characteristic temperature is higher for higher styrene content; for 70/30 it could not be observed above −50°C, the lower limit of our temperature range. This characteristic temperature is approximately the second-order transformation temperature of these substances.[12] As it is assumed that below the transformation point the segments of the chain-molecules "freeze in," and are no longer able to orient as freely as above this temperature, we may conclude that the relaxation phenomena observed are linked to this segment mobility. In agreement with this is the observation that the loss-frequency curve below this temperature has a different character from that above, and does not show the characteristic peak, at least not in our frequency range.

[12] R. F. Boyer and R. S. Spencer, *Advances in Colloid Sciences* (Interscience Publishers, New York, 1946), Vol. II, p. 1.

Electrical Conductivity of GR-S and Natural Rubber Stocks Loaded with Shawinigan and R-40 Blacks*, **

P. E. Wack, R. L. Anthony, and E. Guth
University of Notre Dame, Notre Dame, Indiana

Measurements have been made of the direct current conductivity of rubbers loaded with carbon black. Shawinigan and Continental R-40 blacks compounded in natural rubber and GR-S were studied, and the resistivities were determined as functions of time, temperature, concentration and elongation. Resistance decreased with time, at first very rapidly, then more slowly, approaching an equilibrium value. This behavior seems to be independent of the type of black used. Temperature coefficients of resistance (at 50°C) were positive for Shawinigan stocks, negative for samples containing R-40, and tended to increase with increasing concentration of black and with increasing extension of the sample. At low concentrations, R-40 gave higher conductance in GR-S than did Shawinigan. At high loadings, Shawinigan gave the higher conductance in both GR-S and natural rubber. Resistance increased with elongation for all stocks containing R-40. The Shawinigan GR-S samples showed an inversion; for small elongations the resistance increased on stretching, but for higher extensions the resistance decreased. The results are interpreted on the assumption that the carbon black tends to form chains in the rubber matrix.

I. INTRODUCTION

CARBON black has been used as a reinforcing agent in rubber-like materials for many years. In recent years special grades of carbon black have been developed which serve the purpose of not only reinforcing these materials but also of imparting to them some electrical conductivity. However, our knowledge of the exact mechanisms or processes, which are responsible for this reinforcing action and greatly increased electrical conductivity, is still far from complete. Both effects are closely related, and increased knowledge of one will aid our understanding of the other.

The reinforcing action of fillers has been dis-

* This work was carried out under contract to the Office of Naval Research as a part of Contract N6-ori-83, Task Order 1.

** Presented at the American Physical Society Meeting, Division of High Polymer Physics, held at Columbia University on Jan. 30–31 and Feb. 1, 1947.

cussed in a series of theoretical papers by Rehner,[1] Smallwood,[2] and Guth.[3] A general discussion of the effects of various types of carbon black in GR-S has recently been given by Parkinson.[4] The apparent tendency of the carbon black particles to form chains in the rubber, and possibly even a network structure at high carbon black concentrations has been pointed out by the aforementioned authors and others. Parkinson, in particular, has noted that, in some instances, there is strong evidence that the forces between carbon particles are greater than the forces between the carbon particles and the rubber. The possibility that in some cases the chain of carbon black particles may serve as the major reinforcing agent rather than the individual carbon black particles, was suggested by Guth.[3]

Past studies of the electrical conductivity produced in rubbers by carbon blacks have been confined chiefly to investigations of the effects resulting from varying the type of black, the particle size of the black, and the concentration of the black in the rubber. Cohan and Mackey[5] and Cohan and Steinberg[6] have shown that the specific resistance of a rubber compound at 20% volume concentration decreases with increasing purity of the black, decreases with increasing graphitic structure, and decreases exponentially with decreasing particle size. The progressive decrease in resistance with decreasing particle size had also been noted by Amon and Brown[7] in a study of the electrical resistance of carbon black inks. Hall, Buckley, and Griffith[8] have studied the dependence of the electrical resistance upon the concentration and structure of the black, using Shawinigan black in natural rubber and in GR-S. Bulgin,[9] in one of the most comprehensive papers published to date on this subject, discussed the dependence of the electrical conductivity in conducting rubbers upon the concentration of the black in rubber, its dependence upon the temperature, and its dependence upon the extension. Bulgin[9] employed a large variety of blacks and studied the behavior of these blacks in GR-S, GR-I, and in natural rubber.

In the work reported here, the conductivity has been studied much more completely than in any previous work as a function of time, temperature, extension, and concentration of the black in the rubber. The behavior of two types of conducting blacks, Shawinigan and Continental R-40, in both GR-S and in natural rubber, has been studied. The conductivity of the blacks themselves was also investigated as a function of temperature, under a pressure of approximately 2000 lb. per square inch.

This more complete study was carried out in the expectation that the results might indicate the state of aggregation of the black particles in the rubber and thus lead to conclusions about the relative strength of the carbon black-carbon black and the carbon black-rubber interaction. Since rubber is an insulator, appreciable conduction in a rubber stock loaded with conducting carbon black spheres can take place only if these spheres form a chain. Such chains in turn may form a lattice or network. Our results can be understood on the basis of a simple picture of the formation and breaking up of chains of carbon black particles. Carbon black particles are colloidal in size. To a first approximation, we may neglect the forces between them. Then we can consider the chain formation as a purely

TABLE I.

GR-S stocks	Parts by weight	Natural rubber stocks	Parts by weight
GR-S	100.0 g	Smoked sheet	100.00 g
Zinc oxide	5.0 g	Zinc oxide	7.85 g
Pine tar	5.0 g	Pine tar	3.00 g
Stearic acid	2.0 g	Stearic acid	3.30 g
Sulfur	2.0 g	Sulfur	2.81 g
Captax	1.5 g	Captax	0.743 g
(Shawinigan or R-40)	variable	(Shawinigan or R-40)	variable
Cured for 70 minutes at 40 lbs./in.^{2} steam pressure.		Cured for 90 minutes at 35 lbs./in.^{2} steam pressure.	

[1] J. Rehner, J. App. Phys. **14**, 638 (1943); Rubber Chem. Tech. **17**, 865 (1944).
[2] H. M. Smallwood, J. App. Phys. **15**, 758 (1944); Rubber Chem. Tech. **18**, 292 (1945).
[3] E. Guth, J. App. Phys. **16**, 20 (1945); Rubber Chem. Tech. **18**, 596 (1945).
[4] D. Parkinson, Trans. Inst. Rubber Ind. **21**, 7 (1945); Rubber Chem. Tech. **19**, 100 (1946).
[5] L. H. Cohan, and J. F. Mackey, Ind. Eng. Chem. **35**, 806 (1943); Rubber Chem. Tech. **16**, 918 (1943).
[6] L. H. Cohan, and M. Steinberg, Ind. Eng. Chem. **36**, 7 (1944).
[7] F. H. Amon, and O. J. Brown, American Ink Maker, November, 1941.
[8] R. H. Hall, B. P. Buckley, and T. R. Griffith, Can. Chem. and Process Industries **29**, 587 (1945).
[9] D. Bulgin, Trans. Inst. Rubber Ind. **21**, 188 (1945); Rubber Chem. Tech. **19**, 667 (1946).

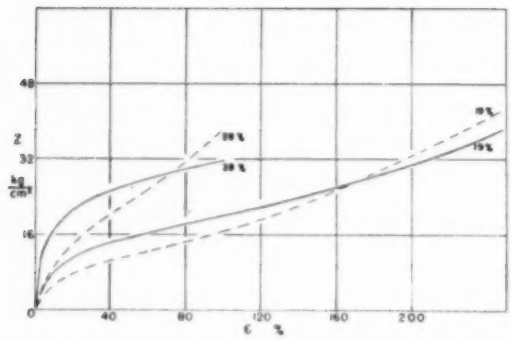

FIG. 1. Fast stress-strain curves at 30°C for GR-S stocks. Shawinigan stocks are denoted by dashed lines and R-40 stocks by full lines.

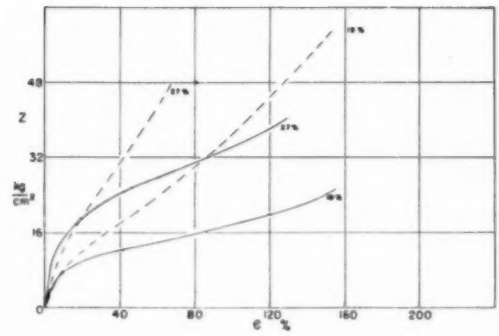

FIG. 2. Fast stress-strain curves at 30°C for natural rubber. R-40 stocks are denoted by full lines and Shawinigan stocks by dashed lines.

kinetic phenomenon regulated only by chance. The probability of formation of a chain becomes appreciable only when the loading is sufficiently high. Changes in temperature and elongation cause a modification of structure of the carbon black chains. This will also change with time. It should be pointed out that the carbon black particles are connected to each other by the flexible long rubber molecules. In the unstretched state, the rubber molecules are curled up, in accordance with the kinetic theory of rubber elasticity. The flexibility of the rubber molecules will permit almost free translational kinetic (Brownian) motion of the carbon black particles, up to the limit given by the length of the rubber molecules. According to this picture, stretching of a loaded stock will limit the region in which the carbon black particles can move, and at sufficiently large extensions, the positions of the carbon black particles are more or less rigidly fixed.

II. EXPERIMENTAL PROCEDURE

All stocks were mixed on a small laboratory size mixing mill and cured in a small platen press. The following base formulae were used for all stocks: Four different loadings of Shawinigan and of R-40 were employed in the GR-S and natural rubber stocks. These were 136.9 g, 80 g, 50 g, and 36.9 g. These loadings gave volume concentrations of 40 percent, 28 percent, 19 percent, and 15 percent, respectively, for the GR-S stocks, and 39 percent, 27 percent, 19 percent, and 15 percent, respectively, for the natural rubber stocks, the slight difference at the two highest loadings being caused by the difference in densities of GR-S and natural rubber. The volume concentration is defined here as the ratio of the true volume of the carbon black to the total volume of the cured rubber. The carbon black volume was calculated from its weight, employing the standard density value of 1.80 g/cm³. The densities (and volume) of the cured rubber stocks were determined by hydrostatic weighing at room temperature. It is of interest to note that the volume of cured loaded stock is equal to the sum of the volumes of the cured gum stock and of the carbon black, to within 1 percent or better, when the carbon black volume is calculated from the density value of 1.80 g/cm³. This was checked

TABLE II. GR-S stocks.

Black	Volume concentration (%)	Tensile strength (lb/in.²)	Elongation at break (%)	Shore hardness (30 sec value)
Shawinigan	40	1270	50	97
Shawinigan	28	2070	300	74
Shawinigan	19	1430	750	57
Shawinigan	15	1080	875	46
R-40	40	1640	150	97
R-40	28	2880	675	74
R-40	19	2820	775	61
R-40	15	3060	925	50

TABLE III. Natural rubber stocks.

Black	Volume concentration (%)	Tensile strength (lb/in.²)	Elongation at break (%)	Shore hardness
Shawinigan	39	1220	50	99
Shawinigan	27	1630	150	81
Shawinigan	19	2060	575	67
Shawinigan	15	2640	500	66
R-40	39	1340	150	95
R-40	27	2060	425	78
R-40	19	2500	425	70
R-40	15	2140	550	60

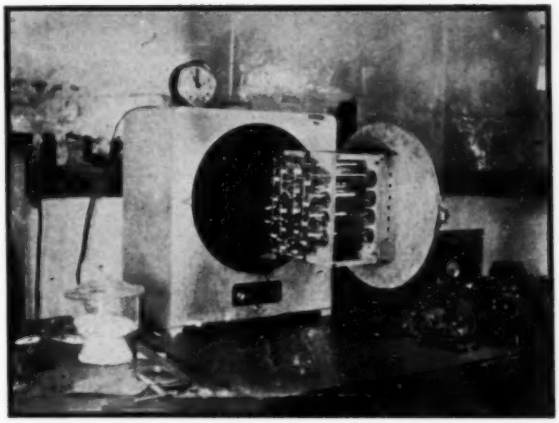

FIG. 3. View of oven with door opened to show mounting rack.

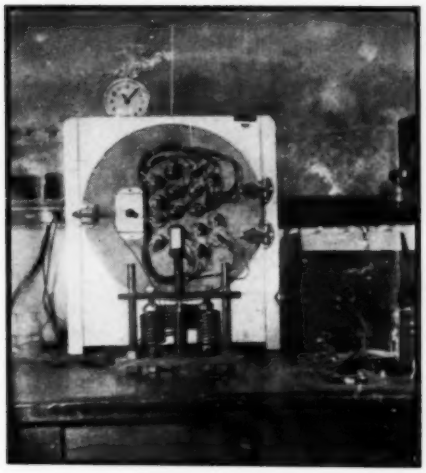

FIG. 4. View of oven with door closed. The apparatus used for measuring resistivities of the blacks is seen in front of the oven.

by hydrostatic weighing of gum stocks and loaded stocks.

The tensile strength, elongation at break and Shore hardness are given in Table II below for the eight GR-S stocks, and in Table III for the eight natural rubber stocks.

Figures 1 and 2 show stress-strain curves at 30°C for the 19 percent and 28 percent concentrations in GR-S, and for the 19 percent and 27 percent concentrations in natural rubber. It is seen that for each loading the R-40 gives higher rigidity in both natural rubber and GR-S at low extensions than does the Shawinigan. At high extensions, the situation is reversed. An explanation for the higher rigidity of Shawinigan stocks at higher extensions will be suggested in connection with the interpretation of resistivity-extension curves (cf. Fig. 14). The data shown in Figs. 1 and 2 were taken with the fast stress-strain machine described in an earlier paper.[10]

The rubber was cured in the form of standard tensile sheets 6 inches square by $\frac{1}{16}$ inch thick. After an aging period of 24 hours or more, the samples for investigation were die-cut from these sheets. These samples were in the shape of square headed dumb-bells, the straight center sections having a width of 0.25 inches and a length of 2 inches. The ends of the samples were placed in flat aluminum clamps which covered only the enlarged end portions of the samples. The clamps served simultaneously as a means of stretching the rubber and also as electrical contacts to the sample. Resistivities of (stretched) samples were measured in the direction of the stretch. The coating of the sample ends with Aquadag before clamping made no appreciable difference in the over-all resistance measurements. After clamping, the samples were mounted in an oven by means of a rack capable of holding eighteen samples, each sample being individually mounted in a horizontal Pyrex glass tube. One end of each sample was held fixed at one end of the glass tube, the other end being attached to a copper rod which protruded through the door of the oven. The elongation of each sample could be adjusted and measured by means of these rods. The time required, after a temperature change, for equalization of temperature throughout the oven, including the interior of the samples themselves, was checked by means of a differential thermocouple. This waiting time was approximately 15 minutes after reaching the desired temperature, as read on a mercury thermometer centrally located in the oven. Good air circulation was maintained by means of a small fan mounted in the base of the oven. Resistances were measured with the aid of a Leeds and Northrup Type H.S. galvanometer and a 2-volt storage battery. For low resistance samples a Leeds and Northrup Testing Set, Model 5430, was also used. Specific resistances were then calculated for each sample from the known sample dimensions.

[10] S. L. Dart, R. L. Anthony, and P. E. Wack, Rev. Sci. Inst. **17**, 106 (1946).

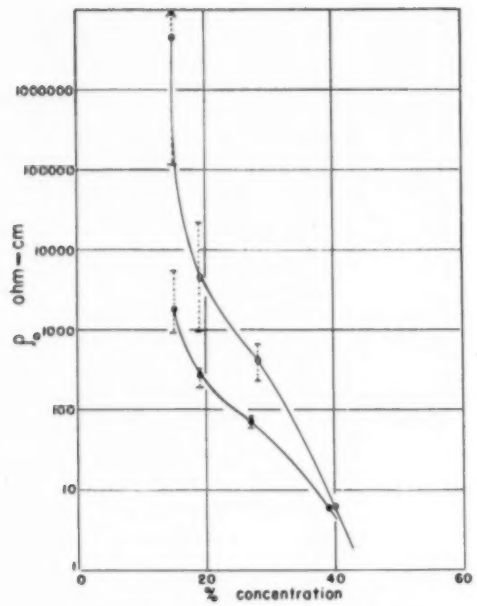

FIG. 5. Resistivity *versus* volume concentration of Shawinigan black at 70°C. Open circles denote GR-S stocks, and black circles denote natural rubber stocks.

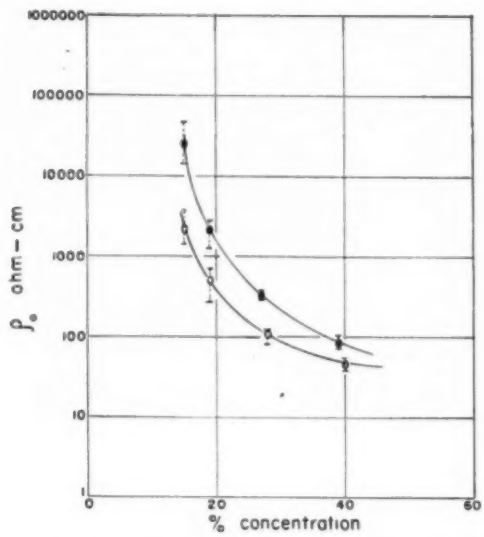

FIG. 6. Resistivity *versus* volume concentration of R-40 black at 70°C. Open circles denote GR-S stocks, and black circles denote natural rubber stocks.

The measurements on the carbon black were made in the oven by inserting the powder in a small Bakelite tube and maintaining a pressure of approximately 2000 lbs./in.^{2} on the black by means of a piston and tension spring device. This pressure, along with considerable tamping down of the black while inserting it in the cylinder, gave apparent densities ranging from 0.36 g/cm^3 to 0.39 g/cm^3.

Figure 3 shows the oven with its door opened, and the rack in which the samples are placed. Figure 4 is a view of the oven with its door closed and shows the copper rods projecting through the door. The device employed in measuring the temperature coefficients of resistivity for the carbon blacks is seen in front of the oven.

Reversal of the direction of current flow during the measurements, as well as several checks employing 60 cycle current, gave no evidence of any important polarization effects, either in the rubber or in the carbon black.

III. RESULTS

A. Dependence of Resistivity Upon Carbon Black Concentration and Upon Time

Initial measurements of the resistivities of several samples showed that the resistivity for each sample was a function of the time which had elapsed after the sample had been cut out and mounted in the clamps in an unstretched condition. In all cases the resistance decreased with time, at first quite rapidly, and then more slowly, and appeared to be approaching a stable value. This behavior is easily explained using our picture of the rubber-black system. As the samples were molded, cured, and cut, strains were set up in their interior. These strains caused a breakage in the carbon black chains, thus leading to an increase in the resistance. In the course of time kinetic (Brownian) motion of the carbon black particles will lead to a re-forming of the chain structure and thus to a decrease in the resistivity. Any small temporary distortion of the sample, for example a small extension followed by an immediate retraction to zero extension, produced a relatively large increase in the resistance, which then decayed in the same manner with time again to a semi-equilibrium value. This behavior had been noted much earlier by Evans[11] and has since been pointed out by Bulgin and others. The approach to a steady state value of the resistance can be greatly accelerated by "annealing" the samples at elevated temperatures. This effect would seem to indicate that any sudden change in

[11] R. D. Evans, Paper presented at the meeting of the Ohio Academy of Science in 1930 and kindly made available to us by W. W. Vogt.

strain disrupts existing carbon networks, which subsequently tend to reform themselves. In the work described here all samples were annealed, in an unstretched condition, for a period of 10 hours at 70°C after they had been mounted in the oven. The value of the resistivity attained at the end of this initial annealing period is denoted by ρ_0 in this work. (It should be noted here that this value of resistivity is not really constant but rather continues to decrease slowly with time. However, the important consideration is that the rate of change of resistance with time must be so small that it cannot appreciably alter the results of some additional experiment.) Preliminary measurements also indicated wide variations between the resistivity values for samples which were supposed to be identical. Resistivities for samples cut from the same tensile sheets were found to vary, in some cases, by as much as a factor of ten. This was particularly true for the Shawinigan black—GR-S stocks at low carbon concentrations. The Shawinigan black—natural rubber stocks were somewhat more uniform. However, the continental R-40 stocks were much superior in this respect. At high concentrations the variations in resistivity values were much smaller for all stocks.

The dependence of ρ_0 upon the volume concentration of the carbon black in the rubber is shown in Figs. 5 and 6. Figure 5 shows the effect on resistivity of four concentrations of Shawinigan in both GR-S and natural rubber, and Fig. 6 shows the behavior of R-40 in these two rubbers. In these two figures each point is an average value of a large number of separate determinations on individual samples. The vertical line drawn through each point shows the range of ρ_0 values for each stock. Comparison of Figs. 5 and 6 shows that at low loadings R-40 gives better conductivity (lower resistivity) in GR-S than does Shawinigan. At the high loadings, Shawinigan gives better conductivity in both GR-S and natural rubbers. The R-40 natural rubber stocks have higher resistivities than the R-40 GR-S stocks. In the case of the Shawinigan black, however, the situation is reversed and here the GR-S stocks have the higher resistivities. The very rapid decrease of resistivity with increasing concentration of Shawinigan black at low concentrations, may explain in part the wide variations found in the resistivity values for identical stocks in this region. Slight variations in concentration of the Shawinigan, from sample to sample, might thus be expected to produce large changes in resistivity in the region of low loadings. Large variations in the resistivities of supposedly identical rubber stocks loaded with Shawinigan black were also found by Hall, Buckley, and Griffith.[8] They suggest that the effect may be due to variations in the degree to which the structure of the Shawinigan black has been broken down during the milling and curing processes.

To minimize the effects of variations in the value of ρ_0 and thus make possible better comparisons between different samples, when studying the dependence of resistivity upon extension, temperature and time, the relative resistivity, ρ/ρ_0, is employed in this work rather than the actual resistivity, ρ. Figure 7 shows the decrease in the relative resistivity with time during the annealing period for 19 percent volume concentrations of R-40 and Shawinigan in natural rubber. Figure 8 shows the decrease in this ratio

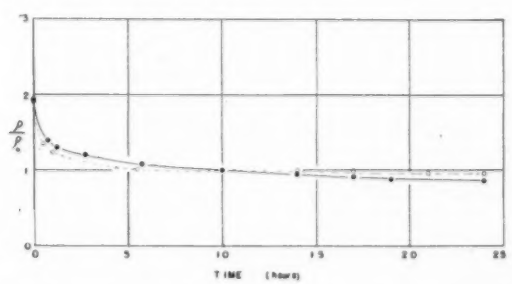

FIG. 7. Annealing curves at 70°C for 19 percent volume concentrations of R-40 (open circles) and Shawinigan (black circles) in natural rubber.

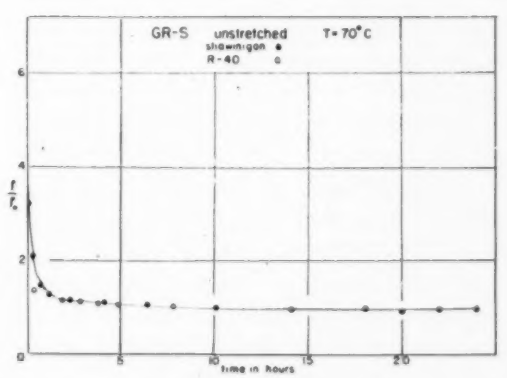

FIG. 8. Annealing curves at 70°C for 19 percent volume concentrations of R-40 (open circles) and Shawinigan (black circles) in GR-S.

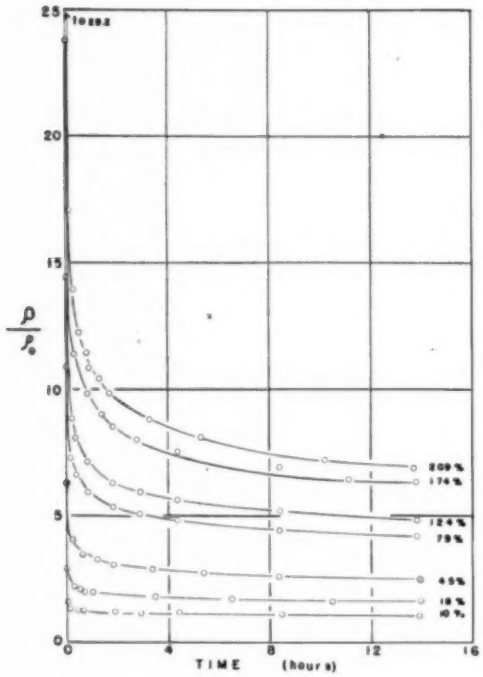

FIG. 9. Decay of resistivity with time at various extensions for a 19 percent volume concentration of R-40 in GR-S. Temperature = 70°C.

with time, during the annealing period, for the same concentrations of these blacks in GR-S. In general, this relative decrease with time was found to be larger for the GR-S stocks than for the natural rubber stocks, and it became progressively smaller for both stocks as the loadings were increased.

B. Dependence of Resistivity of Loaded Stocks upon Extension

At the end of the 10-hour annealing period, the samples were stretched to various elongations, and the temperature was maintained at 70°C for an additional 14 hours. During this period the decay of resistivity with time was again observed. Figure 9 shows the decrease in the relative resistivity with time, at various extensions, for a GR-S stock containing a 19 percent volume concentration of R-40. These curves have been cross-plotted at times of 30 seconds and 14 hours to show the dependence of the resistivity upon the extension. This dependence is shown in Fig. 10. Figure 11 shows the decrease in ρ/ρ_0 with time, at various extensions, for a 19 percent concentration of R-40 in natural rubber. The

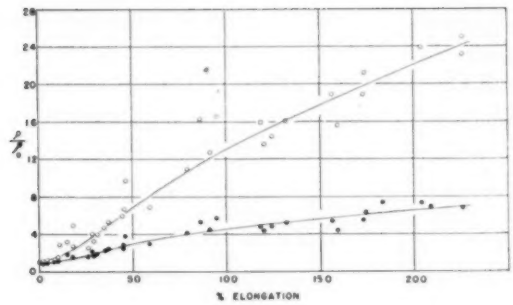

FIG. 10. Cross-plot of Fig. 9 showing the dependence of resistivity upon extension at times of 30 sec (open circles) and 14 hours (black circles).

corresponding dependence of ρ/ρ_0 upon the extension, at times of 30 seconds and 14 hours, is shown in Fig. 12. A very similar behavior was observed for the 15 percent and 28 percent concentrations of R-40 in GR-S and also for the 15 percent and 27 percent concentrations of R-40 in natural rubber. It was not possible to obtain data as a function of extension for the 40 percent loadings in GR-S nor for the 39 percent loadings in natural rubber, because of the extreme stiffness of these stocks.

Figure 13 gives the dependence of ρ/ρ_0 upon time for various extensions of a GR-S stock containing a 19 percent volume concentration of Shawinigan. A very pronounced inversion in the value of the relative resistivity as a function of

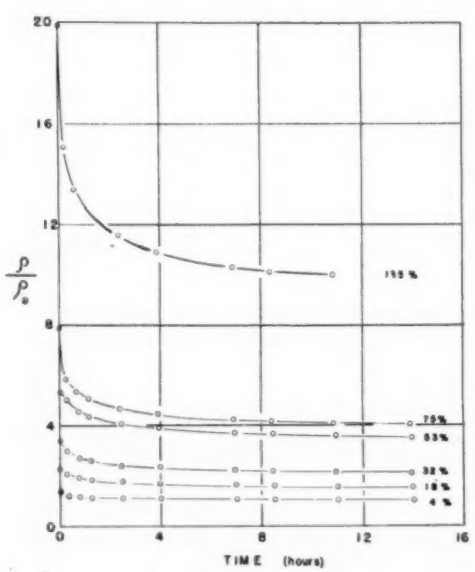

FIG. 11. Decay of resistivity with time at various extensions for a 19 percent volume concentration of R-40 in natural rubber. Temperature = 70°C.

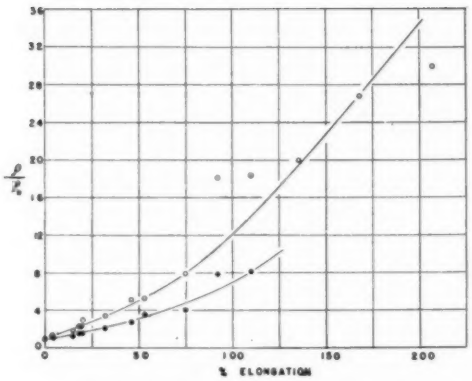

FIG. 12. Cross-plot of Fig. 11 showing the dependence of resistivity upon extension at times of 30 sec (open circles) and 14 hours (black circles).

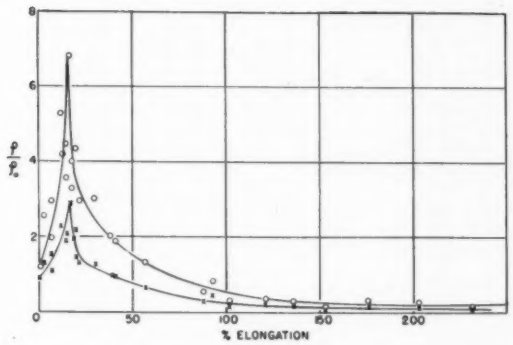

FIG. 14. Cross-plot of Fig. 13 showing the dependence of resistivity upon extension at times of 30 sec (open circles) and 14 hours (crosses).

extension is apparent in the range of low extensions. These curves have been cross-plotted at times of 30 seconds and 14 hours to show the dependence of ρ/ρ_0 upon the extension. This dependence is shown in Fig. 14. Examination of Figs. 13 and 14 shows that for high extensions the resistivities are almost immediately reduced to values which are very considerably less than the values which existed just before the extension. At extensions in the vicinity of 15 percent to 20 percent the resistivities, immediately after stretching for the first time, tend to become quite large and are extremely sensitive to slight differences in extension. Reproducibility of relative resistivities in this region was poor. The general behavior shown in Figs. 13 and 14 is strongly suggestive of a maximum in the resistivity *versus* extension relationship in the region of low extensions. This might, perhaps, be caused by a general breakdown of the carbon black network

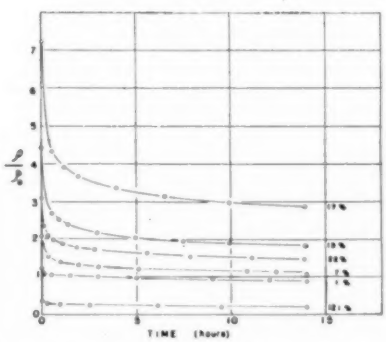

FIG. 13. Decay of resistivity with time at various extensions for a 19 percent volume concentration of Shawinigan in GR-S. Temperature = 70°C.

structure at these extensions, followed by a forced realignment of the carbon chains in the direction of the extension at higher elongations caused by the orientation of the rubber molecules. A process of this nature would account for the increased conductivity in the direction of the extension and might even be accompanied by a reduction in the conductivity in the direction perpendicular to the stretch. The latter possibility has not yet been checked, since the equipment employed in this work was designed to measure resistivities (and conductivities) in the direction of the extension.

A probable explanation of the different behavior of Shawinigan and of R-40 at large extensions may be given. At large extensions of the material the rubber molecules most firmly bound to the carbon black particles will be subject to exceptional high extensions and will make abnormally high contributions to the rigidity. Therefore, we would expect carbon black to increase the rigidity of the material more when it is more firmly bound to the rubber molecules. That this is the case with Shawinigan is indicated by the decrease in resistivity below the initial value at high extensions. However the larger size of the Shawinigan particles may also be of importance both for the increase of rigidity and for the decrease of resistance with increasing extension.

An anisotropic conduction of the type suggested above has been shown by Habgood and Waring[12] to occur in extruded stocks containing

[12] B. J. Habgood, and J. R. S. Waring, Trans. Inst. Rubber Ind. **17**, 51 (1941); Rubber Chem. Tech **15**, 146 (1942).

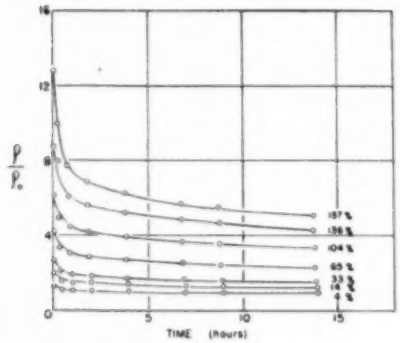

FIG. 15. Decay of resistivity with time at various extensions for a 19 percent volume concentration of Shawinigan in natural rubber. Temperature = 70°C.

Shawinigan black. A similar asymetry in graphite electrodes was also noted by Buerschaper.[13]

The behavior of Shawinigan black in GR-S for the 28 percent loading was similar to that shown in Figs. 13 and 14 for the 19 percent loading. In the case of the 15 percent loading of Shawinigan black in GR-S, the resistivities of the extended samples were too high for measurement with the present equipment. A similar inversion in the resistivity *versus* extension relationship was found for the 27 percent loading of Shawinigan in natural rubber, but was not perceptible for the 15 percent and 19 percent loadings in natural rubber. Figures 15 and 16 show the dependence of relative resistivity upon extension and time for the 19 percent volume concentration of Shawinigan in natural rubber.

C. Dependence of Resistivity of Loaded Stocks upon the Temperature

After the samples had been maintained in an extended condition for a time of 14 hours at 70°C, the temperature was lowered in steps to about 30°C and the corresponding values of resistivity were noted. The temperature was then increased in steps, and readings were taken as a function of increasing temperature. In general the resistance *versus* temperature relationship so obtained was not a linear one, and the two branches of the curve did not coincide. Figures 17, 18, 19, and 20 show the temperature dependence of resistivity at zero extension for all loadings of Shawinigan and R-40 in both natural rubber and GR-S. In general, the agreement between data obtained with decreasing and increasing temperatures becomes better as the loadings are increased. This is particularly true for the Shawinigan stocks. The temperature coefficients of resistivity were determined by constructing tangents to these curves at 50°C, this temperature coefficient being defined as

$$\alpha_{50°C} = \frac{\Delta\rho}{\Delta T \cdot \rho_{50°C}}.$$

The dependence of $\alpha_{50°C}$ upon carbon black concentrations is shown in Fig. 21 for GR-S and in Fig. 22 for natural rubber. Each plotted point is an average of four separate determinations. It is seen that $\alpha_{50°C}$ is positive for all Shawinigan stocks, and increases with increasing loadings. With one exception, namely, the 40 percent volume concentration in GR-S, the temperature coefficient for the R-40 stocks is negative and also increases with increasing loadings. Since the temperature coefficients at 100 percent concentration should correspond to those of the carbon blacks themselves, the possible trend at higher concentrations is indicated in Figs. 21 and 22 by dotted line extensions of the curves.

Figures 23, 24, 25, and 26 show the dependence of the resistivity-temperature relation upon extension for 19 percent volume concentration of both blacks in GR-S and natural rubber. Average temperature coefficients over the range from 30°C to 70°C have been calculated from these curves as follows. Let A be the average value of ρ/ρ_0 at 70°C and B the value of this ratio at 30°C.

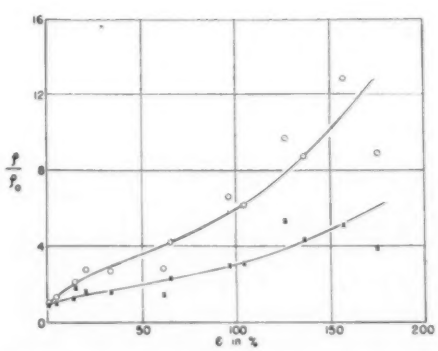

FIG. 16. Cross-plot of Fig. 15 showing the dependence of resistivity upon extension at times of 30 sec (open circles) and 14 hours (crosses).

[13] R. A. Buerschaper, J. App. Phys. **15**, 452 (1944).

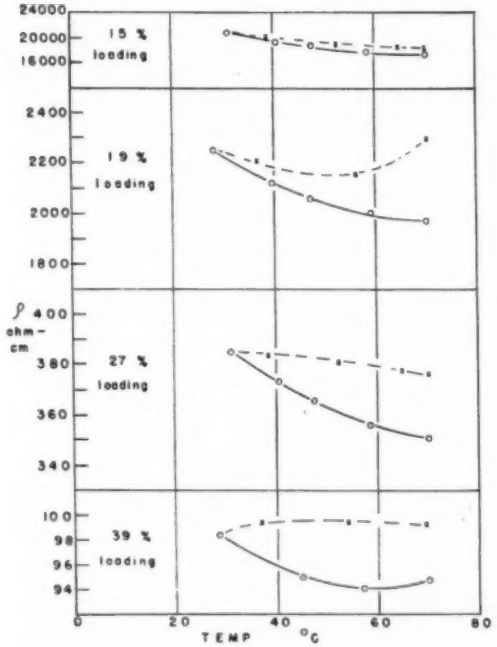

FIG. 17. Resistivity *versus* temperature relationships at zero extension for four loadings of R-40 in natural rubber. Circles indicate decreasing temperature and crosses increasing temperature.

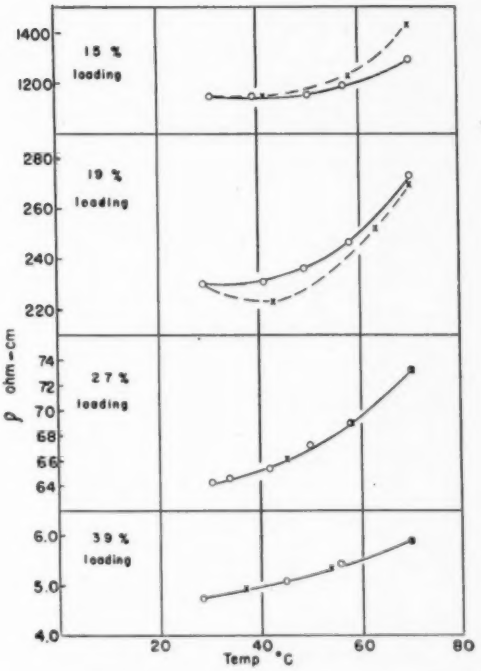

FIG. 19. Resistivity *versus* temperature relationships at zero extension for four loadings of Shawinigan in natural rubber. Circles indicate decreasing temperature and crosses increasing temperature.

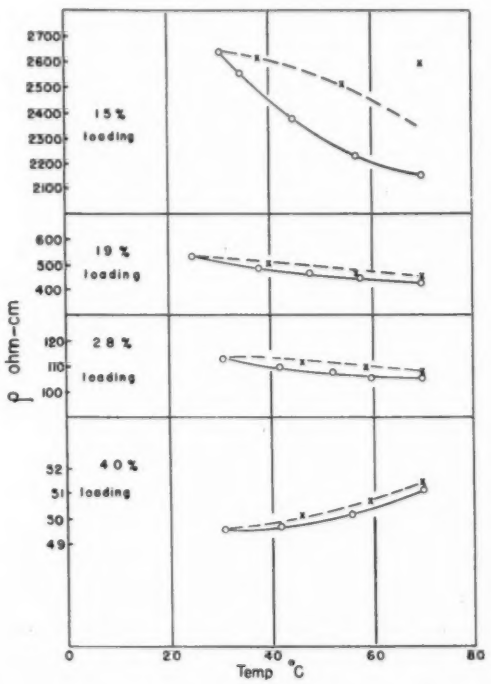

FIG. 18. Resistivity *versus* temperature relationships at zero extension for four loadings of R-40 in GR-S. Circles indicate decreasing temperature and crosses increasing temperature.

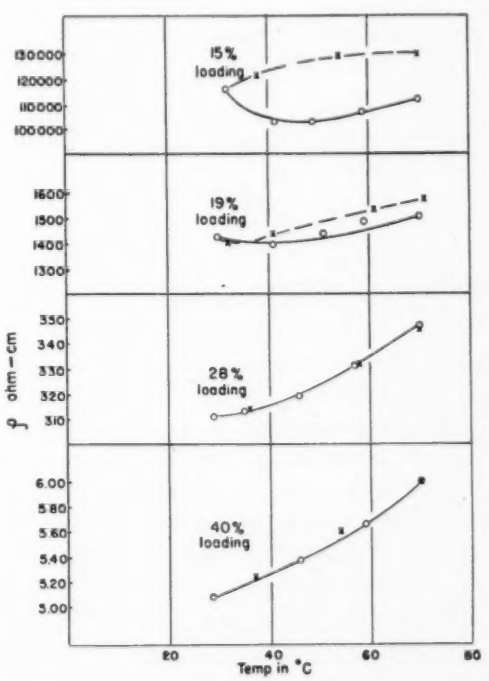

FIG. 20. Resistivity *versus* temperature relationships at zero extension for four loadings of Shawinigan in GR-S. Circles indicate decreasing temperature and crosses increasing temperature.

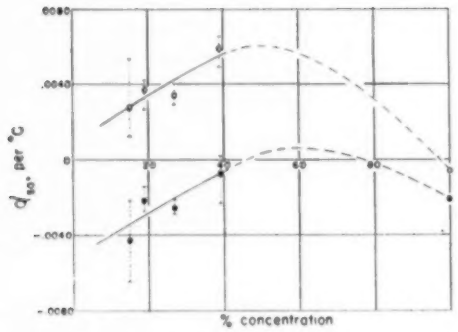

FIG. 21. Dependence of temperature coefficient of resistance upon volume concentration in GR-S. Open circles denote Shawinigan and black circles R-40.

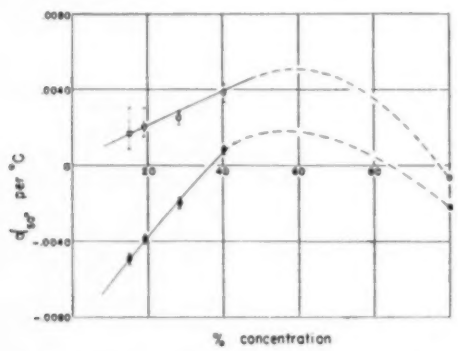

FIG. 22. Dependence of temperature coefficient of resistance upon volume concentration in natural rubber. Open circles denote Shawinigan and black circles R-40.

Then

$$\bar{\alpha}_{50°C}=\frac{A-B}{40\dfrac{(A+B)}{2}}=\frac{A-B}{20(A+B)}.$$

The dependence of this temperature coefficient upon extension for 19 percent volume concentrations of R-40 and Shawinigan is shown in Fig. 27 for natural rubber and in Fig. 28 for GR-S. This coefficient increases with increasing extension in all cases. It is positive for the Shawinigan stocks and negative for the R-40 stocks. A similar behavior was found for the other loadings.

These results show that the temperature coefficient of the resistivity of the loaded stocks depends strongly upon the concentration and upon the extension. The positive coefficient is probably connected with the breaking and reforming of carbon black chains. Such a kinetic effect will, in general, increase with increasing temperature, in contrast to the resistivity of the

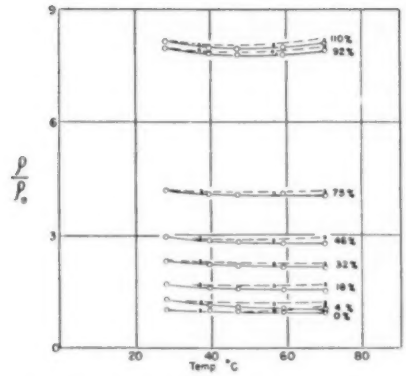

FIG. 23. Relative resistivity *versus* temperature at various extensions for a 19 percent concentration of R-40 in natural rubber.

black itself, which will decrease with rising temperature. The explanation of the negative coefficient at lower black concentrations needs further consideration. It will also be noted that when a run is made first decreasing the temperature and then increasing it again to the original value the final resistivity is (with one exception: 19 per cent concentration Shawinigan in GR-S) larger than the starting value. This fact and the presence of hysteresis effects in general indicates that any disturbances of the material, whether thermal or mechanical, tends to break up some chains and thus increase the resistivity temporarily. This effect is simply superimposed on the other trends which would be observed if measurements could be made on samples in complete statistical equilibrium. The decrease of the area of hysteresis loops on elongation for R-40 and Shawinigan in GR-S may be explained as due to the fixation of black particles as explained in connection with the effect of elongation on resistivity in general.

D. Dependence of Resistivity of the Carbon Blacks upon Temperature

The temperature dependence of the blacks was measured with the aid of the apparatus described in Section II, a pressure of 2000 lbs./in.^{2} being maintained on the blacks during the measurements. The dependence of the resistivity upon the temperature is shown in Fig. 29 for both blacks. The temperature coefficients of resistivity at 50°C, as determined from these curves, are -0.0021/°C for R-40 and -0.0006/°C for Shawinigan.

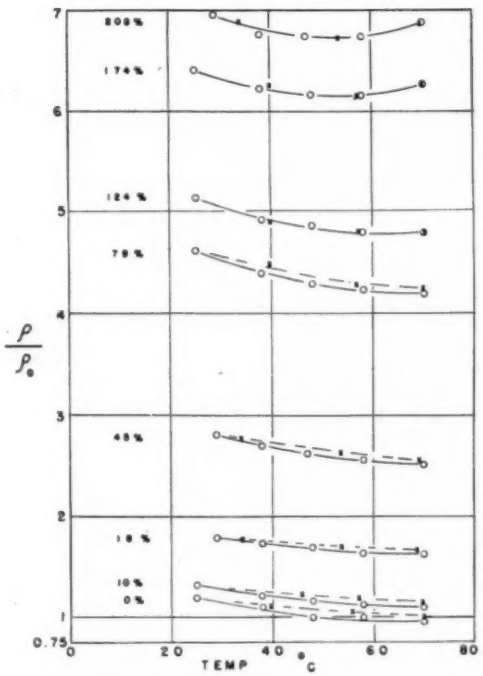

FIG. 24. Relative resistivity *versus* temperature at various extensions for a 19 percent concentration of R-40 in GR-S.

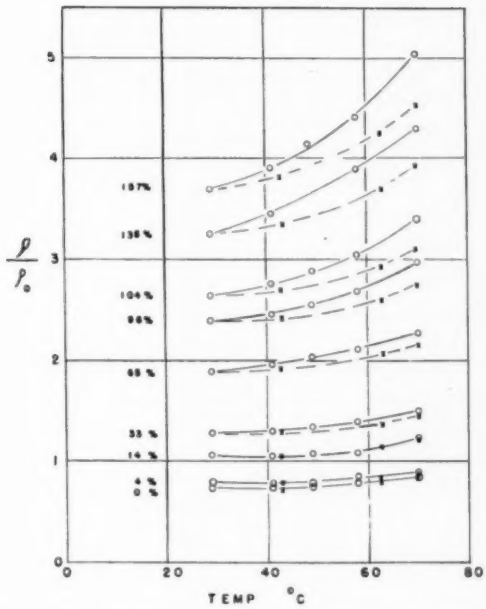

FIG. 25. Relative resistivity *versus* temperature at various extensions for a 19 percent concentration of Shawinigan in natural rubber.

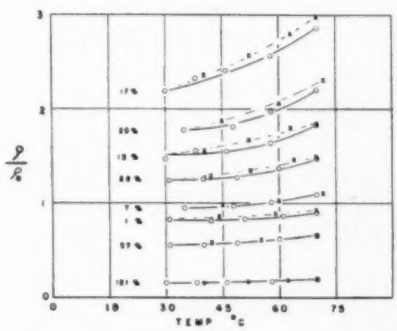

FIG. 26. Relative resistivity *versus* temperature at various extensions for a 19 percent concentration of Shawinigan in GR-S.

It is interesting to note that even at a pressure of 2000 lbs./in.^{2} the apparent density of the carbon black ranged from about 0.36 g/cm^3 to 0.39 g/cm^3, whereas the apparent density of the carbon black in the rubber at the highest loadings was about 0.7 g of carbon black per cubic centimeter of cured rubber. It had originally been expected that pressures of from 1000 to 2000 lbs./in.^{2} would result in a stable value of resistivity for the carbon black, since a previous study of the decrease in resistance of the carbon black with increasing pressure seemed to indicate a leveling off of resistance values in the region of about 1000 lbs./in.^{2} On the basis of this expectation, these resistivity values were at first included in the plots of the logarithm of the resistivity *versus* volume concentration shown in Figs. 5 and 6, as points corresponding to a 100 percent volume concentration. This led to an approximate linear relationship for the R-40 black in GR-S and in natural rubber when log resistivity was plotted *versus* log concentration. However, it has since been discovered that the resistivity of the black itself depended strongly upon its apparent density and that even at constant pressure a wide variation in apparent densities can be obtained by tamping down the black while it is being loaded in the cylinder. Since the carbon black volume, calculated from the density value of 1.8 g/cm^3, plus the gum rubber volume has been shown to be equal to the volume of the cured loaded rubber, it follows that the "apparent" density of the carbon black corresponding to a 100 percent volume loading should be 1.8 g/cm^3. This density value is much greater than any we have been able to produce, and the corresponding resistivity value is therefore unknown. This strong dependence of resistivity upon apparent density of the black has been noted by Benson,

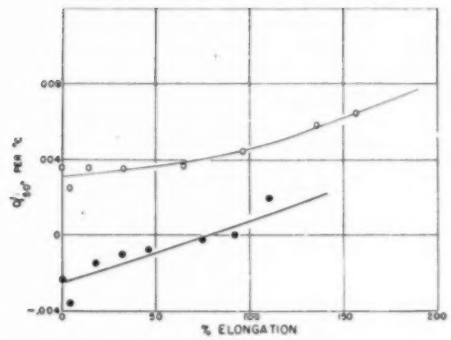

FIG. 27. Dependence of temperature coefficient of resistivity upon extension for 19 percent concentrations of R-40 (black circles) and Shawinigan (open circles) in natural rubber.

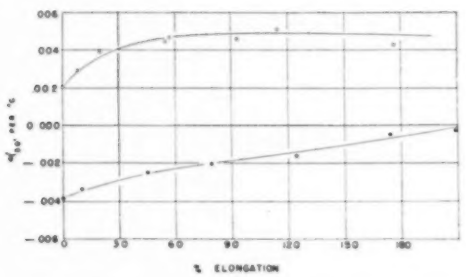

FIG. 28. Dependence of temperature coefficient of resistivity upon extension for 19 percent concentrations of R-40 (black circles) and Shawinigan (open circles) in GR-S.

Gluck, and Kaufmann.[14] They also showed that the density of the black measured at a constant pressure could be increased by as much as a factor of two by various densifying processes, for example by ball-milling.

In contrast to the large variations in the resistivity of the blacks produced by variations in pressure and density, the temperature coefficients of resistivity were found to be nearly independent of pressure and density, provided neither the pressure nor the density was too low. Accordingly these values have been included in Figs. 21 and 22.

IV. SUMMARY

The behavior of two types of conducting blacks, R-40 and Shawinigan, has been studied in natural rubber and in GR-S. A series of four loadings of each black in each type of rubber was employed. These loadings ranged from about 40 grams of black per 100 grams of raw rubber to 140 grams of black per 100 grams of raw rubber, the corresponding true volume concentrations ranging from 15 percent to 40 percent. The resistivities of these stocks were studied as functions of time, temperature, extension, and loading. The following results were observed:

A

Fast stress-strain curves show that in both natural rubber and GR-S, the R-40 black gives the better reinforcement at low extensions, but that Shawinigan gives the better reinforcement at the high extensions.

B

Any small strain produces an increase in resistivity which then decays with time in a nearly exponential fashion. In particular the process of cutting out the samples and mounting them in clamps produces such strains. Annealing the samples at elevated temperatures accelerates the approach to an initial steady-state resistance value. Accordingly, in this work all samples were annealed for 10 hours at 70°C in an unstretched condition. The resistivity value attained at the end of this time is denoted by ρ_0.

C

At the lowest concentrations, R-40 gave better conductivity in GR-S than did Shawinigan, the log resistivity *versus* concentration curve being very steep for the Shawinigan black in this region. At the high loadings Shawinigan gave higher conductance in both GR-S and natural rubber. The R-40 GR-S stocks were better conductors than the R-40 natural rubber stocks. For Shawinigan black, however, the natural rubber stocks were better conductors than the GR-S stocks.

D

For the R-40 stocks, stretching a sample produced an increase in the resistivity, which then decayed with time while the sample was held at a fixed extension. The Shawinigan stocks behaved differently, however. In the case of the 19 percent and 28 percent concentrations in GR-S and also the 27 percent concentration in natural rubber, an inversion was found in the resistivity *versus* ex-

[14] G. Benson, J. Gluck, and C. Kaufmann. In paper presented before the Toronto Meeting of the Electrochemical Society, October 16 to 19, 1946.

tension relationship. The resistivity increased with increasing extensions up to about 20 percent extension and then decreased for higher extensions. For sufficiently high extensions, the resistivities were immediately reduced to values which were very considerably less than the unstretched values. All resistivities were measured along the length of the sample and hence in the direction of the extension.

E

The dependence of resistivity upon temperature was observed for all stocks over the temperature range from 30°C to 70°C. In general, the average temperature coefficient, calculated at 50°C, was positive for the Shawinigan stocks and negative for the R-40 stocks. It increased with increasing carbon black concentration and also increased with increasing extension of the sample.

F

Temperature coefficients of resistivity were also measured for the two blacks at 50°C. The blacks were compressed under a pressure of about 2000 lbs./in.^{2} This pressure was maintained during the measurements, the "apparent" densities ranging from 0.36 to 0.39 g/cm^3. The observed temperature coefficients were -0.0021/°C for the R-40 black, and -0.0006/°C for Shawinigan black.

Our results can, in general, be understood on the basis of a simple picture of the formation and the breaking up of chains of carbon black particles. Thermal and mechanical disturbances both lead to a breakage of the chains and thus to an increase in the resistance. In the course of time Brownian motion of the carbon black particles will re-form the chain structure and thus decrease the resistivity as a function of time.

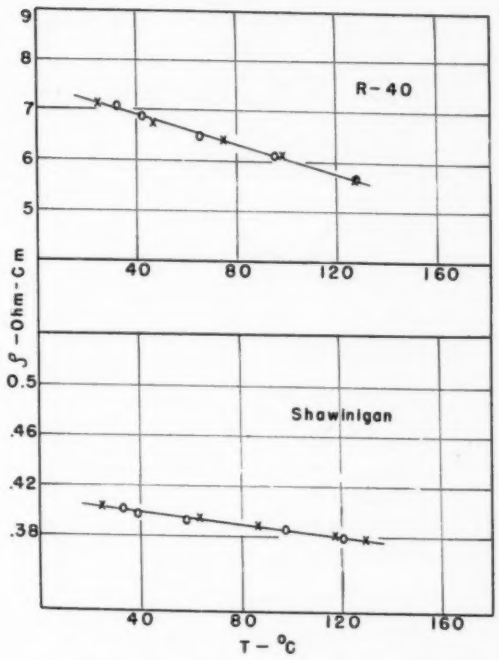

FIG. 29. Dependence of carbon black resistivity upon temperature at a pressure of 2000 lbs./in.^{2}

This explains the decrease of resistance with time of freshly cured and cut and of stretched samples, the increase of resistivity on stretching in general, the fact that the ascending branch of the resistivity-temperature curve lies above the descending branch and a positive temperature coefficient of resistivity. In the case of Shawinigan the greater increase of rigidity and the decrease of resistivity (below the initial value), both at high extensions, is probably determined by the greater strength of the rubber-carbon black bond and the larger size of the black particles as compared with R-40.

It is a pleasure to thank Professor Hubert M. James for frequent consultation and many valuable suggestions in connection with this study.

Elastic Properties of Cork

II. Stress-Temperature Relationship of Compressed Cork

S. L. Dart and Eugene Guth
Polymer Physics Laboratory, University of Notre Dame, Notre Dame, Indiana
(Received October 14, 1947)

In the first paper of this series it was shown that for cork, held at constant compression, the stress as a function of compression, temperature, and time was separable into two factors, one factor representing the load-compression curve and the other describing the decay of stress with time. In the present paper the dependence of the load-compression curve upon temperature is studied. After the sample has relaxed at constant temperature and compression for a time sufficiently long so that the change of stress with time may be neglected, stress-temperature curves were obtained. These curves showed a linear dependence of the stress upon the temperature. From the stress-temperature curves the resolution of the stress into its additive components due to internal energy and entropy was carried out. The physical significance of this resolution is discussed. The experiments were carried out with a refined version of the apparatus described in the first paper. In particular, the apparatus was corrected for rate of thermal expansion.

INTRODUCTION

In a previous paper[1] an account was given of the stress relaxation of cork as a function of compression, temperature, and time. In particular it was shown that the stress decayed to zero in about 1000 years at room temperature and in about 1000 minutes at 200°C, independent of compression. This independence of the decay time on compression was also checked at 80°C and at 130°C. It was also demonstrated that the compressive stress Z as a function of compression, temperature, and time was separable into two factors,

$$Z(\epsilon, T, t) = F(\epsilon, T) \cdot G(t, T), \tag{1}$$

where the factor $F(\epsilon, T)$ is essentially the load-compression curve of cork and the factor $G(t, T)$ describes the decay of stress with time and temperature. In the previous paper it was proved that $G(t, T)$ has the form

$$G(t, T) = a - b \log t \tag{2}$$

where a and b depend on T only. In particular a and b were thrown into the form

$$a = 1$$
$$b = \beta/(\alpha - T)$$

giving as a final equation

$$Z(\epsilon, T, t) = A(\epsilon, T)[1 - [\beta/(\alpha - T)] \log t]. \tag{3}$$

[1] Dart and Guth, J. App. Phys. **17**, 314–318 (1946).

However, the dependence of $A(\epsilon, T) = F(\epsilon, T)$ upon T was left open. The present paper fills in the gap and brings the fundamental stress-temperature relationship for cork.

EXPERIMENTAL METHOD

The apparatus used was described in the previous paper. It consisted of a lever arm for compressing the sample which was automatically kept balanced through a chainomatic drive. Through this drive the force was recorded as a function of time on a clock-driven drum.

The apparatus was carefully rechecked for possible errors in the thermal expansion correction and was also corrected for rate of thermal expansion. This latter is very important in connection with the measurement of stress as a function of temperature at constant compression, since the compression must be maintained constant during the temperature change as well as during the temperature equilibrium. The procedure used was patterned after that of Anthony, Caston, and Guth.[2] That is, the sample was allowed to relax[1] until the rate of change of stress was small enough to make the stress-relaxation negligible during the subsequent stress-temperature determination. The preliminary relaxation time used was 1000 minutes. After this

[2] R. L. Anthony, R. H. Caston, and E. Guth, J. Phys. Chem. **46**, 826 (1942). Reprinted in Rubber Chem. Tech. **16**, 297 (1943).

preliminary relaxation period the temperature was lowered in steps and the corresponding stress changes were noted. Using this procedure one can find the temperature behavior of the stress at temperatures less than the relaxation temperature.

Figure 1 shows the results of such an investigation at the compressions indicated and with the common relaxation temperature of 80°C. It is seen that within the experimental error the stress depends linearly on the temperature. Thus, we may express this by the equation

$$Z(\epsilon, T) = M(\epsilon) + N(\epsilon)T, \qquad (4)$$

where $M(\epsilon)$ and $N(\epsilon)$ are functions of compression alone. We will defer the discussion of the significance of this relation to a later section.

This then gives us the stress as a function of compression and temperature, exclusive of time effects. That is, this Eq. (4) gives us the temperature dependence of the factor $A(\epsilon, T)$ or $F(\epsilon, T)$ in Eq. (3). Before we write down an equation expressing all the experimental results presented, we must recognize that we have measured time effects and temperature effects separately, i.e., time effects were measured at constant temperature and *vice versa*. Let us call the constant relaxation temperature T^* and the temperature which is changed, T. T^* is really a variable separate from T because in order to specify the state of the system one must specify not only the actual temperature T, but also the temperature T^* at which the relaxation took place. This situation was discussed in more detail by Guth, Anthony, and Wack[3] for the case of rubber in extension. They showed, experimentally, that certain ratios (cf. Eqs. (13a, b, c, and d) of their paper) are constant. The constancy of these ratios implies the validity of "generalized similarity and separability" expressed by the equation

$$Z(\epsilon, T, T^*, t) = F(\epsilon, T) \cdot G(T^*, t). \qquad (5)$$

It seems reasonable to assume that "generalized similarity" will also hold for cork, though this was not checked directly. Taking into account (3) we can then identify more explicitly the factors F and G.

$$F(\epsilon, T) = M(\epsilon) + N(\epsilon) \cdot T;$$
$$G(T^*, t) = \{1 - [\beta/(\alpha - T^*)] \log t\}. \qquad (6)$$

Then our generalized equation of state takes the form

$$Z(\epsilon, T, T^*, t) = [M(\epsilon) + N(\epsilon)T] \times \{1 - [\beta/(\alpha - T^*)] \log t\} \qquad (7)$$
$$= F(\epsilon, T) \cdot G(T^*, t).$$

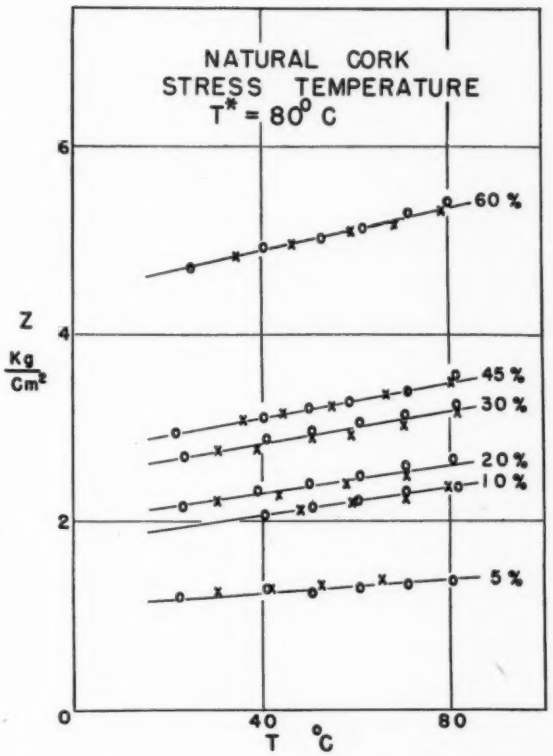

FIG. 1. Stress-temperature curves for cork previously relaxed at $T^* = 80°C$ for 1000 minutes. Circles indicate points obtained on lowering the temperature. Crosses are the points obtained on raising the temperature.

DISCUSSION OF EXPERIMENTAL RESULTS

A. Stress Relaxation

The discussion so far has been concerned solely in presenting the experimental results of our investigation of the elastic properties of cork. We shall now try to give a more fundamental discussion of these results in the light of present day theories. Consider first, the stress relaxation. The general equation for the time dependency of stress as given by Boltzmann has been generalized for the non-Hookean case, by Guth, Wack,

[3] E. Guth, P. E. Wack, and R. L. Anthony, J. App. Phys. **17**, 347 (1946).

and Anthony.[3] This may be written as follows:

$$Z(t)=F[\epsilon(t)]-\beta'\int_{-\infty}^{t}\phi(t-t')F[\epsilon(t')]dt', \quad (8)$$

where β' is a small constant, $F=F(\epsilon)$ gives the stress-strain relationship, and $\beta'\phi(t-t')$ is the memory function of Boltzmann. For relaxation we have $\epsilon(t)=\epsilon(t')=0$ for $t<0$ and $\epsilon(t)=$constant for $t>0$. Thus, Eq. (8) becomes

$$Z(t)=F(\epsilon)[1-\beta'\psi(t)], \quad (9)$$

where

$$\psi(t)=\int_{0}^{t}\phi(t-t')dt'. \quad (9a)$$

It is to be noticed that Eq. (9) is identical in form with the experimental Eq. (3). Thus, we can describe the time dependency by means of the generalized Boltzmann theory. Also, for the case of cork, comparison of (3) and (9) shows that

$$\beta'\psi(t)=[\beta/(\alpha-T)]\log t, \quad (10)$$

while (9a) shows that

$$\phi(t-t')=1/(t-t'). \quad (10a)$$

A relation of the type (10) holds for many materials in a limited range of t values. The remarkable result for cork is the validity of the relation (10) over a very wide range of t values. As a matter of fact, (10) is valid for cork in the range $t=1$ min. We plan to discuss the theoretical significance of this fact at a later time.

If the stress-time curve is an exponential in t, we have

$$Z=Z_0\exp(-K't), \quad (11)$$

where K' is given by

$$K'=(kT/h)e^{-\Delta H/RT}.$$

Here ΔH is the activation energy and kT/h is the rate factor as given by Eyring.[4] This equation is a straight line on a log$Z$ *vs.* t plot. Such a plot was tried on a relaxation run at 200°C and 4.86 percent compression and the result was far from linear. However, activation energies were calculated using a straight line portion of the curve and also using the time for the stress to drop to a value $1/e$ times the first value. These activation energies were 38.0 and 36.8 kilocalories per mole, respectively. These results are slightly larger than the corresponding values for rubber-like materials, which have activation energies of about 32 kilocalories per mole.

In Eq. (3), $F(\epsilon, T)$ designates the value of the stress at $t=1$ min. Expressing this fact more explicitly, Eq. (7) may be written

$$Z(\epsilon, T, T^*, t)=F(\epsilon, T)\times\{1-[\beta/(\alpha-T^*)]\log t/t_0\}, \quad (12)$$

where $t_0=1$ min. For $\alpha\leq T^*$ Eq. (12) was not established experimentally and it cannot be extrapolated to this range without further considerations. At any rate theoretical arguments show that a logarithmical relationship of the type of Eq. (12) will not hold for very small times, i.e., for times much smaller than 1 min.

In the first installment of this series[1] the time τ needed for the stress to decay to zero, for a sample held at constant compression, was shown to be independent of the compression strain. To show the dependence of τ upon the relaxation temperature T^*, a plot of T^* *versus* logτ was used. The curve so obtained was a straight line.

Instead of a T^* *vs.* logτ plot, a logτ *vs.* $1/T^*$ plot may also be used. A straight line does not fit in the latter representation as well as the former one, but still gives a reasonable fit, if one considers the unavoidable experimental errors. We then have the relation

$$1/T^*=a+b\log\tau.$$

Solving for τ we obtain

$$\tau=\tau_0\exp(V/RT^*), \quad (13)$$

i.e., an infinite decay time at absolute zero, which is reasonable. The constants in Eq. (13) have the values

$$\tau_0=1.6\cdot10^{-3}\text{ min.},$$
$$V=9\text{ kilocalories per mole.}$$

B. Stress-Temperature

Concerning the stress-temperature relationship, we can proceed as follows:

We start from the well-known energy equation of thermodynamics

$$\left(\frac{\partial U}{\partial V}\right)_T=T\left(\frac{\partial P}{\partial T}\right)_V-P. \quad (14)$$

[4] Cf. for instance, S. Glasstone, K. Laidler, and H. Eyring, *The Theory of Rate Processes* (McGraw-Hill, New York, 1941).

Using the Maxwell relation

$$\left(\frac{\partial P}{\partial T}\right)_V = \left(\frac{\partial S}{\partial V}\right)_T, \tag{15}$$

we can write

$$\left(\frac{\partial U}{\partial V}\right)_T = T\left(\frac{\partial S}{\partial V}\right)_T - P. \tag{16}$$

Applying this to our case of unilateral compression we must substitute $1-\epsilon$ for V, and Z for P, since we plot actually the pressure or the negative of the tension stress. This gives

$$-\left(\frac{\partial U}{\partial \epsilon}\right)_T = -T\left(\frac{\partial S}{\partial \epsilon}\right)_T - Z$$

or

$$Z = \left(\frac{\partial U}{\partial \epsilon}\right)_T - T\left(\frac{\partial S}{\partial \epsilon}\right)_T = Z_U + Z_S, \tag{17}$$

where Z_U is the contribution of the internal energy to the stress, Z_S is the entropy contribution, and Z is, of course, the total stress. (Actually the experiments are carried out at constant pressure and constant compression. Nevertheless, Eq. (17) is valid in sufficient approximation, when derivatives are taken at constant temperature and constant pressure.) Equation (17) has the same form as our experimental Eq. (4). Thus, using the curves shown in Fig. 1 we can calculate Z_U and Z_S as a function of ϵ. In doing this one must remember that the T in Eq. (17) is absolute temperature. The results of such a calculation are shown in Fig. 2. Here one can see that the entropy is responsible for most of the stress in the first two regions, i.e., for the stiffness of the sample at small compressions and during the breakdown of the structure. However, when the actual material of the cell walls begins to be compressed, at 60 percent or so, the internal energy contribution becomes appreciable.

The negative internal energy contribution in the first range of (small) compressions is at least partly caused by the thermal expansion of the uncompressed cork. This is similar to the behavior of rubber at small extensions. The internal energy contribution is partly caused by the thermal expansion of the unstretched rubber.

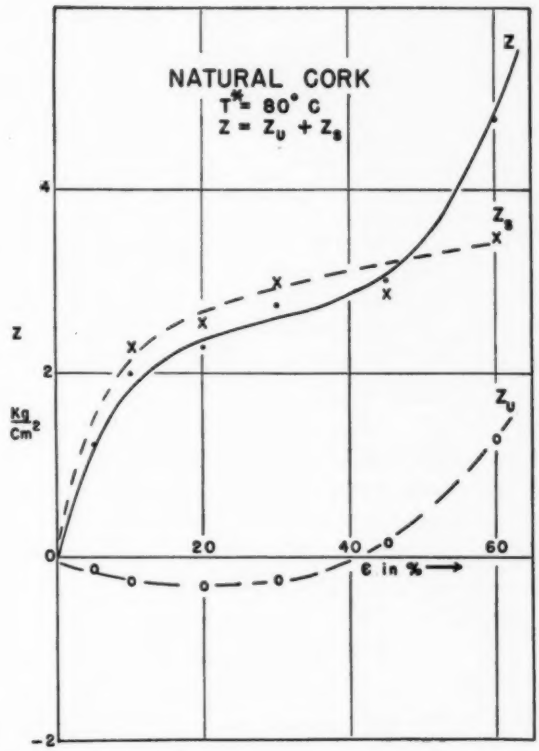

FIG. 2. Resolution of the stress of Fig. 1 at $T=25°C$ into its components Z_U and Z_S due to internal energy and entropy, respectively.

The large contribution to the stress due to entropy is presumably connected with the bending of the cell walls. The material of the cell walls is likely to consist of long chain molecules with at least some degree of free rotation. On this basis a large entropy contribution can be understood. The increase of internal energy, on further compression, is presumably caused by intermolecular forces coming into prominence as compression increases.

ACKNOWLEDGMENT

The authors wish to express their appreciation to Dr. H. A. Robinson, Chief Physicist, Armstrong Cork Company, for valuable discussions and for furnishing the samples used in this investigation. They also wish to express their appreciation to Mr. E. Claxton, Director of Research, and to Dr. R. B. Rohrer, Assistant Director of Research, Armstrong Cork Company, for the benefit of valuable discussions and for the support of this work.

Elastic Properties of Cork

III. Hydrostatic and Ordinary Load-Compression Curves for Cork

S. L. Dart,* Howard A. Robinson,** and Eugene Guth*

(Received October 14, 1946)

Load-compression curves were taken for natural cork. The S-shape of the curves is discussed and a theoretical fit is made for the high end of the curve, assuming an initial stiffness and an incompressible part of the cork material. A comparison is made between repeated compressions, with and without a recovery period of time.

Pressure-volume curves were also taken and their significance discussed in connection with the load-compression curves leading to an evaluation of Poisson's ratio.

DETERMINATION of the load-compression curves of cork under various experimental conditions is of great theoretical and practical interest. The load-compression curves for cork show a peculiar S-shape. The proper interpretation of this S-shape should throw considerable light on the structure of cork. A knowledge of the structure of cork, in turn, will facilitate the design of corky materials for practical applications, and enable one to predict their behavior under a great variety of conditions.

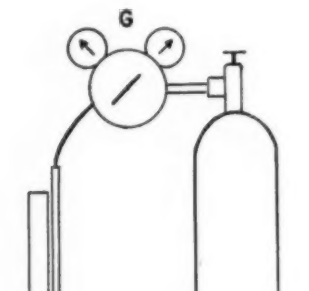

Fig. 1. Apparatus for hydrostatic compression of cork. T: high pressure tank; G: gauge and reducing valve; S: scale; C: glass capillary tube; A: compression chamber.

In this paper an attempt is made to interpret the S-shaped load-compression curve of cork as the result of the cellular structure and of the two-phase structure of cork, namely, the corky material *and* the air trapped in the cork cells. Load-compression curves were obtained in two ways: in the ordinary way, and second, by measuring the change in volume caused by hydrostatic pressure.

These two methods lead actually to somewhat different load-compression curves; their mutual relation will be explained in this paper in the section on hydrostatic curves.

DESCRIPTION OF THE EXPERIMENTAL METHOD

A. Ordinary Load-Compression Curves

These curves were obtained by means of the apparatus described in a previous paper[1] (cf. Fig. 1 there). The same sample was used to obtain the complete load-compression curves up to 70 percent compression by gradually increasing the load, and reading the corresponding compressions on the dial gauge.

B. Hydrostatic Volume-Pressure Curves

These curves were obtained on an experimental arrangement shown in Fig. 1. A cork

* Polymer Physics Laboratory, University of Notre Dame, Notre Dame, Indiana.
** Research Laboratories, Armstrong Cork Company, Lancaster, Pennsylvania.

[1] Dart and Guth, J. App. Phys. 17, 314 (1946).

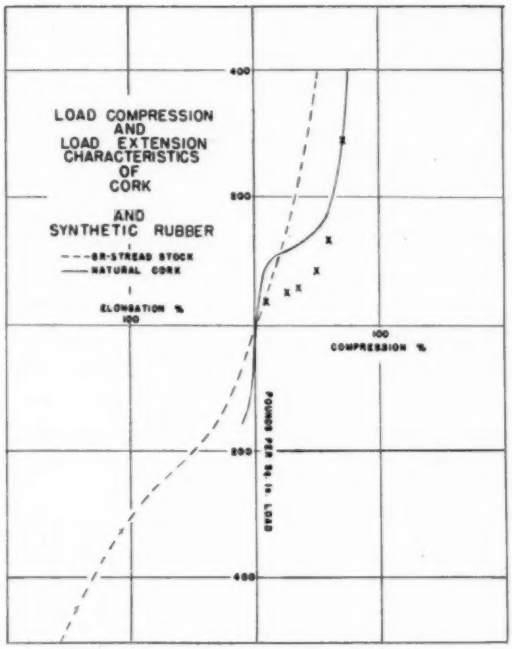

FIG. 2. Load compression and extension characteristics of cork and of GR-S tread. The crosses indicate the curve obtained by repeating the loading a second and a third time on the same sample.

sample of about six cubic centimeters volume is placed in the compression chamber which is then bolted shut. Water is then forced into the stopcock at the bottom until it rises near the top of the glass tube and scale. The stopcock is then closed and any air bubbles are made to rise to the top of the tube by tapping. Care must be taken to get all air bubbles out as they would cause an error in the volume-pressure curve. A zero reading on the scale is taken of the water level, and the whole unit is connected through a reducing valve to a high pressure tank (of nitrogen in our case). The pressure is then increased in units of 5 p.s.i. every 30 seconds, and the corresponding water-level readings on the scale are taken at the end of each 30-second period. This procedure was used in order to simulate as closely as possible the procedure used in taking an ordinary load-compression curve. The pressure was read from the reducing gauge and the volume change was calculated from the scale readings (knowing the diameter of the glass tube). It was interesting to note that there was a great deal of flow of the cork during a run, as is the case during an ordinary load-compression run. This implies that the flow is caused by the cork structure itself and not by the escape of air from the cells, which would be impossible in the hydrostatic case.

ORDINARY LOAD-COMPRESSION CURVES FOR CORK

Figure 2 represents load-compression curves obtained at the Armstrong Research Laboratories. Up to the breaking point the extension branch of this curve is also given for cork. The crosses indicate the load-compression curve for cork obtained by repeating the loading a second and a third time on the same sample. Twenty-four hours elapsed between consecutive loadings.

Figure 3 shows a somewhat more extensive study of the repeated load-compression curves carried out at Notre Dame. The consecutive curves were taken one after the other without giving time for the sample to recover. Complete hysteresis loops were obtained.

Figures 2 and 3 reveal a series of interesting features important for the interpretation of the load-compression curves.

The extension branch is monotonic. The tensile strength and breaking elongation are low. They

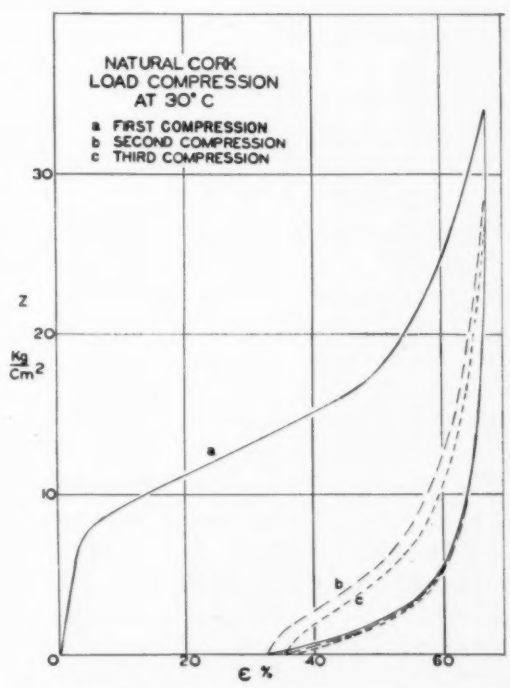

FIG. 3. Load-compression curves for repeated compressions including hysteresis loops.

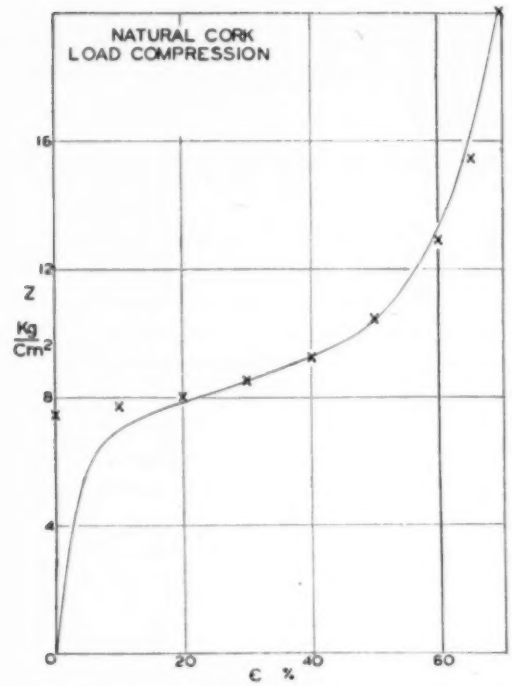

FIG. 4. Load-compression curve of cork. Crosses indicate theoretical Eq. (1) of text.

are chiefly determined by the cuts or cracks invariably present in cork, and the propagation or growth of these cracks. The tensile strength may be compared with the tear resistance of a compact material like rubber, the tear being natural and unavoidable for cork.

The compression branch shows a characteristic S-shape. On repeated compression the S-shape tends to be washed out and the curve approaches somewhat the monotonic behavior shown by GR-S tread.[2] This is shown with particular clarity in Fig. 3, but to a lesser degree in Fig. 2 because of the recovery of the sample between consecutive loadings.

A simple explanation of the S-shape may be based on the known cellular and two-phase structure of cork: the corky material (including various organic substances) constituting the cell walls and the air trapped in the cells. We notice that the knee of the compression curve occurs roughly at a compression corresponding (on inversion at the origin) to the breaking elongation, and for a load somewhat smaller than the negative of the tensile strength. On repeated stretching the knee occurs for a lower critical load. The equal order of absolute magnitude of the critical load and compression of the knee and of the tensile strength suggest that a certain breakdown of the cells may have taken place at the knee. The difference in the lowering of the knee as shown in Fig. 2 with recovery period between repeated loadings, and in Fig. 3 without a recovery period, indicates that the breakdown of the cells is partially reversible.

For the part above the knee of the compression curve we have tried a preliminary quantitative representation. That part of the compressive stress Z may be represented fairly accurately by the equation

$$(Z-a)(L-l_0)=\text{const}; \qquad (1)$$

L is the relative length, a and l_0 are constants. The quantity a should be independent of the compression, and represents the critical stress necessary for the partial destruction of the cork structure (*not* the *cells*).

The plateau after the knee is interpreted as largely caused by the failure of the resistance of the cork (through buckling of the cell walls for instance). The upward turn is interpreted as a compression of the almost incompressible part of

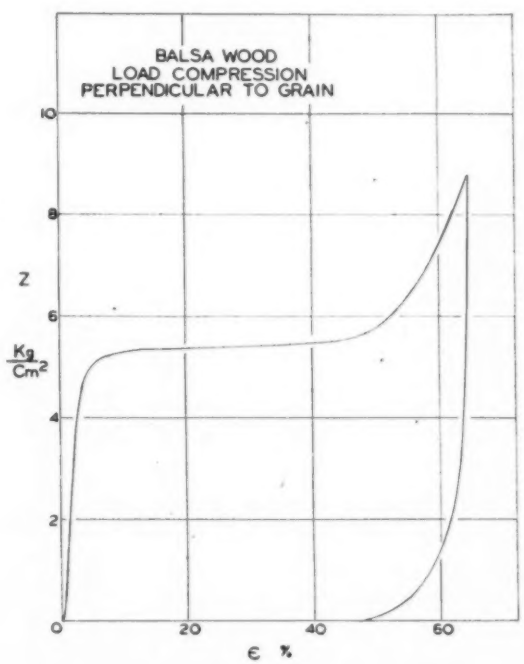

FIG. 5. Load-compression loop for balsa wood.

[2] Synthetic rubber compound containing carbon black as used for the tread surface of tires.

cork. Of course, the van der Waals b of the air comes in also. The constant on the right side of Eq. (1) should be of the order RT. According to this equation, Z should be a linear function of the temperature at constant compression (since the constant on the right side of Eq. (1) should be proportional to T)

$$Z = M(L) + N(L) \cdot T. \qquad (2)$$

This conclusion was checked in the second paper of this series by our relaxation method. Equation (1) checks well with a load-compression curve, as shown in Fig. 4. However, the true significance of this apparent agreement has not been established. For some samples the plateau above the knee was practically straight. The possible significance of this finding, at some variance with Eq. (1), needs further study.

It is interesting to note that balsa wood, when compressed perpendicular to the grain, also shows a pronounced S-shaped load-compression curve, with an almost horizontal plateau, as shown in Fig. 5. The large set (46 percent) after compression disappears almost completely when the sample is soaked in water.

LOAD COMPRESSION CURVE OF HIGHLY COMPRESSED CORK

In connection with the interpretation of the S-shaped load-compression curve it was interesting to see how a high hydrostatic pressure would change the shape of the load-compression curve. At our request Dr. P. W. Bridgman[3] was kind enough to apply to cork a pressure of 29,000 kg/cm² in isopentane. The initial dimensions of the sample on April 11, 1945, were 0.324″×0.319″ ×0.312″. After exposure to high pressure the dimensions were 0.297″×0.301″×0.283″. On February 6, 1946, the dimensions were 0.302″ ×0.306″×0.287″. In view of the magnitude of the hydrostatic pressure employed in the test, it is remarkable that the permanent set of the linear dimensions was only about 8 percent on the average immediately after the exposure. After ten months' rest the permanent set was somewhat less.

In Fig. 6 the dotted line shows the load-compression curve taken in June, 1946, on the same piece of cork which had been subjected to the high pressure by Dr. Bridgman on April 11, 1945. The full line shows the load-compression curve of Fig. 2, which was obtained on a piece of cork not previously compressed. It is seen that the initial part of the two curves is almost the same. We interpret this initial part as resulting from the initial bending of the cell walls. The comparison of the two curves exhibits nicely the fact that the cells were not crushed by the high hydrostatic pressure. The plateau of the curve for the pre-compressed sample is, however, much less developed than in the case of the previously uncompressed sample. We attribute this plateau to the failure of the resistance of the cork cells. The comparison of the two curves shows that the hydrostatic compression must have driven a large amount of the air out of the cells. The steep part of the two curves has about the same slope, as one would expect.

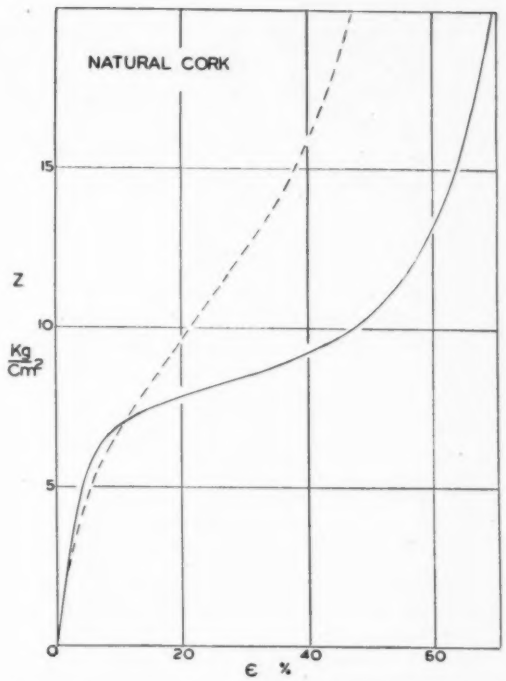

FIG. 6. Comparison of load-compression curves for cork; dashed line shows curve for sample hydrostatically compressed by P. W. Bridgman, applying a pressure of 29,000 kg/cm². Full line shows behavior of a sample which was not previously compressed.

HYDROSTATIC CURVES

It is clear from the description of this method in the first section that hydrostatic compression

[3] Jefferson Physical Laboratory, Harvard University, Cambridge, Massachusetts.

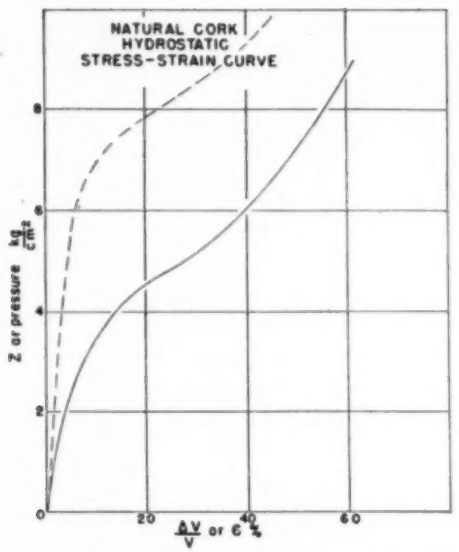

FIG. 7. Comparison of hydrostatic (full line) and ordinary load-compression (dashed line) curves for cork.

leads to a pressure-volume relationship, different from the ordinary load-compression relation. The connection between these two types of relations may be exhibited simply and quantitatively, referring to the elements of the theory of elasticity. The slope at the origin of a load-compression curve $Z=Z(\epsilon)$ is Young's modulus

$$dZ/d\epsilon=E. \tag{3}$$

Similarly, the slope at the origin of the pressure-volume relation, $P=P(V)$, is the bulk modulus K

$$VdP/dV=K. \tag{4}$$

Now according to the theory of elasticity, Young's modulus, E, and the bulk modulus K are connected as follows:

$$E=3K(1-2\mu), \tag{5}$$

where μ is Poisson's ratio (ratio between lateral contraction and longitudinal extension). Knowing E and K Eq. (5) enables us to obtain μ.

$$\mu=\tfrac{1}{2}(1-E/3K). \tag{6}$$

Figure 7 shows a hydrostatic pressure-volume change curve with the corresponding load-compression curve for cork. When inserted into Eq. (6), comparison of the slopes of the two curves yields

$$\mu=0.04. \tag{7}$$

Another method of obtaining μ is to measure the change of volume on ordinary compression. According to the theory of elasticity the following relation holds:

$$\Delta V/V=\epsilon(1-2\mu). \tag{8}$$

This relation permits one to compute μ if $\Delta V/V$ is measured for a given compression ϵ. This method, however, was not used in the present work.

ACKNOWLEDGMENT

The authors wish to express their appreciation to Mr. E. Claxton, Director of Research, and to Dr. R. B. Rohrer, Assistant Director of Research, Armstrong Cork Company, for the benefit of valuable discussions and for the support of this work.

Contributed Original Research

A Cold Cathode Rectifier

WILLARD H. BENNETT*

(Received October 21, 1946)

A cold cathode rectifier is described in which corona discharge is used at atmospheric and higher pressures in hydrogen and nitrogen free of electron-attaching impurities. This kind of tube has advantages where the current demands upon a rectifier are small.

IN the course of some experimental studies of corona discharge, methods were found for producing and maintaining conditions for free electron discharge in gases at pressures of the order of magnitude of atmospheric and higher. The very large difference in mobility between free electrons and positive ions is illustrated in Fig. 1, in which are shown the negative and positive corona current-voltage characteristics for a 1-mil tungsten wire-end discharging in hydrogen at atmospheric pressure towards a plane electrode at a distance of 3 cm. Characteristics for wire sizes between 0.4 and 3 mil, and for distances to the plane electrode between 0.3 cm and 10 cm were measured and are summarized in an earlier report.[1]

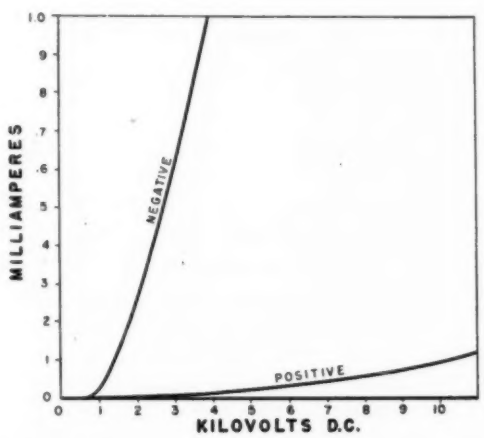

FIG. 1. Current-voltage characteristics for negative and positive corona.

As will be seen from the figure, the very large difference between the mobilities of electrons and positive ions is quite unusual for corona discharges. These can only be attained by using means for eliminating electron-attaching components from the gas in the tube to a degree estimated as less than one part per hundred million and keeping the gas free of these components to this degree.

Cold cathode rectifiers were developed taking advantage of this large difference in mobilities. It is believed that these rectifiers have peculiar advantages over conventional types of rectifiers in many applications, particularly where the

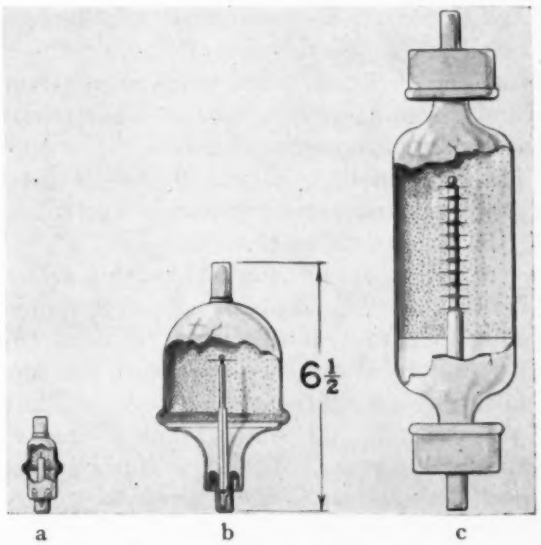

FIG. 2. Representative types of tube. (The dimension 6½ is in inches.)

* Now at the National Bureau of Standards. This work was performed in 1939–1941 at the Electronic Research Corporation, Newark, Ohio.

[1] Willard H. Bennett, Phys. Rev. **58**, 992–997 (1940), see Figs. 2 and 3, p. 994. The abscissae in those figures were incorrectly labelled and should have been "kilovolts difference" instead of "log voltage difference."

FIG. 3. A representative type of rectifier using ten tubes of the type shown in Fig. 2b. The condensers are 0.5 microfarad each and rated at 20 kilovolts d.c. each. The multiplier can be a spiral ink line resistor on a Bakelite or formica cylinder with 100 megohms per stage.

current requirements are small, and that a description of this kind of rectifiers would be of interest.

GENERAL DESCRIPTION

Some representative types of tube are illustrated in Fig. 2. In these tubes, the discharge electrodes are one- or two-mil tungsten wire-ends. The collecting electrode in each is an Aquadag coating on the glass wall shown as the shaded area in the broken sections.

The tubes in Figs. 2a and 2b are filled with hydrogen at atmospheric pressure. The tube in Fig. 2c is filled at eight atmospheres with 30 percent hydrogen and 70 percent nitrogen.

Because there is no filament heating requirement with a tube of this kind, rectifiers built using these tubes are simpler, lighter, and more compact, than rectifiers using conventional types of tubes. As an illustration, Fig. 3 shows a rectifier supplying 100 kilovolts using a 10 kilovolt transformer in a Cockcroft-Walton circuit. In this kind of circuit, if conventional types of tubes were used, the need for filament heating current at each stage would make necessary a filament transformer with high voltage insulation between primary and secondary for each stage. Such a requirement would make necessary a bulkier and more complicated equipment than that shown in Fig. 3.

There is no requirement for filament heat-up time and no devices are needed for tube protection on this account.

Rectifiers can readily be designed with clips for holding the tubes so that simply reversing the tubes in the clips reverses the output polarity of the rectifier.[2]

Although these tubes do not waste electric power in heating a filament, they suffer from loss of efficiency from another cause. Under normal conditions of operation, there is a small positive-ion current on the reverse half-cycle. This effect together with the fact that even the high free electron mobilities are not sufficient to give as high current densities as are obtainable with electrons in vacuum, has served to hold these tubes to an efficiency of about 20 percent to 50 percent which is lower than most conventional types of rectifier unless no greater output currents are required than can be adequately supplied by these cold cathode tubes.

In Figs. 4 and 5 are shown some efficiency data taken on a rectifier using the type of tube shown in Fig. 2c. In Fig. 4, the transformer supplies 10 kilovolts a.c., and in Fig. 5, the supply is 20 kilovolts a.c. Observations were obtained for hydrogen (shown with full lines) and a mixture of 30 percent hydrogen and 70 percent nitrogen (shown with dashed lines). War work prevented completing these data, but from some observations in a single wire experimental tube, a good estimate was obtained for 20 percent deuterium and 80 percent nitrogen (shown with the dotted lines). From mobility data[3] it is to be expected that the efficiency would be still higher for a mixture of 5 percent deuterium and 95 percent nitrogen. For comparison purposes, representative curves for a vacuum-tube rectifier are included.

PREPARATION OF A TUBE

As discharge electrodes, wire-ends with any diameter between about 0.4 mil and 3 mils seem

[2] Additional engineering data is given in Trans. A.I.E.E. **64**, 164–7 (1945); and Electronics Industries, p. 106 (November, 1945).

[3] W. H. Bennett and L. H. Thomas, Phys. Rev. **62**, 41–47 (1942).

to be about equally effective. The reason for this is that in the initial conditioning of the tube, there is an etching of the wire-ends to a sharp conical tip whose radius of curvature is of the order of magnitude of 0.2 mil.[4] In tubes containing six or more wire-ends, the maximum number that can usefully be grouped with bases adjoining is six, and even with six wires in a group, the maximum current per wire-end that can be drawn without arc-over is less than six times the current that could be drawn from a single wire, the other electrode spacings being the same but the other five wires removed. The discharge spreads laterally from a wire-tip and adjacent discharges interfere with each other to some extent.[5]

It is important that the electric field diverge all the way to the collecting electrode. Aquadag or metal collecting electrodes can be used.

After filling the tube with gas and sealing the tube, a.c. voltage is applied directly. The resulting discharge eliminates the electron-attaching impurities and sharpens the wire-ends, slowly at first. The current rises quite rapidly during the last stages of the conditioning, however, and unless a circuit breaker is used in the a.c. supply, the tube may be greatly over-heated.

This does not complete the conditioning. If the tube is allowed to stand, it will probably decondition to some extent after a day, that is, the electron mobilities will have decreased by a large amount. This is probably caused by the liberation into the gas of some electron-attaching impurities from the walls of the tube and from the electrodes. For this reason, immediately following the first run-up, the tube is put on a reduced a.c. voltage sufficient to maintain a current of about 100 microamperes per wire. After about three hours, the tube is permanently conditioned.

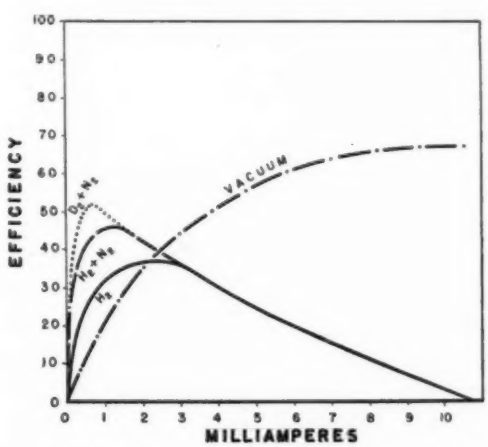

FIG. 4. Efficiency with 10 kv a.c., applied.

[4] Willard H. Bennett, Phys. Rev. **61**, 55 (1942). See also reference 1.

[5] Willard H. Bennett, Phys. Rev. **61**, 53–56 (1942).

OPERATION

One of the convenient features of this kind of tube is that the full rated voltage can be thrown on without any preliminaries.

There is a definite output voltage at which a tube arcs over and the maximum d.c. output rating of the tube can be given as about 10 percent under that value. The tube never "arcs-back" at unexpectedly low voltages as some of the conventional mercury vapor tubes do occasionally.

There is no observable consumption of discharge electrodes or other materials in these tubes and there is no known reason for these tubes to have other than an indefinitely long life when operated within the ranges of rated current and voltage.

Surges in the high voltage a.c. supply, caused by opening or closing the primary circuit, cannot puncture the tube with cold emission because the tube is filled with gas.

The small positive-ion current on the inverse half-cycle serves a useful purpose. When the output of the rectifier is being smoothed with a condenser, resetting the input a.c. voltage to a

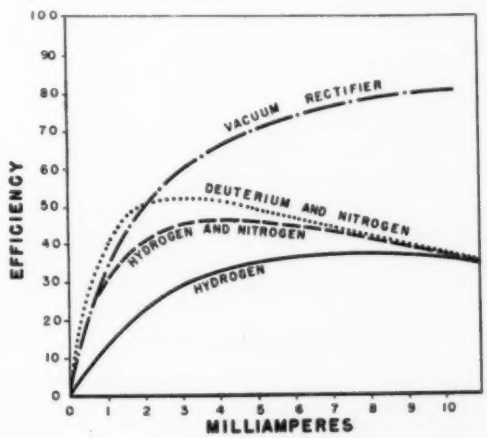

FIG. 5. Efficiency with 20 kv a.c., applied.

lower value results in the condenser voltage dropping correspondingly because of the positive-ion current in the tube.

As long as the rated inverse voltage is not exceeded with these tubes, no damage results from drawing more than the rated current through the tubes momentarily. The only damage that eventually occurs is caused by over-heating the tube as a whole and this takes at least several minutes for all types of tubes. The largest tubes, containing part nitrogen, decondition at currents of about 0.2 milliampere per wire because of a slow formation of ammonia. Operation at 0.06 milliampere per wire slowly disassociates the ammonia and reconditions the tube.

At the higher values of current, ionization by collision occurs between the sheath and the collector in a tube and a high pressure glow discharge makes its appearance. This glow discharge has a positive resistance characteristic for currents up to a higher order of magnitude than the limiting current for the corona discharge, and is not to be confused with normal high pressure arcs. This is not a disruptive kind of arc (that is, it is not abruptly initiated with a streamer and a spark) because of the absence of electron-attaching gaseous components.[6]

In tubes containing part nitrogen, at currents of the order of ½ milliampere per wire-end, the wire-ends become heated, and at currents of between 1 and 5 milliamperes per wire-end, the wire-ends attain temperatures as high as 2000°C. The energy necessary to produce these temperatures cannot be accounted for by the impact energies of positive ions striking the wire-ends following their last free paths. Such heating does not occur in discharges in pure hydrogen at the same currents.[7] It appears that either an active state of nitrogen, or else an excessive concentration of atomic hydrogen caused by the presence of nitrogen, is produced in the ionization sheath and is responsible for this excessive heating which occurs only in part nitrogen.

When the wire-ends heat to more than about 1000°C, a reduction in sheath drop in potential[1] occurs both for positive and negative discharge because of the thermal reduction in gas density immediately adjacent to the wire-end. There is a corresponding reduction in arc-over voltage for the tube on the inverse half-cycle. This effect is reduced by using the finest wires (0.4 mil) but is not entirely overcome by this means.

CONCLUSION

It is not believed that the full potentialities of this kind of discharge in a rectifier have been realized. Further studies of the diffuse kinds of arcs which occur in these gases should prove profitable. It is thought that a wider appreciation of the advantages of a cold cathode gas-filled rectifier may bring an increased interest in studies of the properties and methods for control of these arcs.

[6] Willard H. Bennett, J. App. Phys. **13**, 199–200 (1942). William H. Otto and Willard H. Bennett, J. Chem. Phys. **8**, 899–903 (1940).

[7] Willard H. Bennett, Phys. Rev. **62**, 369–371 (1942).

The Hydrodynamic Lubrication of Finite Sliders

CHARLES P. BOEGLI
Springfield, Ohio

(Received December 17, 1946)

Two approximations are made in the solution of Reynolds' lubrication equation for the case of a finite slider. These approximations lead to a series of equations that are easy and rapid to use for flat sliders, and which are also applicable to curved sliders. Examples of their use are presented, and a number of calculations are made to determine the range of slider proportions to which they may be applied with sufficient accuracy. The method is of special value for wide sliders which are difficult or impossible to analyze by other methods.

INTRODUCTION

THE solution of the basic Reynolds differential lubrication equation for the case of a slider bearing of finite width has always been beset with great difficulties. Reynolds[1] did not succeed in finding a general solution to the

[1] O. Reynolds, "On the theory of lubrication and its application to Mr. Beauchamp Tower's experiments," Phil. Trans. Roy. Soc. **177**, part 1, 157–234 (1886).

equation, and it was not until nineteen years after his presentation that Michell[2] provided a satisfactory attack to the problem.

Michell's method involves no assumptions that affect the accuracy of the solution for the specified conditions. It is, however, applicable only to sliders with flat surfaces, and even for such simple cases the solution is so tedious that only a very small amount of data has yet been computed. R. O. Boswall, working with an assumption credited to Stodola, succeeded in developing an approximate method[3] that gives results negligibly different from those of the exact method in cases where comparisons are possible. Here again the analytical solution can only be made for flat sliders; for other shapes resort is had to a graphical method that actually consists in estimating by eye the shape of one of the pressure distribution curves.

More recently, Muskat, Morgan, and Meres published another solution to the original differential equation.[4] They presented their solution as a series of graphs that serve better for the solution of problems of operation than problems of design. Again, only bearings with flat surfaces are considered.

There is great need for a set of equations that will provide, with a minimum of effort, a good approximation to the actual behavior of a wider variety of sliders than can now be handled. The need for a very high degree of accuracy is, for several reasons, not great. One reason is that it is never possible to predict closely the behavior of the viscosity of the lubricant as it passes through the bearing; the assumption of constant viscosity is generally made, and the practical value of the solution is limited by this approximation. Also, it would be very difficult actually to construct a bearing in exact conformity with a specified design; such a small difference, for example, as a slight rounding of the leading edge, would have considerable effect upon the performance. Therefore, a solution that predicts to a fair degree of accuracy the performance of a great many types of slider bearings would be at least as valuable as one that predicts very closely the performance of only a narrow range.

Such a solution is provided through two simple assumptions. The first is that used by Boswall in his derivation of an approximate method; namely, that the pressure functions along the length and width of the slider are independent. The second is that the pressure function along the length of the slider (that is, the dimension in the direction of motion) is the *same as that for an infinite slider.*

This paper presents analyses based upon these two assumptions; an analytical solution for the case of the flat slider and an arithmetical method for curved sliders. Since with any approximate method some estimate of the accuracy and range of applicability is desirable, the report also presents a comparison of the results obtainable with the new method to any available data found in other manners.

ANALYSIS

The general differential equation of Reynolds serves as the starting point for this analysis of slider lubrication.

$$\frac{\partial}{\partial x}\left(\frac{1}{\mu}\frac{\partial P}{\partial x}h^3\right)+\frac{\partial}{\partial z}\left(\frac{1}{\mu}\frac{\partial P}{\partial z}h^3\right)=6\frac{d}{dx}Uh. \quad (1)$$

In this equation μ, h, U, and P are the oil viscosity, the oil-film thickness, the slider velocity, and the oil pressure at any point on the slider surface. If the substitutions are made:

$$x=x_0+Lx_1,$$
$$z=Bz_1,$$
$$h=h_0\beta,$$

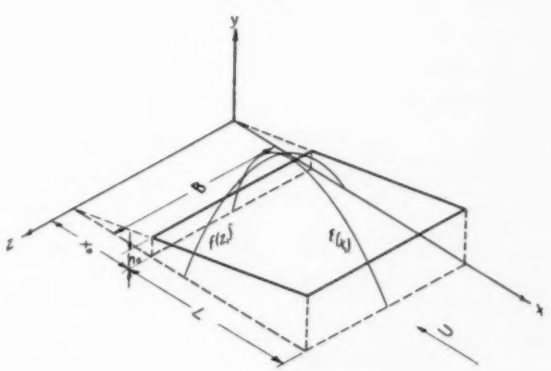

FIG. 1.

[2] A. G. M. Michell, "The lubrication of plane surfaces," Zeits. f. math. Physik **50**, 1073–1099 (1904).

[3] R. O. Boswall, *The Theory of Film Lubrication* (Longmans, Green, and Company, New York, 1928), pp. 141–158.

[4] Muskat, Morgan, and Meres, "Studies in lubrication. VII. The lubrication of plane sliders of finite width," J. App. Phys. 11, 208–219 (March 1940).

where L and B are the length and width of the slider, h_0 represents the oil-film thickness at the outlet edge, and β is a function of x_1 (see Fig. 1); and if viscosity is assumed constant, the equation becomes

$$\frac{\partial}{\partial x_1}\left[\beta^3\frac{\partial P}{\partial x_1}\right]+N^2\beta^3\frac{\partial^2 P}{\partial z_1^2}=A\frac{d\beta}{dx_1}. \tag{2}$$

In Eq. (2), N is the ratio of slider length to slider width (L/B) and A is the product $6\mu UL/h_0^2$ containing all the dimensional terms. The new variables x_1 and z_1 are the fractional distances along the length and width of the slider, and range in value from 0 to 1.0.

It will now be assumed, following the method in reference 3, page 141, that the pressure at any point can be expressed as the product of two functions

$$P=A\cdot f(x_1)\cdot f(z_1). \tag{3}$$

This product is substituted for P in Eq. (2), yielding

$$\frac{\partial}{\partial x_1}\left[\beta^3 f(z_1)\frac{df(x_1)}{dx_1}\right]+N^2\beta^3 f(x_1)\frac{d^2 f(z_1)}{dz_1^2}=\frac{d\beta}{dx_1}. \tag{4}$$

To find the form of $f(z_1)$ Eq. (4) is solved along the line where $f(x_1)$ is a maximum; that is, where $df(x_1)/dx_1$ is zero. This yields

$$\frac{d^2 f(z_1)}{dz_1^2}+\frac{\left[\dfrac{1}{f(x_1)}\dfrac{d^2 f(x_1)}{dx_1^2}\right]_{x_m}}{N^2}f(z_1)=\frac{\left[\dfrac{1}{\beta^3 f(x_1)}\dfrac{d\beta}{dx_1}\right]_{x_m}}{N^2}, \tag{5}$$

in which x_m indicates the value of x_1 for which $f(x_1)$ is a maximum. This equation can be simplified by considering that since $f(x_1)$ is the same as that for an infinite slider, this being the second basic assumption, this function was derived from the differential equation

$$\frac{d}{dx_1}\left(\beta^3\frac{dP}{dx_1}\right)=A\frac{d\beta}{dx_1},$$

which, upon substitution of $P=A\cdot f(x_1)$ and performance of the indicated differentiation, gives

$$3\beta^2\frac{df(x_1)}{dx_1}+\beta^3\frac{d^2 f(x_1)}{dx_1^2}=\frac{d\beta}{dx_1}.$$

Where $f(x_1)$ is a maximum, this equation shows that

$$\left[\frac{d^2 f(x_1)}{dx_1}\right]_{x_m}=\left[\frac{1}{\beta^3}\frac{d\beta}{dx_1}\right]_{x_m} \tag{6}$$

and consequently Eq. (5) is reduced to

$$\frac{d^2 f(z_1)}{dz_1^2}+\frac{M}{N^2}f(z_1)=\frac{M}{N^2}$$

where M is equal to the expression on either side of Eq. (6) divided by $f(x_m)$. The solution is

$$f(z_1)=1-\left(\frac{e^n-1}{e^n-e^{-n}}\right)(e^{-nz_1}+e^{-n(1-z_1)}), \tag{7}$$

where

$$n^2=-\frac{M}{N^2}.$$

Up to this point the treatment has been general, and applicable to both flat and curved sliders. In the case of flat sliders,

$$\beta=1+bx_1$$

and

$$M=-\tfrac{1}{2}\frac{(b+2)^4}{(b+1)^2}$$

while $f(x_1)$ is simply[5]

$$f(x_1)=\frac{bx_1(x_1-1)}{(b+2)(bx_1+1)^2}. \tag{8}$$

For curved sliders, an arithmetic or graphical evaluation of $f(x_1)$ is usually preferred to an analytical solution. Such methods result in a series of tabulated values of the function for various values of x_1, and it is necessary to find x_m and $f(x_m)$ from this table. An excellent method of finding the required values is presented in *Empirical Formulas*.[6] To evaluate n, the value of M must be known; it can be calculated from the expression on the right side of Eq. (6), which is to be preferred to the quantity on the left, because the former does not require the finding of second derivatives from graphical data.

The important equations and constants are

[5] Reference 3, page 44.

[6] T. R. Running, *Empirical Formulas* (John Wiley and Sons, Inc., New York, 1917), pp. 100–113.

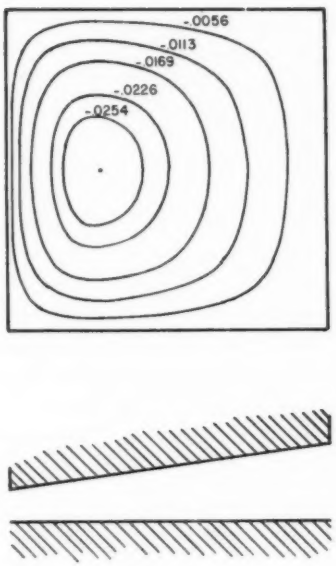

FIG. 2.

summarized below:

$$P = A \cdot f(x_1) \cdot f(z_1) \tag{3}$$

$$f(z_1) = 1 - \left(\frac{e^n - 1}{e^n - e^{-n}}\right)(e^{-nz_1} + e^{-n(1-z_1)}) \tag{7}$$

$$f(x_1) = \frac{bx_1(x_1 - 1)}{(b+2)(bx_1+1)^2} \quad \text{for flat sliders only} \tag{8}$$

in which

$$A = \frac{6\mu UL}{h_0^2}$$

$$n^2 = -\frac{M}{N^2}$$

$$M = \left[\frac{1}{f(x_1)}\frac{d^2f(x_1)}{dx_1}\right]_{x_m} = \left[\frac{1}{\beta^2 f(x_1)}\frac{d\beta}{dx_1}\right]_{x_m}$$

$$= -\tfrac{1}{2}\frac{(b+2)^4}{(b+1)^2} \quad \text{for flat sliders only}$$

$$N = L/B.$$

EXAMPLES OF FLAT-SLIDER ANALYSIS

To illustrate briefly the use of the equations, let it be desired to analyze the lubrication of a slider for which $N=1.0$ and $b=1.5$. For this slider, $M=-12.0$ and n is thus found to be 3.46. The pressure functions are then

$$f(x_1) = \frac{1.5x_1(x_1-1)}{(3.5)(1.5x_1+1)^2}$$

$$f(z_1) = 1 - 0.97(e^{-3.46z_1} + e^{-3.46(1-z_1)}).$$

Graphs of these two functions can be drawn, and by finding curves of constant $f(x_1)\cdot f(z_1)$ the isobars over the slider surface can be located. This has been done in Fig. 2. The numbers on the isobars are values of $f(x_1)\cdot f(z_1)$. The actual pressure at each isobar is, of course, this value of $f(x_1)\cdot f(z_1)$ multiplied by the quantity A.

For the case of wide sliders, where N becomes small, the analysis by means of the rigorous equations, or even by the approximate treatment in reference 3 becomes more difficult, but that with the new equations becomes simpler. For a slider where $N=0.01$ and $b=1.5$, M is still -12.0 but n is now 346. Then,

$$f(z_1) = 1 - (e^{-346z_1} + e^{-346(1-z_1)}).$$

It is observed that the value of this function, although zero at $z_1=0$ and 1.0, rises very rapidly to 1 between these endpoints; at $z_1=0.02$ or 0.98, for example, the value of $f(z_1)$ is 0.999. The function $f(z_1)$ may therefore be considered as a correction to be applied to the ends of a slider which would otherwise be considered infinite. Under such conditions, the value of $f(z_1)$ should be directly dependent upon z_1/N, the actual width represented by z_1; that this is actually the case is illustrated by finding the point at which $f(z_1)=0.999$ for a slider for which $N=0.0001$ and $b=1.5$. This value turns out to be $z_1=0.0002$, which is 0.01 times that for a slider of $N=0.01$. Since, however, this second slider is 100 times as wide, the actual distance from the ends of both sliders to the points at which $f(z_1)=0.999$ is the same. This type of relationship in fact exists up to the point where the quantity

$$(e^n - 1)/(e^n - e^{-n})$$

becomes significantly different from 1.0.

EXAMPLE OF CURVED-SLIDER ANALYSIS

For purposes of illustration, a slider will be analyzed for which $\beta = (2.50)^{x_1}$ and $N=0.5$. The

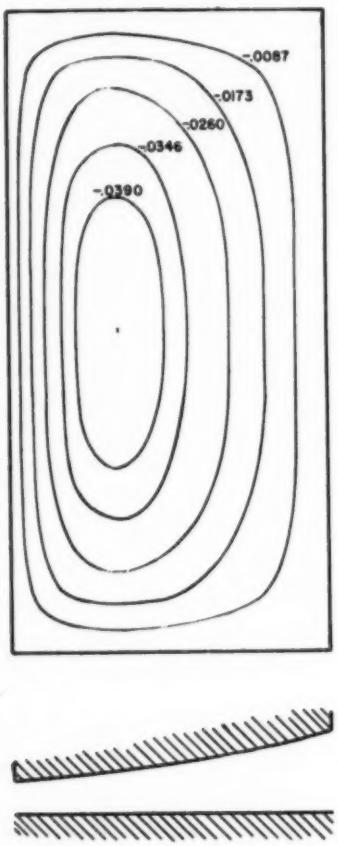

FIG. 3.

customary approximate method leads to a series of values for $f(x_1)$:

x_1	β	$f(x_1)$
0.0	1.000	0.0000
0.1	1.096	−0.0273
0.2	1.201	−0.0414
0.3	1.316	−0.0466
0.4	1.443	−0.0459
0.5	1.582	−0.0414
0.6	1.733	−0.0349
0.7	1.899	−0.0273
0.8	2.081	−0.0192
0.9	2.281	−0.0112
1.0	2.500	0.0000

By the use of Lagrange's interpolation formula, x_m is found to be 0.338 and $f(x_m) = -0.0470$. At this point $\beta = 1.363$ and $d\beta/dx_1 = 1.249$

$$M = \frac{1.249}{(-0.0470)(1.363)^3} = -10.50.$$

The value of n is then

$$n = (10.50)^{\frac{1}{3}}/0.5 = 6.482.$$

All the necessary constants have now been calculated. The shapes of the isobars over the surface are illustrated in Fig. 3. The value marked on each isobar gives, when multiplied by A, the magnitude of the pressure at that isobar.

TABLE I.

	$b=1.0$			$b=2.0$		
N	W/W_∞ (new)	W/W_∞ (actual)	Error %	W/W_∞ (new)	W/W_∞ (actual)	Error %
0	1.000	1.000	0	1.000	1.000	0
0.5	0.687	0.695	−1.2	0.735	0.714	2.9
1.0	0.421	0.434	−3.0	0.493	0.460	7.2
1.5	0.259	0.279	−7.2	0.322	0.297	8.4
2.0	0.168	0.185	−9.2	0.219	0.208	5.3

APPLICABILITY OF EQUATIONS

Although the new equations are especially useful in analyzing cases that are difficult or impossible to solve by the more exact and involved methods, the only available accurate data are for flat sliders, and these must consequently serve as a basis for estimating the accuracy of the solutions obtained by the new method. The comparison thus made is presumed to hold also for curved sliders.

W/W_∞ Ratio

By W/W_∞ ratio is designated the ratio of the total load carried by the slider to that which would be carried by an equal length of an infinitely wide slider. Since $f(x_1)$ in the new equations is the same as that for an infinite slider, the W/W_∞ ratio is merely the integral of $f(z_1)$ (Eq. (7)), which is

$$\frac{W}{W_\infty} = 1 - \frac{2}{n}\frac{(1-e^{-n})^2}{(1-e^{-2n})}. \qquad (12)$$

Values computed from this equation are compared to those computed by Michell's method for $b=1.0$ and 2.0 in reference 3, page 137 (Table I).

TABLE II.

$b=2.0$	N	D (new)	D (actual)	Error %
	0	−0.0246	−0.0246	0
	0.5	−0.0181	−0.0175	3.4
	1.0	−0.0122	−0.0113	8.0
	1.5	−0.0079	−0.0073	8.2
	2.0	−0.0054	−0.0051	5.9

It will be shown later that the error in the W/W_∞ ratio is of the same magnitude as that in many other derived characteristics of the slider bearing. Figure 4 compares values of W/W_∞ obtained with the new equations to those found by several investigators with various methods, for $N=0.5$, 1.0, and 2.0. The values due to Kingsbury are from "Optimum Conditions for Journal Bearings"[7] and those credited to Muskat, Morgan, and Meres were actually found by a series of graphical calculations with the charts in *Lubrication*,[8] pages 162–66. The latter cannot therefore be considered extremely accurate, but they extend over a greater range than the other published values.

It can be seen that the ratio given by the new equations is in good agreement with those computed by other methods.

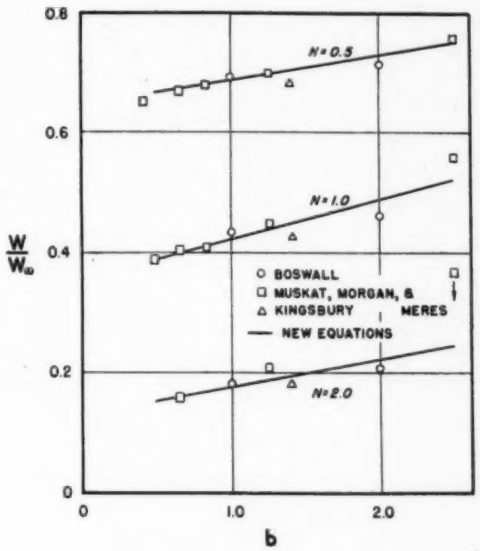

FIG. 4.

Total Load

The total load carried by the slider is given by the expression

$$W=ALBD,$$

following the notation of Boswall. The new method yields, for the value of D,

$$D=\int_0^1 f(z_1)dz_1 \int_0^1 f(x_1)dx_1,$$

because the variables x_1 and z_1 are independent. Comparison of the values of D from the new and from the Michell solution is sufficient because the factors A, L, and B are the same for both methods. The accurate data are again obtained from reference 3, page 137 (Table II). It could have been expected that the error in total load be somewhat greater than that in W/W_∞ ratio, because here the variation of $f(x_1)$ from the actual form is also taken into account. Nevertheless, the accuracy is still surprisingly good.

TABLE III.

$b=2.0$	N	$\bar{x}_1$ (new)	$\bar{x}_1$ (actual)	Error %
	0	0.392	0.392	0
	0.5	0.392	0.386	1.5
	1.0	0.392	0.374	4.9
	1.5	0.392	0.359	10.5
	2.0	0.392	0.341	12.6

Center of Pressure ($\bar{x}_1$)

The center of pressure is the value of x_1 at which the integrated effect of the pressure is directed. It is thus the line along which the slider would be pivoted. This depends, in the new method, only upon $f(x_1)$ which keeps the same form regardless of N. The value of $\bar{x}_1$ is therefore a constant depending only upon b, and is equal to $\bar{x}_1$ for an infinite slider. It is, of course, known that the value of $\bar{x}_1$ is actually dependent upon N, but the error introduced by assuming it constant remains to be found. The actual values are obtained from the same source previously quoted (Table III). The error in $\bar{x}_1$ is still not excessively great, and the assumption of the constant value would lead to no serious difficulty in most cases.

TABLE IV.

$b=2.0$	N	H (new)	H (actual)	Error %
	0	1.82	1.82	0
	0.5	2.00	2.02	−1.0
	1.0	2.30	2.38	−3.4
	1.5	2.74	2.83	−3.2
	2.0	3.23	3.32	−2.7

[7] Albert Kingsbury, "Optimum conditions for journal bearings," Trans. ASME RP-54-7, **54**, 123–148 (1932).
[8] A. E. Norton, *Lubrication* (McGraw-Hill Book Company, Inc. New York and London, 1942), pp. 162–166.

TABLE V.

$b=2.0$	N	V_0 (new)	V_0 (actual)	Error %
	0	0.288	0.288	0
	0.5	0.225	0.227	−0.9
	1.0	0.169	0.172	−1.8
	1.5	0.126	0.130	−3.1
	2.0	0.100	0.115	−14.0
$b=2.0$	N	V_1 (new)	V_1 (actual)	Error %
	0	0.288	0.288	0
	0.5	0.313	0.313	0
	1.0	0.306	0.299	2.3
	1.5	0.274	0.262	4.7
	2.0	0.240	0.245	2.0

TABLE VI.

$b=2.0$	N	W/W_∞	D	$\bar{x}_1$	H	V_1	V_0
	0	0	0	0	0	0	0
	0.5	2.9	3.4	1.5	−1.0	0	−0.9
	1.0	7.2	8.0	4.9	−3.4	2.3	−1.8
	1.5	8.4	8.2	10.5	−3.2	4.7	−3.1
	2.0	5.3	5.9	12.6	−2.7	2.0	−14.0

Frictional Force

In reference 3, page 145, the frictional resistance is given by the equation

$$R=W\left(\frac{\mu_0 U}{W_1}\right)^{\frac{1}{2}}H,$$

where H is an expression involving integrals of $f(x_1)$ and $f(z_1)$. As in the case of total load, a comparison of values of H is sufficient, since the remaining terms are identical for both methods (Table IV). Here, the error is very small indeed.

Quantity of Lubricant

The following expressions are given for the quantity of lubricant in reference 3:

$$V_1=\tfrac{1}{2}(6D)^{\frac{1}{2}}\left[\beta_1-\frac{{\beta_1}^3}{\epsilon}G_1\int_0^1 f(z_1)dz_1\right]$$

where

$$G_1=\left[\frac{df(x_1)}{dx_1}\right]_{x_1=1},$$

$$V_0=\tfrac{1}{2}(6D)^{\frac{1}{2}}\left[1-G_0\int_0^1 f(z_1)dz_1\right]$$

where

$$G_0=\left[\frac{df(x_1)}{dx_1}\right]_{x_1=0}.$$

V_1 and V_0 are the inlet and outlet quantities, respectively. Substitution of the proper values into these equations yields the results given in Table V. The error in V_0 is too large at $N=2.0$ but is certainly sufficiently small at $N=1.5$. The error in V_1 is small enough over the entire considered range of N.

Estimation of Error

It was noted previously that the value of W/W_∞ is very easily calculated by the new method, and it would be desirable to use the error in this quantity as a criterion of the accuracy of the method. For purposes of comparison, then, the errors are tabulated in Table VI. It is considered that the W/W_∞ ratio forms a fair, if not slightly pessimistic, criterion of the accuracy of D, H, and V_1, while for $\bar{x}_1$ and V_0 the error is likely to be greater in magnitude than that estimated from W/W_∞ when N becomes large. For the great majority of sliders, for which $N\leqslant 1.0$, the W/W_∞ criterion is satisfactory.

Since Fig. 4 shows good agreement between actual and computed W/W_∞ ratios even at $N=2.0$, it can be concluded that the new equations hold with good accuracy for all sliders for which N is 1.0 or less, and they provide an excellent basis for estimating the behavior of even narrower sliders.

ACKNOWLEDGMENTS

The original work on this project was carried out at the National Advisory Committee for Aeronautics, Aircraft Engine Research Laboratory, Cleveland, Ohio, and was published as ARR E4122. The present report constitutes a refinement in treatment and a considerable expansion of that work.

The assistance of Miss Thelma Bresser in reading the proofs is gratefully acknowledged.

Letters to the Editor

Measurements of Base Pressure on a Missile in Free Flight*

F. K. Hill and R. A. Alpher
Applied Physics Laboratory, The Johns Hopkins University, Silver Spring, Maryland
February 24, 1947

In a series of experiments now under way, missiles of simple geometry (see Fig. 1), differing only in length, are rocket-launched to supersonic velocities; telemetering installed in the missiles transmits to a ground receiver the aerodynamic data measured during flight. Among the significant data being obtained are base pressures; such data are important in the extrapolation of wind-tunnel studies on models to full-scale performance of missiles, where large Reynolds numbers are encountered under ordinary atmospheric conditions.

The missiles have a 14-caliber ogival nose joining tangentially to a cylindrical body of 4-inch diameter, the base of the cylinder being flat and closed. Four fins of bi-convex section are added to give flight stability. The yaw of the missile (in the plane including the missile axis and base pressure measurement port) with respect to the flight path is determined by differential pressure measurements near the nose tip. These differential pressure measurements may be correlated with yaw by means of laboratory experiments in an open supersonic jet or in wind tunnels, as well as by calculations based on linearized supersonic flow theory. It is found in these experiments that the yaw angles encountered are of the order of 1° or less and that no measurable effects caused by angle of attack are observed on base pressure data here reported. Missile velocities are obtained both by an optical tracking system and by stagnation pressure measurement on the missile with a Pitot tube.

Base pressures were measured at a 0.040″ port located ½″ from the center line of the missile. Observed base pressures were converted to pressure coefficients by dividing them by the dynamic head (namely, ½×density×velocity²); corrections caused by change in altitude during flight were made. Coefficients thus computed are shown (Fig. 2) for missiles of the first two lengths of the series to be studied. It is to be noted that the coefficients show at most a small variation with Mach number in the supersonic range covered by the tests, where the value is about 0.3. This result is significantly different from previously used theoretical values.[1] While present information indicates that pressure is essentially independent of position on the base of such missiles, an experimental check of this will be made in free flight.

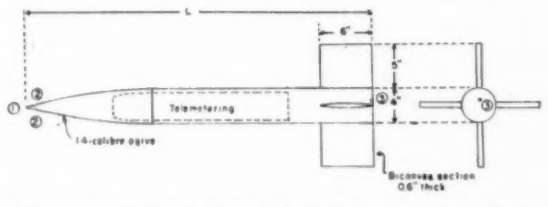

Fig. 1. Scale effect test missile. Telemetering to record: (1) Pitot tube stagnation pressure, (2) differential pressure at nose ports, (3) base pressure at port ½″ from center. All pressure ports in the same plane through missile axis.

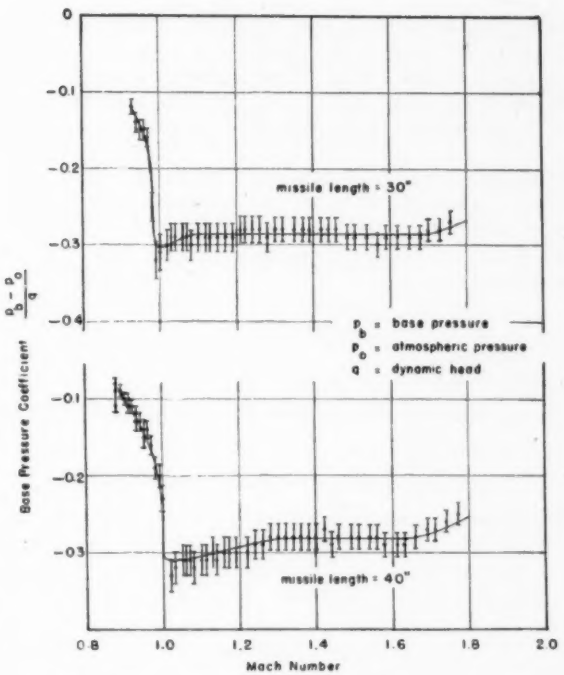

Fig. 2. The probable errors indicated are based upon fairly well-known inaccuracies in the determination of the dynamic head and static pressure throughout flight, and an assumed inaccuracy in the telemetering records based on laboratory tests. All errors are believed to be random.

Similar missiles with lengths up to 120″, as well as a series differing only in diameter, and a series of homologous models, are to be studied, with maximum velocities corresponding to Mach number 3.

This study is part of a general investigation of scale effects which is to be reported in detail after completion of all the tests. It provides the first direct measure of base pressure on such high speed missiles.

* Work being performed by a group under contract NOrd 7386 with the Bureau of Ordnance, U. S. Navy.
[1] 0.2 given by von Kármán and Moore, Trans. ASME **54**, 303 (1932).

Direction of Maximum Crystal Elongation during Metal Cutting

G. H. Townend
Metropolitan-Vickers Electrical Company, Ltd., Manchester, England
March 17, 1947

In an interesting paper by Dr. M. E. Merchant on "Mechanics of the Metal Cutting Process,"[1] an error was made in the expression connecting shear angle, rake angle, and direction of maximum crystal elongation (Eq. (1), page 269). I have written to Dr. Merchant and he confirms the new expression derived below.

Let α = rake angle,
ϕ = the angle between the shear plane and the surface of the workpiece.

Consider a section of the workpiece $ABCD$ such that $\angle CBD = 90°$. Then after shearing this section will become the parallelogram $BFEC$. The dimension perpendicular to the shear plane must be unchanged during shearing.

$$\therefore \quad BD = BH = a.$$

Consider a line CG in the chip making an angle ψ with the plane of shear. Then the corresponding line in the workpiece is DJ. The condition that CG shall be the direction of maximum crystal elongation is that CG/DJ is a maximum.

$$CG = a \operatorname{cosec}\psi,$$
$$DJ = \{a^2 + (a\cot\phi - a\cot\psi + a\tan\langle\phi-\alpha\rangle)^2\}^{\frac{1}{2}}.$$

The condition is that

$$\{\sin^2\psi + (\cot\phi\sin\psi - \cos\psi + \tan\langle\phi-\alpha\rangle\sin\psi)^2\}^{-\frac{1}{2}}$$

is a maximum. That is,

$$\sin^2\psi + \{\sin\psi(\cot\phi + \tan\langle\phi-\alpha\rangle - \cos\psi\}^2$$

is a minimum. Let

$$\cot\phi + \tan\langle\phi-\alpha\rangle = \epsilon,$$
$$\epsilon^2\sin 2\psi - 2\epsilon\cos 2\psi = 0.$$

If $\epsilon \neq 0$

$$2\cot 2\psi = \epsilon,$$
$$2\cot 2\psi = \cot\phi + \tan\langle\phi-\alpha\rangle.$$

Alternatively it is easily shown that a circle on the workpiece becomes an ellipse on the chip and that the principal axes of the ellipse make an angle ψ with the shear plane, where

$$2\cot 2\psi = \cot\phi + \tan\langle\phi-\alpha\rangle.$$

[1] J. App. Phys. **16**, 267 (1945).

Here and There

Printing Electronic Circuits

According to a recent release from the National Bureau of Standards prepared by Cledo Brunetti and Philip J. Franklin, new techniques, developed by the National Bureau of Standards in cooperation with electronic manufacturers, for electronic devices promise to simplify production methods and to accelerate the manufacture of cheaper, more compact, and more uniform electronic equipment. These techniques, representing the perfection of a method of printing wiring and circuit components on an insulated surface, is one of the new processes and techniques evolved from research and development during the war.

The methods are applicable in the design of numerous industrial and commercial devices where extreme ruggedness and small size are imperative. By means of the printing process the electronic circuit of a conventional radio—now characterized by a maze of wires, resistors, inductors, and condensers—may be replaced by a compact circuit printed on a small flat plate, eliminating much of the third dimension and making it simple to check and repair. Other specific applications lie in the fields of pocket radios, personal radio telephones, miniature hearing aids, meteorological instruments, and various miniature electronic control circuits.

Present investigations at the National Bureau of Standards of the various means available for reducing the size of electronic assemblies and for mechanization of chassis wiring reveal a number of feasible and practical electronic printing methods. Variations of the stenciled screen-printing process include hand printing or spraying of the components and leads on suitable surfaces. Another method involves the use of photography and an abrasive blast. A third is an adaptation of the chemical methods of silvering mirrors. Mechanical processes include metal spraying, metal sputtering or evaporation, the use of foils, and stamping. As an example, loop antennas are now stamped out in a single operation by a variation of the printed wiring techniques and have shown improved performance over wire-wound loops in addition to reduced cost of production. The principal effect of these methods is to reduce electronic circuit wiring to two dimensions. The effect is enhanced where it is possible to employ sub-miniature tubes and compact associated components.

New Appointments

Leonard I. Schiff, theoretical physicist who worked on the Los Alamos atom bomb project, has joined the faculty of Stanford University as associate professor of physics.

H. B. G. Casimir, co-director of the Philips Research Laboratories, Eindhoven, Holland, is delivering a series of invitation lectures at Johns Hopkins University on the properties of matter at low temperatures and on problems in quantum electrodynamics.

Leo L. Beranek, formerly director of the electro-acoustic and systems research laboratories of Harvard University, has been appointed associate professor of communications engineering in the Department of Electrical Engineering of the Massachusetts Institute of Technology.

Alfred J. Reis, Austrian-born scientist, was recently appointed a research specialist in the Engineering Experiment Station at Rutgers University. He will conduct a series of studies in the engineering properties of materials and in powder metallurgy.

John A. Hipple has been named chief of the Atomic Physics Section at the National Bureau of Standards.

John L. Abbott recently joined North American Philips Company, Inc., as application engineer in the industrial x-ray division.

Awards

James I. Hoffman of the National Bureau of Standards has been awarded the 1946 Hillebrand Prize for significant contributions to chemical science.

The John Price Wetherill and the Howard N. Potts medals of The Franklin Institute of Philadelphia were awarded at ceremonies on April 16. Kenneth S. M. Davidson of Stevens Institute of Technology received the Wetherill medal for his contributions to the improved design of ships through experiments on ship hull models. Vladimir K. Zworykin, director of electronic research of the Radio Corporation of America, and Robert H. Kent, associate director of the ballistics research laboratories,

Aberdeen Proving Ground, were each awarded a Potts medal. Zworykin received the medal for his inventions of the iconoscope and kinescope, which are essential to modern commercial television. Kent was honored for contributions to the science of ballistics and particularly for his effective operation of the Aberdeen Wind Tunnel, which is doing a large part of the supersonic testing for the armed forces.

The seven winners of Frank B. Jewett fellowships for research in the physical sciences for 1947–1948, announced by the American Telephone and Telegraph Company, are as follows: M. G. Ettlinger of California Institute of Technology and Austin, Texas; Wallace D. Hayes of California Institute of Technology and Palo Alto, California; Paul Olum of Harvard University and Winchester, Massachusetts; Aadne Ore of Yale University and Oslo, Norway; Alfred Schild of the Carnegie Institute of Technology and Pittsburgh, Pennsylvania; Robert L. Scott of the University of California and Santa Ana, California; and Edwin H. Spanier of the University of Michigan and St. Paul, Minnesota. Two of the winners are chemists, two physicists, two mathematicians, and the seventh is an aeronautical engineer.

General Electric-Yale University Joint Research

At the Dunham Laboratory of Electrical Engineering at Yale University, research is being conducted on controls for a flight simulator or dummy rocket for duplicating flight characteristics of a rocket missile, as part of General Electric Company's long-range rocket research program. The project at Yale is under the direction of John L. Bower, Assistant Professor of Electrical Engineering.

Biological Photographic Exhibition

An international exhibition of biological photography of interest to all photographers in the scientific field will be held September 10–27, 1947, under the sponsorship of the Biological Photographic Association at the Rochester Public Library, Rochester, New York. Three judges who are prominent in their fields will select all entries. Membership in the Association is not a requisite for participation in the exhibition. Entry blanks for contributors may be obtained from Mr. H. Lou Gibson, 343 State Street, Rochester 4, New York. The entry fee is $1, and the last day for receiving entries is August 1, 1947.

Information concerning the convention program of the Biological Photographic Association to be held September 10–13 may be obtained from Mr. John V. Butterfield, 635 St. Paul Street, Rochester 4, New York.

General Electric Educational Fund Awards

Research fellowships totaling $20,500 have been awarded to fourteen graduate students by the General Electric Educational Fund. Eight of the winners received Charles A. Coffin Fellowships awarded for research in the fields of electricity, physics, and physical chemistry. The other six young men obtained Gerard Swope Fellowships for advanced study in industrial management, engineering, the physical sciences, and other scientific and industrial fields.

M.I.T. Summer Session in Applied Mathematics

Massachusetts Institute of Technology has announced a special summer session in applied mathematics from August 4 to September 19, 1947. The following graduate courses will be offered:

1. **Theory of Plates and Shells.** By Professors F. B. Hildebrand and E. Reissner.
2. **Theoretical Hydromechanics.** By Professors E. Reissner and C. C. Lin.
3. **Advanced Topics in Applied Mathematics.** By Professors J. L. Synge, H. Reissner, W. Prager, F. B. Hildebrand and P. D. Crout.
4. **Tensors in Mechanics.** By Professor D. J. Struik.

Further information concerning the program may be obtained by writing to Department of Mathematics, Massachusetts Institute of Technology, Cambridge 39, Massachusetts.

Centenary of Association of Engineers

The Association of Engineers, with headquarters at the University of Liége in Belgium, celebrates this year its 100th anniversary. For the occasion it is sponsoring a congress and an exhibition to which engineers and industry representatives are cordially invited. The congress will take place in Liége from August 30 to September 13, and is entitled "Past, Present and Future of Our Industry." For further information address Association des Ingenieurs, 12, Quai Paul Van Hoegaerden, Liége, Belgium.

National Electronics Conference

The National Electronics Conference, Inc., whose purpose is to serve as a national forum on electronic developments and their application, is sponsored jointly by Illinois Institute of Technology, Northwestern University, American Institute of Electrical Engineers, Institute of Radio Engineers, and the University of Illinois, with the Chicago Technical Societies Council a cooperating organization. Plans are now being formulated for the 1947 National Electronics Conference, which will be held on November 3, 4, and 5 at the Edgewater Beach Hotel, Chicago.

Course in Statistical Quality Control

An advanced eight-day course in quality control by statistical methods is to be presented June 27 through July 5 at Purdue University, Lafayette, Indiana. It is intended for those who already have some acquaintance with statistical quality control from such a course as the War Production Board organized during the war. Anyone desiring further information should write to Professor I. W. Burr at Purdue.

Marconi Anniversary

An International Congress will celebrate the fiftieth anniversary of the discovery of radio by Marconi, September 28 to October 5, 1947, in Rome, Italy. The event is being organized by the Italian National Council of Research. It aims at providing a complete picture of the progress of radio in the world from the scientific, technical, and industrial point of view, and giving world radio experts the opportunity of meeting and studying plans for a future international collaboration.

The Bulletin of Mathematical Biophysics

Following is the table of contents for *The Bulletin of Mathematical Biophysics* for June 1947:

Mathematical Theory of Motivation Interactions of Two Individuals: II. ANATOL RAPOPORT

A Theory of Membrane Permeability: III. The Effect of Hydrostatic Pressure. INGRAM BLOCH

The Mechanism of the Middle Ear: II. The Drum. MARTINUS H. M. ESSER

A Mathematical Description of Metabolizing Systems: II. HERMAN BRANSON

Outline of a Matrix Calculus for Neural Nets: II. H. D. LANDAHL

The University of Chicago Press, Chicago, Illinois, Volume 9, Number 2.

Meeting of the Division of Solid State Physics

A Division of Solid State Physics in the American Physical Society, recently authorized by the Council, is in the process of formation and a corresponding announcement is being sent out to the members of the society. The organizing committee of the division is planning for a meeting of the division in conjunction with the Montreal meeting of the American Physical Society June 19 to 21, 1947. In view of the fact that the American Society for X-Ray and Electron Diffraction is having a meeting near Montreal starting Monday, June 23, the meeting of the division will take place on Saturday, June 21, so as to make it convenient for those interested in solid state to attend both meetings.

The program will be composed of four invited papers:

"Diffraction of Neutrons in Crystals," F. SEITZ,
"Theory of Crystal Rectifiers with Application to Copper Oxide," J. BARDEEN,
"The Relaxation Spectrum of Metals," C. ZENER,
"Nuclear Magnetic Resonance Absorption in Solids and Liquids," E. M. PURCELL,

and contributed papers in the field of solids. It is suggested that those who have papers in the field of the division would present them at the June meeting in Montreal.

The Organizing Committee of the Division of Solid State:

T. A. Read	S. Siegel
F. Seitz	R. Smoluchowski
W. Shockley	C. Zener

Calendar of Meetings

May

26–27	Institute of Aeronautical Sciences, Detroit, Michigan
31	American Physical Society, New England Section, Amherst, Massachusetts

June

1–6	Society of Automotive Engineers, French Lick, Indiana
8–10	American Society of Refrigerating Engineers, Los Angeles, California
9–13	American Institute of Electrical Engineers, Montreal, Quebec, Canada
9–14	Symposium on Molecular Structure and Microscopy, Ohio State University, Columbus, Ohio
12–14	Canadian Association of Professional Physicists, University of Western Ontario, London, Canada
16–19	American Society of Mechanical Engineers, Chicago, Illinois
16–20	American Society for Testing Materials, Atlantic City, New Jersey
18–20	American Association of Physics Teachers, Regional Meeting, University of Minnesota, Minneapolis, Minnesota
18–21	Society for the Promotion of Engineering Education, Minneapolis, Minnesota
23–25	American Society for X-Ray and Electron Diffraction, Montreal, Quebec, Canada

July

11–12	American Physical Society, Stanford University, California
16–19	American Society of Civil Engineers, Duluth, Minnesota

August

21–23	Society of Automotive Engineers, Los Angeles, California (Transportation and Maintenance Meeting)
26–29	American Institute of Electrical Engineers, San Diego, California

New Booklets

Dow Corning Corporation, Midland, Michigan, has announced a new technical pamphlet, *DC Antifoam A*, which discusses a silicone compound recently developed for killing foam in aqueous systems. 4 pages.

The December 1946 issue of *The Frontier*, published by the Armour Research Foundation of Illinois Institute of Technology, Chicago 16, Illinois, includes the following articles: "A Unique Torquemeter," "Classification of Analytical Methods," "Processing and Use of Zircon for Refractory Electrical Insulating Compositions." 20 pages.

Nickel Steel Topics for February 1947, published by The International Nickel Company, Inc., 67 Wall Street, New York 5, New York, features an article on the "refrigerator car of the future," built largely of stainless and low nickel alloy steels. 12 pages.

Fish-Schurman Corporation, 230 East 45th Street, New York 17, New York, makers of raw optical, technical, and scientific glass and optical parts and specialties, recently issued bulletin MI-318 on *FS Multi-Layer Interference Films; Dichroic and Achromatic Beam Splitters*. 2 pages.

The Aerovox Research Worker, monthly house organ of the Aerovox Corporation, New Bedford, Massachusetts, in its December 1946 edition discusses "The Rectifier-Amplifier V. T. Voltmeter." 4 pages.

Pittsburgh Plate Glass Company, Columbia Chemical Division, Fifth Avenue at Bellefield, Pittsburgh 13, Pennsylvania, has published *Form A-100*, a new Columbia Caustic Soda Book, 72 pages, printed in three colors. Many photographs. Write for a copy on your company letterhead.